

2014

## Dynamic Constitutive Equation For A Syntactic Foam Under Multi-Axial Stress State

Rafid M. Kully  
*North Carolina Agricultural and Technical State University*

Follow this and additional works at: <https://digital.library.ncat.edu/dissertations>

---

### Recommended Citation

Kully, Rafid M., "Dynamic Constitutive Equation For A Syntactic Foam Under Multi-Axial Stress State" (2014). *Dissertations*. 81.  
<https://digital.library.ncat.edu/dissertations/81>

This Dissertation is brought to you for free and open access by the Electronic Theses and Dissertations at Aggie Digital Collections and Scholarship. It has been accepted for inclusion in Dissertations by an authorized administrator of Aggie Digital Collections and Scholarship. For more information, please contact [iyanna@ncat.edu](mailto:iyanna@ncat.edu).

Dynamic Constitutive Equation for a Syntactic Foam under Multi-axial Stress State

Rafid M. Kully

North Carolina A&T State University

A dissertation submitted to the graduate faculty  
in partial fulfillment of the requirements for the degree of

DOCTOR OF PHILOSOPHY

Department: Mechanical Engineering

Major: Mechanical Engineering

Major Professor: Dr. Kunigal Shivakumar

Greensboro, North Carolina

2014

The Graduate School  
North Carolina Agricultural and Technical State University  
This is to certify that the Doctoral Dissertation of

Rafid M. Kully

has met the dissertation requirements of  
North Carolina Agricultural and Technical State University

Greensboro, North Carolina  
2014

Approved by:

---

Dr. Kunigal Shivakumar  
Major Professor

---

Dr. Mannur Sundaresan  
Committee Member

---

Dr. Sameer Hamoush  
Committee Member

---

Dr. Dhananjay Kumar  
Committee Member

---

Dr. Samuel P. Owusu-Ofori  
Department Chair

---

Dr. Julius Harp  
Committee Member

---

Dr. Sanjiv Sarin  
Dean, The Graduate School

© Copyright by

Rafid M. Kully

2014

### Biographical Sketch

Rafid Kully was born on November 18<sup>th</sup>, 1976, in Baghdad, Iraq. He received his bachelor's degree in Mechanical Engineering from The College of Engineering at Baghdad University in 1999. He was ranked tenth among 35 graduates. He worked with the Iraqi Ministry of Housing and Reconstructions for five years as a mechanical engineer. He was involved with the installation of the HVAC equipment for new and renovated sites. Then he worked for two years as a military interpreter for U.S. military. In 2009 he went back to school at North Carolina A&T State University seeking a master's degree in engineering. He worked with the school performing energy auditing for buildings inside the university campus and other commercial facilities in the area. Besides, he taught HVAC laboratory while he was a teaching assistant in the Civil Engineering Department. He was awarded his master's degree in Civil Engineering (Energy Major) with a GPA of 4.0 in 2010.

In the same year (2010) he was admitted to a Ph.D. program in Mechanical Engineering at North Carolina A&T State University and worked at the Center for Composite Materials Research (CCMR) through funding from the US Army and NASA's Center for Aviation Safety (CAS). During his time at CCMR and CAS, he worked in the area of multi-axial high strain rate characterization of syntactic foams. He also taught a measurement laboratory while he was a teaching assistant in the Mechanical Engineering Department. He maintained a GPA of 4.0 throughout all his years in the graduate school.

## Dedication

After praising god, I would like to dedicate this work to my beloved parents back in Iraq, since my success is their only comfort for being me away from them. Also I dedicate it to my loving wife Jehan for her support and encouragement, to my brothers and sisters for their support and to my baby girl Lara for the hope in life I feel just looking into her eyes.

## Acknowledgments

I would like to express my greatest gratitude to the many individuals who supported and encouraged me both professionally and personally for the completion of this work. Especially, I would like to thank my advisor Professor Dr. Kunigal Shivakumar. Certainly, without his continued support, encouragement, patience and valuable advice, this work would not be possible. I sincerely acknowledge to my committee members Dr. Mannur Sundaresan, Dr. Dhananjay Kumar, Dr. Sameer Hamoush and Dr. Julius Harp for reviewing my work and offering many useful recommendations. Also I want to express my gratefulness to Dr. Trisha Sain for volunteering to participate in my dissertation defense. I express my sincerest appreciation to the Center for Composite Materials Research (CCMR) and the Department of Mechanical Engineering at the North Carolina A&T State University for the opportunity to enroll me in this program.

This research has been funded and supported by various organizations including Office of Naval Research (Dr. Yapa Rajapakse), NASA University Research Center (URC)-Center for Aviation Safety CAS) and U.S. Army Research Office (Dr. Larry Russell). I truly acknowledge these organizations and personnel for their financial and technical support to accomplish this research work. I would like to thank CCMR staff, especially, Mr. Matthew Sharpe and Mr. John Skujins and Ms. Latoya Best for various assistance in completion of this work. It is my pleasure to acknowledge the contribution of my lab mates and, senior alumni specially Dr. Raghu Pandurangha, Dr. Paul Akangah, Dr. Rupan Talucdher, Anthony Cunningham, Hiba Ahmed and Kazi Al Imran for their support. Finally, I would like to express my deepest appreciation to my parents, my wife Jehan Ali and other family members for their lifelong sacrifices and belief in me. Their consistent moral support and love always played a significant role in my life.

## Table of Contents

|  |      |
|--|------|
| List of Figures .....  | xi   |
| List of Tables .....   | xvi  |
| List of Symbols .....  | xvii |
| Abstract .....   | 1    |
| CHAPTER 1 Introduction.....                                    | 2    |
| 1.1 Background.....  | 2    |
| 1.2 Literature Review .....                                    | 6    |
| 1.3 Confinement .....  | 10   |
| 1.3.1 Sleeve (mechanical) confinement.....                     | 10   |
| 1.3.2 Hydrostatic confinement. ....                            | 11   |
| 1.3.3 Electro-magnetic confinement.....                        | 12   |
| 1.3.4 Self confinement.....                                    | 13   |
| 1.4 Sandwich Structures .....                                  | 14   |
| 1.5 Strain Rate .....  | 16   |
| 1.6 Challenges.....  | 17   |
| 1.7 Rationale of the Study .....                               | 17   |
| 1.8 Objectives of the Research .....                           | 17   |
| 1.9 Scope of the Dissertation.....                             | 18   |
| CHAPTER 2 Processing of Eco-Core and Specimen Fabrication..... | 19   |
| 2.1 Material.....  | 19   |
| 2.2 Panels Fabrication.....                                    | 21   |
| 2.3 Preparation of Test Specimen .....                         | 28   |
| 2.3.1 Preparation of static test specimens.....                | 28   |

|   |    |
|---|----|
| 2.3.2 Preparation of dynamic test specimens. ....             | 30 |
| 2.4 Summary.....  | 32 |
| CHAPTER 3 Static Confined Compression Tests.....              | 33 |
| 3.1 Methodology.....  | 33 |
| 3.2 Confined Compression Testing .....                        | 33 |
| 3.2.1 Test setup.....   | 33 |
| 3.2.2 Testing.....  | 36 |
| 3.3 Test Results.....   | 38 |
| 3.3.1 Aluminum sleeve.....                                    | 38 |
| 3.3.2 Rubber sleeve.....                                      | 41 |
| 3.3.3 Effect of sleeve type.....                              | 43 |
| 3.4 Development of Static Constitutive Equation .....         | 47 |
| 3.4.1 Frictional stress ( $\sigma_{\mu}$ ).....               | 48 |
| 3.4.2 Net-deviatoric stress ( $\sigma_{d-\mu}$ ).....         | 48 |
| 3.4.3 Development of constitutive equation.....               | 50 |
| 3.5 Summary.....  | 54 |
| CHAPTER 4 Dynamic Confined Compression Tests .....            | 55 |
| 4.1 High Strain Rate Testing .....                            | 55 |
| 4.1.1 SHPB test apparatus and analysis.....                   | 55 |
| 4.1.2 Calibration of strain rate versus gas gun pressure..... | 58 |
| 4.1.3 Validation of SHPB apparatus.....                       | 59 |
| 4.2 High Strain Rate Testing of Confined Eco-Core.....        | 61 |
| 4.2.1 Design of specimen.....                                 | 61 |
| 4.2.2 Confined compression test fixture.....                  | 63 |

|   |    |
|---|----|
| 4.2.3 Testing of confined Eco-Core. ....                            | 63 |
| 4.3 Test Results of Confined Eco-Core .....                         | 65 |
| 4.3.1 Typical stress-strain response.....                           | 65 |
| 4.3.2 Results for different strain rates. ....                      | 68 |
| 4.4 Derivation of Dynamic Constitutive Equation .....               | 72 |
| 4.5 Energy Absorption.....  | 75 |
| 4.6 Summary.....  | 78 |
| CHAPTER 5 Simulation by LS-DYNA .....                               | 79 |
| 5.1 Background.....   | 79 |
| 5.2 Challenges.....   | 81 |
| 5.3 Material Model .....  | 81 |
| 5.3.1 Selection of LS-DYNA material model. ....                     | 81 |
| 5.3.2 Modification of material model by constitutive equation. .... | 82 |
| 5.4 Simulation of Static Test .....                                 | 85 |
| 5.4.1 Finite element model of static test. ....                     | 85 |
| 5.4.2 Results of static test simulation. ....                       | 87 |
| 5.4.3 Validation of static test simulation results.....             | 89 |
| 5.5 Simulation of Dynamic Test.....                                 | 89 |
| 5.5.1 Finite element model of dynamic test. ....                    | 89 |
| 5.5.2 Results of dynamic test simulation.....                       | 92 |
| 5.5.3 Validation of dynamic test simulation results. ....           | 94 |
| 5.6 Applications of the LS-DYNA Simulation.....                     | 97 |
| 5.7 Summary.....  | 99 |

|  |     |
|--|-----|
| CHAPTER 6 Concluding Remarks and Future Work ..... | 100 |
| 6.1 Concluding Remarks .....                       | 100 |
| 6.2 Future Work.....                               | 102 |
| References .....                                   | 104 |
| Appendix A.....                                    | 109 |
| Appendix B .....                                   | 111 |
| Appendix C .....                                   | 112 |
| Appendix D.....                                    | 115 |
| Appendix E .....                                   | 119 |

## List of Figures

|  |    |
|--|----|
| Figure 1.1. Schematic of unconfined stress state, (b) Schematic of confined stress state. ....   | 6  |
| Figure 1.2. Schematic of sleeve confinement. ....  | 11 |
| Figure 1.3. (a) Photograph of pressure cell, (b) Schematic of pressure cell. ....  | 12 |
| Figure 1.4. Schematic of Electro-magnetic confinement.....   | 13 |
| Figure 1.5. Schematic of self-confinement. ....  | 14 |
| Figure 1.6. Schematic of typical sandwich structure. ....  | 14 |
| Figure 2.1. Typical microscopic structure of Cenosphere. ....  | 20 |
| Figure 2.2. Fly ash-resin mixing process. ....   | 22 |
| Figure 2.3. (a) Photograph of fly ash-resin mixture in the mold, (b) Distribution process. ....  | 23 |
| Figure 2.4. Photograph of preheating of mold and Eco-Core mixture. ....  | 23 |
| Figure 2.5. Photograph of cured Eco-Core panel. ....   | 24 |
| Figure 2.6. Time, temperature and pressure cycle for curing Eco-Core. ....   | 24 |
| Figure 2.7. Post curing time-temperature cycle. ....   | 25 |
| Figure 2.8. Post cured Eco-Core panel. ....  | 25 |
| Figure 2.9. Locations of measurements on Eco-Core panel. ....  | 27 |
| Figure 2.10. Process flow diagram for producing Eco-Core panel.....  | 27 |
| Figure 2.11. SEM micrograph of broken piece of Eco-Core. ....  | 27 |
| Figure 2.12. (a) Photograph of cutting of panels, (b) Photograph of core drilling. ....  | 28 |
| Figure 2.13. (a) Photograph of specimen turning on lathe machine, (b) Photograph of static test specimens, (c) Schematic of static test specimen. .... | 30 |
| Figure 2.14. Fixture to adjust the length of the dynamic test specimen. ....   | 31 |

|  |    |
|--|----|
| Figure 2.15. (a) Photograph of dynamic test specimens, (b) Schematic of dynamic test specimen.<br>.....  | 31 |
| Figure 3.1. (a) Static test fixture, (b) Axial and cross sections of test specimen and sleeve. ....  | 35 |
| Figure 3.2. Confined compression test setting.....   | 35 |
| Figure 3.3. Stress-strain response of five Eco-Coe specimens with aluminum sleeve.....   | 38 |
| Figure 3.4. Mean stress-strain response of five Eco-Core specimens with aluminum sleeve. ....  | 39 |
| Figure 3.5. Mean Hoop strain versus axial stress of Eco-Core with aluminum sleeve<br>confinement.....  | 40 |
| Figure 3.6. Hoop stress versus axial stress of Eco-Core with aluminum sleeve confinement. ....   | 40 |
| Figure 3.7. Confinement stress versus axial stress of Eco-Core with aluminum sleeve<br>confinement.....  | 41 |
| Figure 3.8. Axial stress-strain response for five specimens with rubber confinement. ....  | 42 |
| Figure 3.9. Mean stress-strain response of Eco-Core with thin rubber sleeve confinement. ....  | 42 |
| Figure 3.10. Axial stress-strain response for five specimens with acrylic sleeve.....  | 43 |
| Figure 3.11. Axial stress-strain response for five specimens with copper sleeve.....   | 44 |
| Figure 3.12. Axial stress-strain response for five specimens with steel sleeve. ....   | 44 |
| Figure 3.13. Stress-strain response of Eco-Core under different types of sleeve confinement. ...   | 45 |
| Figure 3.14. Mean Hoop strain of different sleeves versus axial stress of Eco-Core. ....   | 46 |
| Figure 3.15. Hoop stress of different sleeves versus axial stress of Eco-Core. ....  | 46 |
| Figure 3.16. Confinement stress versus axial stress of Eco-Core under different sleeves<br>confinement.....  | 47 |
| Figure 3.17. (a) Stress state on Eco-Core specimen confined by sleeve, (b) Derivation of<br>principal axial stress, (c) Derivation of net-deviatoric stress..... | 49 |

|   |    |
|---|----|
| Figure 3.18. Net-deviatoric stress of Eco-Core under different types of sleeve confinement. ....  | 50 |
| Figure 3.19. Comparison of curve fitting equation (3.5) and experiment. ....  | 51 |
| Figure 3.20. Comparison between constitutive equation and experimental data (aluminum sleeve). ....   | 52 |
| Figure 3.21. Comparison between constitutive equation and experiments (copper sleeve). ....   | 53 |
| Figure 3.22. Comparison between constitutive equation and experiments (steel sleeve). ....  | 53 |
| Figure 4.1. (a) Schematic of SHPB testing, (b) Photograph of SHPB testing. ....   | 56 |
| Figure 4.2. A one-dimensional strain/stress wave propagation analysis. ....   | 56 |
| Figure 4.3. Calibration of strain rate of confined Eco-Core versus pressure of gas gun. ....  | 58 |
| Figure 4.4. Axial stress-strain response of polycarbonate at about 1200/s strain rate. ....   | 59 |
| Figure 4.5. Axial stress-strain response of nylon 6/6 at about 1250/s strain rate. ....   | 60 |
| Figure 4.6. Axial stress-strain response of unconfined Eco-Core at different strain rates. ....   | 61 |
| Figure 4.7. (a) Typical compression response of foam, (b) Effect of Eco-Core specimen length on response. ....  | 62 |
| Figure 4.8. (a) Schematic of dynamic test fixture, (b) Photograph of dynamic test fixture. ....   | 63 |
| Figure 4.9. Typical time history of strain pulses of confined compression test at 3120/s. ....  | 66 |
| Figure 4.10. Dynamic balance response of SHPB. ....   | 67 |
| Figure 4.11. (a) strain rate versus time response, (b) axial strain versus time response, (c) Axial stress versus time response, (d) Axial stress-strain response at 3120/s strain rate. .... | 68 |
| Figure 4.12. Axial and confinement stresses versus axial strain at 500/s strain rate. ....  | 69 |
| Figure 4.13. Axial and confinement stresses versus axial strain at 1574/s strain rate. ....   | 69 |
| Figure 4.14. Axial and confinement stresses versus axial strain at 2220/s strain rate. ....   | 70 |
| Figure 4.15. Axial and confinement stresses versus axial strain at 3120/s strain rate. ....   | 70 |

|   |    |
|---|----|
| Figure 4.16. Axial stress-strain response at different strain rates. ....   | 71 |
| Figure 4.17. Confinement stress versus axial strain at different strain rates. ....   | 72 |
| Figure 4.18. Net-deviatoric stress-strain response at different strain rates. ....  | 74 |
| Figure 4.19. Comparison of Eq. 4.9 and experimental net-deviatoric stress versus axial strain at different strain rates. ....   | 74 |
| Figure 4.20. Validation of constitutive equation (Eq. 4.10) by experiments. ....  | 75 |
| Figure 4.21. Stress-strain curve of Eco-Core for energy absorption at 3120/s. ....  | 76 |
| Figure 4.22. (a) Energy absorption per unit volume of different core materials, (b) Energy absorption per unit mass of different core materials. ....                 | 77 |
| Figure 5.1. LS-DYNA material models. ....   | 80 |
| Figure 5.2. (a) Static test setup, (b) A 2-d axisymmetric model of static test setup. ....  | 86 |
| Figure 5.3. Finite element model of static test. ....   | 87 |
| Figure 5.4. Nodal selection for monitoring stress and strain. ....  | 87 |
| Figure 5.5. (a) Disp. response, (b) Strain response, (c) Stress response (d) Stress-strain response. ....   | 88 |
| Figure 5.6. (a) Displacement response of Node 22, (b) Stress response of Node22. ....   | 89 |
| Figure 5.7. Comparison of LS-DYNA and experimental results for static test. ....  | 90 |
| Figure 5.8. Schematic of SHPB apparatus, test fixture and specimen. ....  | 90 |
| Figure 5.9. A 2-dimensional axisymmetric model of SHPB with specimen (hatched section). ....  | 91 |
| Figure 5.10. Finite element model of SHPB set up with zoomed sections. ....   | 92 |
| Figure 5.11. (a) Strain response at 3120/s, (b) Stress response at 3120/s, (c) Strain rate response at 3120/s, (d) Stress-strain response at 3120/s strain rate. .... | 93 |
| Figure 5.12. LS-DYNA results for different strain rates. ....   | 93 |

|   |    |
|---|----|
| Figure 5.13. LS-DYNA predicted deformed shapes of specimen at four different time steps. ....     | 94 |
| Figure 5.14. Comparison of LS-DYNA with experiment for 500/s strain rate. ....                    | 95 |
| Figure 5.15. Comparison of LS-DYNA with experiment for 1574/s strain rate. ....                   | 95 |
| Figure 5.16. Comparison of LS-DYNA with experiment for 2220/s strain rate. ....                   | 96 |
| Figure 5.17. Comparison of LS-DYNA with experiment for 3120/s strain rate. ....                   | 96 |
| Figure 5.18. Axial stress response at different locations of 13.2 mm long specimen at 4000/s. ... | 98 |
| Figure 5.19. Axial stress propagation in a 100 mm long specimen at 140/s strain rate. ....        | 98 |

## List of Tables

|   |    |
|---|----|
| Table 2.1 <i>Physical properties of Cenosphere</i> .....                            | 19 |
| Table 2.2 <i>Chemical properties of Cenosphere</i> .....                            | 20 |
| Table 2.3 <i>Physical and chemical properties of phenolic resin</i> .....           | 20 |
| Table 2.4 <i>Properties of static test panels</i> .....                             | 26 |
| Table 2.5 <i>Properties of dynamic test panels</i> .....                            | 26 |
| Table 2.6 <i>Dimensions and densities of static test Eco-Core specimens</i> .....   | 29 |
| Table 2.7 <i>Dimensions and densities of dynamic test Eco-Core specimens</i> .....  | 31 |
| Table 3.1 <i>Material properties of sleeves</i> .....                               | 34 |
| Table 3.2 <i>Static test results</i> .....  | 37 |
| Table 4.1 <i>Strain rates and compression strengths of Eco-Core specimens</i> ..... | 71 |

## List of Symbols

$\sigma_a$  = axial stress

$\sigma_r$  = radial stress

$\sigma_\theta$  = Hoop stress

$\sigma_d$  = deviatoric stress

$\sigma_{\mu-d}$  = net-deviatoric stress

$\sigma_\mu$  = axial friction stress

$\sigma_{conf}$  = confined axial stress

$\sigma_{unconf}$  = unconfined axial stress

$\sigma_c$ ,  $\sigma_y$  or  $\sigma_{ys}$  = yield compression strength

$\sigma_{pl}$  = plastic strength

$\varepsilon_a$  = axial strain

$\varepsilon_\theta$  = Hoop strain

$\varepsilon_d$  = densification strain

$\varepsilon_{crush}$  = crushing strain

$\varepsilon_c$ ,  $\varepsilon_y$  or  $\varepsilon_{ys}$  = yield compression strain

$t$  = time

$\varepsilon_i(t)$  = incident strain

$\varepsilon_r(t)$  = reflected strain

$\varepsilon_t(t)$  = transmitted strain

$\dot{\varepsilon}$  = strain rate

$\dot{\varepsilon}_0$  = reference strain rate

$P_f$  = failure load

$\mu$  = coefficient of static friction

$F_\mu$  = friction force in axial direction

$\tau_\mu$  = friction shear

$q$  = confinement stress

$h$  = thickness

$d$  = diameter

$l$  = length

$A_c$  = cross section area

$A_b$  = cross section area of bars

$E$  = modulus of elasticity

$E_b$  = modulus of elastic of bar

$c_b$  = speed of sound in bar

$T$  = material temperature

$T_g$  = glass transition temperature

$P$  = pressure

$T$  = time period

$f$  = frequency

$V$  = velocity

## Abstract

Eco-Core is a fire resistant structural core material that was developed at North Carolina A&T State University in 2003. During the last 10 years, mechanical, fracture and fatigue properties as well as resistance to sea water were established for Eco-Core. A design methodology for Eco-Core in sandwich structures was provided. The objective of this research was to develop a dynamic constitutive equation for Eco-Core in a multi-axial stress state that is valid for both static and dynamic loadings, and then demonstrate the model to be used in a commercial code to solve real life problems. A special tri-axial loading and strain measurement test fixture was developed and used in static and dynamic tests. The material was tested at strain rates ranged from  $10^{-3}$ /s to 3500/s. Analysis of the results showed that the net-deviatoric stress is independent of lateral stress. Based on the test results and a multi-variable regression analysis, a two part constitutive equation was developed. The first part was for the linear response and the second part was for the non-linear response that covers translation, crushing and densification of micro bubbles in the Eco-Core. The equation was validated by independent experiments and simulation by LS-DYNA. The dynamic energy absorption capability for Eco-Core was found to be superior compared to commercial materials such as PVC foam, Rohacell foam and Balsa wood.

## **CHAPTER 1**

### **Introduction**

This chapter presents a background and historical facts about fire resistant materials and Eco-Core, detailed literature review about constitutive modeling of foams and other similar materials, confinement techniques and types, sandwich structure concept, strain rate definition, challenges of this research, rationale of the study, objectives of the research and finally the scope of this dissertation.

#### **1.1 Background**

In the era of lightweight structures where weight plays the major role for classifying materials; there is no doubt that composite sandwich structures are desirable. They are highly desired because of their superior stiffness-to-weight ratio, high strength-to-weight ratio, good endurance under cyclic loading and high resistance to corrosion [1]. Furthermore, composite sandwich structures are perfect for applications that require high specific flexural properties and not too sensitive to weight [2]. Hence, composite sandwich structures are replacing metals in a long list of civilian and military applications including air-craft, aerospace, naval, ships, submarines, infrastructures and others.

Advanced composite materials like Polymer Matrix Composites (PMC) and their sandwich structures have been widely used in the military applications for the last 40 years. Also, civilian and military aircraft manufacturers have been using ever-increasing amounts of advanced composite materials and their sandwich structures in their designs since 1940s. For example the Airbus A320 currently contains over 9,000 pounds of composite materials and the C-17 has more than 15,000 pounds of composite materials [3].

Despite of the entire success that polymer composite sandwich structures achieved, fire continues to be a major obstacle in their growth. Accidental or deliberate fire may ignite, spread and engulf the composite releasing both heat and toxic gases and smoke. Thus, a localized fire may propagate to an uncontrolled larger structural fire in polymer composite structures. One of the main reasons is that polymer composites contain about 25% of weight as volatiles; once it is ignited it fuels the fire. The National Fire Protection Association reported that in 2011, U.S. fire departments responded to about (1,389, 500) fires. These fires caused about 3000 citizens their lives and caused other 17,500 sever injuries. On average, a fire department responded to a fire every 23 second, a structure fire every 65 second, a vehicle fire every 144 second [4].

Nevertheless, on the military vehicles aspect, fire and toxicity has been a significant concern. In enclosed and confined spaces such as aircrafts, ships, submarines and others the growing fire can lead to a flashover condition in which all combustible materials within the enclosure ignite and generate enormous amounts of toxic smoke. If the burning composite is part of the primary structure; it may also collapse. In aircraft, composite matrices may be combustible contributing to the fuel load in making the situation even more critical. In submarines, the use of the composites was based on assumptions that the fire must be extinguished or brought under control within 5 minutes and in surface ships, fire should be controlled within 30 minutes [3]. These requirements are very difficult to achieve. US Navy currently uses unprotected sandwich composites do not meet the fire growth requirement of ISO 9705. Thus, Navy has invested \$10M toward the development of new fire restricting resins and foams over the last 5-10 years [5].

Because of the never ending demand for composite material that meets both, fire and toxicity safety and superior mechanical properties requirements, extensive research is being conducted by many national laboratories and universities. In 2003, fire resistant syntactic foam

called “Eco-Core” was conceived and developed by Shivakumar and his co-researchers in NCA&T State University [6]. It is a fly ash based core material for sandwich structures that contains or mitigates fire.

Hollow ceramic microspheres extracted from fly ash called Cenospheres were pressed and banded by small quantity of high char yield binder to make the syntactic foam [6]. The Cenospheres withstand temperatures in excess of 1,000° C. The small percentage of high char binder deprives the fire from fueling because it essentially reduces or eliminates the volatile content. Eco-Core has successfully passed the ASTM-1354 fire ( $75\text{kW/m}^2$ ) and toxicity safety [6, 7]. The cost of processing Eco-Core is low since it uses the waste product of coal fired from electric power plants. The most important advantages of Eco-Core can be listed as:

- Inexpensive material (from a waste product).
- Excellent fire resistant [7].
- Nontoxic in fire [7].
- Superior mechanical properties [6, 7].
- Good thermal and sound insulator.
- Adaptable to existing manufacturing facility.
- Moldable and shapeable to complex configurations.

Comprehensive studies were made on Eco-Core to understand and improve its mechanical properties. These studies can be summarized as follows: study on mechanical and fracture properties [1, 6, 7], sea water resistance [8], compression, shear and flexural fatigue of sandwich structures [9-11], design guidelines of Eco-Core sandwich composite structures [12], fracture toughness enhancement [13], energy absorption for blast applications [14], unconfined high strain rate constitutive equation [15].

Eco-Core has the potential to be used in military as well as civilian applications, transportation, buildings and other industries where fire and toxicity safety are major requirement. These applications might be subjected to blast, shocks, high speed projectiles and other high strain rate impacts. Thus, high strain rate constitutive equation for Eco-Core is needed for designing structures.

Panduranga and Shivakumar [14-16] studied the static and dynamic compression under unconfined and rigid confinement conditions. Results showed that the constitutive equation for static with rigid confinement [14, 16] is:

$$\frac{\sigma_a}{\sigma_c} = 1 + 45\varepsilon_a^{5.4} \quad (1.1)$$

and the unconfined high strain rate equation [15, 16] is:

$$\frac{\sigma_a(t)}{\sigma_c} = 1 + 90\varepsilon_a^{5.4}(t) \quad (1.2)$$

Where  $\sigma_a$  is axial stress,  $\sigma_c$  is compression strength (20 MPa), and  $\varepsilon_a$  is axial strain. The constants in the equation are the results of equation fit to experimental data. Also, note that the Eco-Core was found to be strain rate insensitive.

Eco-Core is primarily used as a core material in sandwich structures where the stress state is 3-dimensional (see Figure 1.1). Thus, a multi-axial constitutive equation of the material is needed for general structural application and designs. Therefore, the overall objective of this research is to develop a multi-axial constitutive equation for Eco-Core for both static and dynamic loadings.

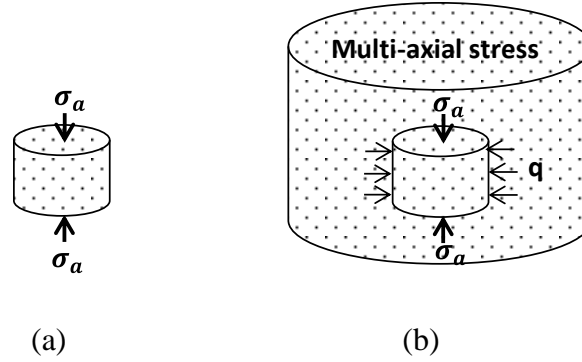


Figure 1.1. Schematic of unconfined stress state, (b) Schematic of confined stress state.

## 1.2 Literature Review

Many efforts have been made in the literature to provide constitutive equation of nonlinear materials. Only important and relevant models are presented here. In 1943, Ramberg and Osgood [17] expressed deformation of metals in power law form as:

$$\varepsilon = \frac{\sigma}{E} + k \left( \frac{\sigma}{E} \right)^m \quad (1.3)$$

Where  $\sigma$  is static stress,  $\varepsilon$  is strain,  $E$  is modulus of elasticity and  $k$  and  $m$  are material constants. In 1952, Cowper and Symonds [18] extended Ramberg and Osgood's static model for metals to the dynamic condition by introducing the strain rate effect term in the form:

$$\frac{\sigma_{dy}}{\sigma_{st}} = 1 + \left( \frac{\dot{\varepsilon}}{C_1} \right)^{\frac{1}{C_2}} \quad (1.4)$$

Where  $\sigma_{dy}$  is dynamic stress,  $\sigma_{st}$  is static stress and  $C_1$  and  $C_2$  are material constants. In 1983, Johnson and Cook [19] introduced the temperature effects in addition to the strain rate effect to the metals model as:

$$\sigma = \left[ \sigma_{ys} + B \varepsilon^n \right] \left[ 1 + C \ln \dot{\varepsilon} \right] \left[ 1 - T^m \right] \quad (1.5)$$

Where  $\sigma$  is stress,  $\varepsilon$  is strain,  $\dot{\varepsilon}$  is strain rate,  $\sigma_{ys}$  is yield strength,  $T$  is the temperature and  $B$ ,  $n$ ,  $C$  and  $m$  are material constants. In 1987, Zerilli and Armstrong [20] introduced their version of the material model that included the strain rate and the temperature effects in the form:

$$\sigma = C_1 + [C_2 + C_3\sqrt{\dot{\varepsilon}}]e^{(-C_4 + C_5 \ln \dot{\varepsilon})T} + C_6\varepsilon^n \quad (1.6)$$

Where  $C_1$ ,  $C_2$ ,  $C_3$ ,  $C_4$ ,  $C_5$ ,  $C_6$  and  $n$  are material constants. Among these models Johnson and Cook model is widely used by researches.

Three references were found in the literature for foam type materials. Gibson and Ashby model for polymeric foam in 1997 [21], Song et al model for epoxy syntactic foam in 2005 [22] and Subhash and Liu model for epoxy polymeric foam in 2009 [23]. Gibson and Ashby's study was based on unconfined test ( $\sigma_r = 0$ ) with using the assumption of Poisson's ratio is zero. In this model, stress-strain response is divided into three parts: Linear, plateau and densification parts. They are expressed as:

$$\left. \begin{array}{l} \text{Linear part,} \quad \sigma = E\varepsilon \quad \text{for} \quad \varepsilon < \varepsilon_y \\ \text{Plateau part,} \quad \frac{\sigma}{\sigma_{pl}} = 1 \quad \text{for} \quad \varepsilon_y \leq \varepsilon \leq \varepsilon_D \left(1 - \frac{1}{D}\right) \\ \text{Densification part,} \quad \frac{\sigma}{\sigma_{pl}} = \frac{1}{D} \left( \frac{\varepsilon_D}{\varepsilon_D - \varepsilon} \right)^m \quad \text{for} \quad \varepsilon > \varepsilon_D \left(1 - \frac{1}{D}\right) \end{array} \right\} \quad (1.7)$$

Where  $\sigma$  is stress,  $\varepsilon$  is strain,  $E$  is modulus of elasticity  $\varepsilon_y$  is yield strain,  $\varepsilon_D$  is densification strain,  $\sigma_{pl}$  is yield strength and  $D$  and  $m$  are material constants. In dynamic condition, the static yield strength of the foam ( $\sigma_{pl}$ ) is replaced by the dynamic yield strength as:

$$\sigma_{pl} = (\sigma_{pl}^0) \left( 1 - \frac{AT}{T_g} \ln \frac{\dot{\varepsilon}_0}{\dot{\varepsilon}} \right) \quad (1.8)$$

Where  $\sigma_{pl}$  is dynamic yield strength,  $(\sigma_{pl}^0)$  is static yield strength,  $T$  is material temperature,  $T_g$  is glass transition temperature,  $\dot{\varepsilon}_0$  is a reference strain rate and  $A$  is material constant. Gibson and Ashby model was found to be valid for low density foam used in packaging industries.

Song et al model was developed for syntactic foam under rigid confinement condition. The constitutive equation is divided into two parts, first part represents the linear response and the other part represents the plateau and densification responses, given as:

$$\sigma = \begin{cases} \left( \sigma_{ys} + \alpha \left( \frac{\varepsilon}{\dot{\varepsilon}_0} \right)^m \right) \frac{\varepsilon}{\varepsilon_y} & \text{for } \varepsilon < \varepsilon_y \\ \sigma_{ys} \left( \frac{\varepsilon}{\varepsilon_y} \right)^n + \alpha \left( \frac{\varepsilon}{\varepsilon_y} \right) & \text{for } \varepsilon_y < \varepsilon < \varepsilon_d \end{cases} \quad (1.9)$$

Where  $\sigma_{ys}$  is yield strength,  $\varepsilon_y$  and  $\varepsilon_d$  are yield and densification strains, respectively,  $m$  and  $n$  are material constants. The third model was developed by Subhash and Liu. Again the model is for syntactic foam with rigid confinement. It captured the three responses: Linear, plateau and densification parts in one equation. But, this equation requires a look up table of constants for each strain rate. The equation is given by:

$$\sigma_a = \sigma_{ys} \left( \frac{e^{\alpha\varepsilon-1}}{1+e^{\beta\varepsilon}} \right) + Ke^c (e^{\gamma\varepsilon} - 1) \quad (1.10)$$

Where  $\alpha, \beta, \gamma$  and  $c$  are material constants and  $K=1$  with stress units.

All of the three equations (models) discussed above were one-dimensional. No attempt was made to quantify the radial confinement stress (this is also referred to as lateral stress at some places). In order to introduce the effect of lateral (radial) stress to the stress-strain relation, direct measurement of this lateral stress is required in the experiment. Although, the concept of tri-axial stress is widely adopted in soil and sand mechanics to build earthen dams and retention walls, but, such model has not been evaluated for syntactic foams like Eco-core. The key difference between the above and the syntactic foam is the compressibility. The soil and sand are assumed incompressible but Eco-Core is not.

Several authors have tried to measure confinement stress and relate it to compression yield strength for solid materials: Rittel and Hanina et al [24] worked on pressure insensitive materials like metals and introduced direct determination of confinement pressure, Rittel and Brill [25] and Forquin and Nasraoui et al [26] worked on a PMMA and found that the confinement increases the compression strength of the material. Similar results were also noted by Hung and Subhash [27] for basalt rock; and Bentayeb and Taher et al [28] for concrete. However, the measurement of confinement stress and relating it to static and dynamic constitutive equation of syntactic foam has not been established. The present study focuses on this subject for Eco-Core material.

Finally, It is important to mention other study by Chun and Lim et al [29] involved static compression under hydrostatic confinement of expanded polystyrene (EPS) geo-foam. They conducted the study for different levels of hydrostatic pressure and different densities of the foam. A hyperbolic model for the static stress–strain behavior as a function of hydrostatic stress and density was developed as:

$$\sigma = \frac{a\varepsilon^b}{c + b\varepsilon} \quad (1.11)$$

Where  $a$ ,  $b$ , and  $c$  are material constants as function of density and confinement stress (pressure).

### 1.3 Confinement

Confinement simply refers to a technique that constrains material from lateral deformation. Because of Poisson deformation, the lateral strain develops under an axial stress. Confinement reduces the lateral deformation by applying lateral constraint. In this study axisymmetric problem in cylindrical shell is considered. Therefore, the terminologies are confined to this type of problems; however, this can be extended to other class. Several types of confinement were studied in the literature, they are reviewed below:

**1.3.1 Sleeve (mechanical) confinement.** This is the most commonly used type of confinement. It is practical and easy to conduct experimentally. In this case, a metallic sleeve is used to encase the specimen and provide the required level of lateral stress (see Figure 1.2). It can be either a tight fit (about 25  $\mu\text{m}$  clearance) or otherwise a loose fit if clearance is more than the mentioned one [30]. The confinement level is controlled by the dimensions and material of sleeve. With this type of confinement, the lateral confinement stress is initially zero and then it develops as the axial stress is applied on the specimen.

When specimen inside the sleeve goes under elastic axial deformation, a lateral deformation occurs according to Poisson's effects. The resistance of sleeve to the lateral deformation develops the lateral confinement stress. If the specimen undergoes plastic deformation beyond the elastic limit, then the confinement stress will be almost constant while the material is deforming under constant axial stress. But, when specimen undergoes densification mode it bulges laterally causing the confinement stress to increase rapidly. The sleeve can be designed to be rigid as in [22], deforms only elastically during the test (in this case most often a strain gauge is mounted on the sleeve to measure circumferential strain) as in [31],

deforms elastically and plastically (in this case an analytical or numerical simulation is required to determine confinement stress) as in [26] and finally, in some cases the sleeve is designed to yield at early stage of specimen deformation to apply nearly constant lateral confinement stress while deforming plastically [32].

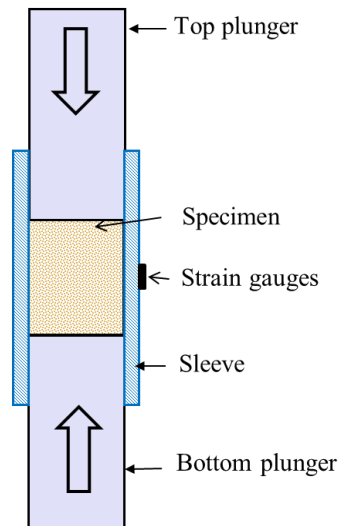


*Figure 1.2.* Schematic of sleeve confinement.

**1.3.2 Hydrostatic confinement.** This kind of confinement can be provided by a hydrostatic pressure cell that connected to either a manual or electrical pressure pump. The specimen is placed inside the pressure cell to be pressurized radially by the cell and axially by two plungers. The cell, specimen and plungers assembly is placed in between the two platens of the test apparatus. The beauty of this method it allows for applying initial confinement pressure before applying axial strain on the specimen, which is not possible with other methods. Radial pressure may vary from few to hundreds of thousands of pounds per square foot; it all depends on the application and the design of the pressure cell.

In general pressure cells consist of a hollow steel cylinder with threaded removable ends, a urethane rubber or other material bladder incorporating a seals at both ends to form a pressurization chamber for the hydraulic fluid within the cell. A spherical seat at each end

applies an axial load to the flattened ends of the specimen. Pressure sensor is installed on the cell to measure confinement pressure. A strain gauge can be installed on the specimen to measure lateral strain. Photograph and schematic of a pressure cell provided by ROCTEST Company are shown in Figures 1.3a and b, respectively. Typical type of pressure cell can be seen in [33, 34].

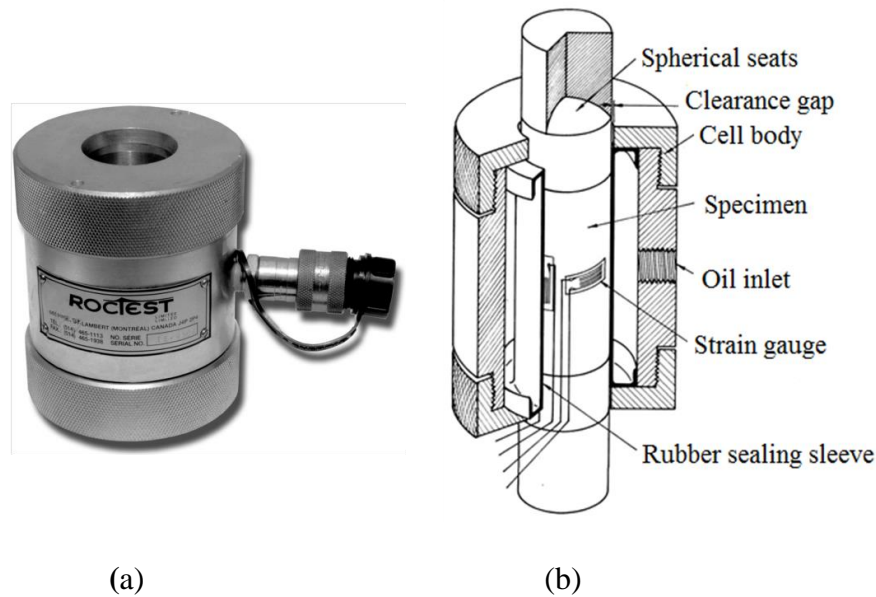


Figure 1.3. (a) Photograph of pressure cell, (b) Schematic of pressure cell.

**1.3.3 Electro-magnetic confinement.** This method is usually used with dynamic tests. The lateral confinement is achieved by using an electro-magnetic force generator. It consists of a copper or other metal strip surrounding the specimen and a capacitor bank. The capacitor bank consists of capacitors connected by inductances such that the capacitors will discharge in a given sequence. The copper strip provides a path for high intensity electric currents moving in opposite directions around the specimen. Copper strips are arranged as two layers forming two coils one inside the other.

When current passes through the copper strip, the resulting electro-magnetic force will move the two layers apart from each other's in two opposite directions. The outer layer of the copper strip tends to expand outwards but is restricted by a rigid mass, since the inner strip tends

to move inwards against the specimen. Thus, the electro-magnetic force will generate a lateral confinement pressure on the specimen. It is preferred to use a cylindrical specimen to obtain an evenly distributed confining pressure over the lateral surface of the specimen [35]. Figure 1.4 shows a schematic of the electro-magnetic confinement system.

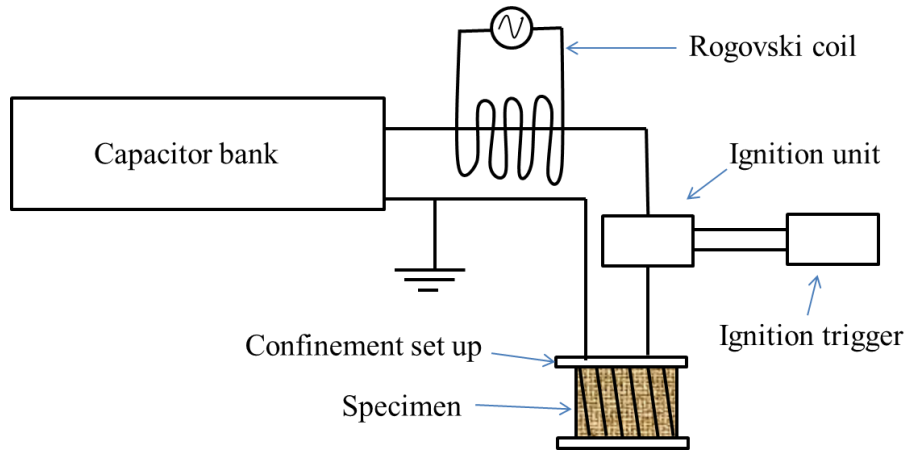


Figure 1.4. Schematic of Electro-magnetic confinement.

This method of confinement has two advantages: First is pulse tailoring, where the dynamic confinement pressure pulse can be tailored to the desired shape. Amplitude and duration of the pulse can be controlled through proper design of the capacitor bank circuits. Second is timing, as this method provides a precise timing control for the confinement pressure pulse to initiate and terminate with the axial loading while using for example Split Hopkinson Pressure Bar (SHPB) apparatus or other impact machine. Timing can be controlled by an ignition trigger delay circuit and a thyatronmercury switch ignition unit.

**1.3.4 Self confinement.** When a normal force acts on a part of object in the axial direction for example, that part develops an axial stress/strain. According to the Poisson's effect the part tends to expand laterally. The rest of the object material will constrain that lateral deformation and will develop a lateral stress or confinement stress. Since the material provides a confinement for itself, it is called self-confinement in this research. Figure 1.5 shows a schematic

expresses the self-confinement. This type of confinement is the most related to the real life applications. The multi-axial stresses acting on the core material of a sandwich structure is a good example for this type of confinement.

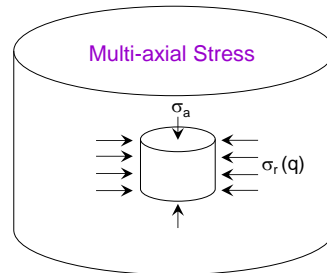


Figure 1.5. Schematic of self-confinement.

#### 1.4 Sandwich Structures

Sandwich-structure is a special class of structural construction fabricated by attaching two thin and stiff layers called face sheets to the top and bottom surfaces of a lightweight and thick core material as shown in Figure 1.6. Typically core material is of low strength, low density and inexpensive. But, its high thickness provides the sandwich structure with superior bending stiffness with overall low density. First sandwich structure appeared in 1820 when Delau introduced the principal of using two cooperating faces with a distance between them. Then during the World War 2 sandwich panels were extensively used for the first time in the Mosquito Aircraft. The demand for sandwich structure increased because of the shortage of the other materials in England during the war. Veneer was used to make the skin or the face and balsa wood to make the core.

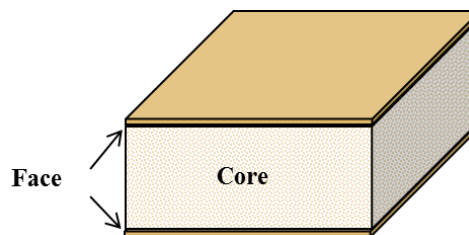


Figure 1.6. Schematic of typical sandwich structure.

The first theoretical writing about sandwich structures appeared during the World War 2 as well. During the 50's, the development focused mainly on the honeycomb materials when it mainly used as core materials in the aircraft industry. However, honeycomb had some limitations like corrosion problem. During the 60's, different cellular plastic core materials were produced. In the beginning, soft core materials like polystyrene and polyurethane were used because of their insulation properties. Later on, harder cellular plastics were produced with higher densities. By that time sandwich structure became a very useful and flexible concept. The aim was to use materials with a maximum of efficiency.

The two faces are placed at a distance from each other's to increase the moment of inertia and the flexural rigidity about the neutral axis of the structure. A sandwich beam of the same width and weight as a solid beam has become remarkably stiffer because of its higher moment of inertia [36]. Nowadays, sandwich structures are extensively used in many applications like aircraft, aerospace, ships, infrastructures and others due to their superior mechanical properties.

Core can be open or closed-cell structured foams like polyvinylchloride, polyurethane, polyethylene or polystyrene foams. Also it can be balsa wood, synthetic foam or metal foam and finally it can be honeycombs. Face material can be a laminate of glass or carbon fiber reinforced polymers or it can be a sheet of metal. The faces are usually bonded to the core with an adhesive. If the adhesive bond between the core and the face is not strong enough that results in delamination [37]. The function of each component in the sandwich structure can be summarized as following:

**Faces** carry the tensile and compression stresses of the bending moment acting on the sandwich structure. They also carry local pressure; if the local pressure is high the face should be designed to carry the shear forces associated with it.

*Core* keeps the distance between the two faces constant, so it has to be stiff enough. Also it has to be rigid if shear forces tend to slide the faces against each other. Otherwise the structure will lose its stiffness.

*Adhesive* keeps the faces and core bonded and cooperated with each other's. It has to be able to carry and transfer the shear forces between the faces and the core. At least it must withstand shear and tensile stresses as much as the core does [36].

### **1.5 Strain Rate**

Strain rate is the rate of applying strain (load) on the material. If the strain rate is about  $0.01\text{s}^{-1}$  or less, then this is called a static or quasi-static condition. It can be achieved using a universal static test apparatus like MTS Machine. With this process the acceleration effect on load measuring devices is insignificant and the stress wave propagation effect can be ignored. Intermediate strain rate is in the range of  $0.1 - 100\text{ s}^{-1}$ . It is generally covered by universal test instruments, standard servo-hydraulic test instruments, specialized drop towers and high-speed servo-hydraulic test instruments. The strain rates above  $100\text{ s}^{-1}$  are considered to be high strain rates. They require apparatus that includes stress wave propagation such as Split Hopkinson Pressure Bar (SHPB) apparatus.

The physical properties of many materials are sensitive to the strain rate. However, some materials are more sensitive to strain rate than others. It makes sense to observe these changes over orders of magnitude of strain rate. Changing the strain rate by the order of doubling or halving may generate very small structural changes that are difficult to observe. But, Strain rate measurements over orders of magnitude change in strain rate such as  $0.1, 1, 10$  and  $100\text{s}^{-1}$  will produce meaningful results [38].

## **1.6 Challenges**

Static and dynamic response of syntactic foams like Eco-Core under confinement stress is not well understood. The models reviewed previously treated the problem either as free of confinement or under rigid confinement conditions. The challenge has been the measurement of lateral strain while the axial stress is applied. This problem has been encountered in both static and dynamic loadings. This research attempts to develop appropriate test fixtures to measure the lateral strain/stress for both of these conditions. Then effect of lateral stress is included in obtaining the constitutive equation of the Eco-Core.

## **1.7 Rationale of the Study**

The development of a material model is very important to conduct analytical simulation studies of real life problems using commercial codes like ANSYS, LS-DYNA, ABACUS and others. Accuracy of the prediction depends on the accuracy of the material model used. Therefore, development of material model that accounts for stress state, failure onset and progression is very important. Thus, this study carries significant importance as it establishes the basics for development of multi-axial material models, in particular syntactic foams like Eco-Core. That helps to understand and improve their mechanical properties to expand their usage in the sandwich structures applications. Finally, introducing fire resistant material like Eco-Core for the sandwich structures in the high strain rate applications saves lives and possessing.

## **1.8 Objectives of the Research**

The overall objective of this work is to develop a dynamic constitutive equation for Eco-Core material under multi-axial stress state. However, this first attempt was to develop the constitutive equation for problems of axisymmetric type. The specific objectives are:

- Identify the stress-state that causes the failure.

- Develop a static constitutive equation and validate it by experiments.
- Develop a dynamic constitutive equation and validate it by experiments.
- Develop a single constitutive equation that covers static and dynamic conditions.
- Validate the model by dynamic simulation using LS-DYNA code.
- Assess the energy absorption of Eco-Core and compare it with other core materials.

### **1.9 Scope of the Dissertation**

This dissertation consists of six chapters. Chapter One consists background of Eco-Core, literature review about available material models, some related general concepts, importance of the study and objectives of the research. Chapter Two explains the processing of Eco-Core and specimen preparation. Chapter Three presents the static confined compression test, identification of stress state that controls the failure process of Eco-Core and development of static constitutive equation. Chapter Four presents the dynamic confined compression testing using Split Hopkinson Pressure Bar apparatus and development of dynamic constitutive equation. Chapter Five discusses the finite element simulation using LS-DYNA code to simulate static and dynamic tests. Chapter Six contains the concluding remarks and suggestions for future work.

## CHAPTER 2

### Processing of Eco-Core and Specimen Fabrication

This chapter describes processing of Eco-Core material and preparation of test specimens in details. It explains the fabrication of Eco-Core panels including preparation of fly ash mixture, molding, curing and post curing. The same procedure followed in references [6, 9, 10, 16] was followed and explained in this work. Specimen preparation for the static and dynamic tests is also discussed in details in this chapter.

#### 2.1 Material

A class of fly ash known as Cenosphere (BIONIC BUBBLE™-XL-150 was obtained from Sphere Services Inc. was used. The binder resin was a phenol-formaldehyde resole resin, Durite SC 1008 supplied by Borden Chemical Company. The physical properties of the Cenosphere, chemical properties of Cenosphere and the physical and chemical properties of the phenolic resin as provided by the material supplier are listed in Tables 2.1, 2.2 and 2.3, respectively. Typical microscopic structure of the treated Cenosphere as received from the supplier is shown in Figure 2.1. This figure shows the spherical shape of the bubbles that are evolved in the coal fire power plant.

Table 2.1

*Physical properties of Cenosphere*

| Size                 | 10-350 $\mu\text{m}$ (63 $\mu\text{m}$ at 50% Passing) |
|----------------------|--|
| Wall thickness       | 10-30 $\mu\text{m}$                                    |
| pH in water          | 6.0-8.0  |
| Bulk density         | 0.29-0.32 g/cc   |
| Specific gravity     | 0.5-0.6  |
| Compressive strength | 12 MPa (Average)                                       |
| Softening point      | Above > 1000° C  |
| Shape                | Spherical  |
| Color                | Off white to light grey                                |

Table 2.2

*Chemical properties of Cenosphere*

| Composition | Wt.%      |
|-------------|-----------|
| Silica      | 15%-50%   |
| Aluminum    | 30%-35%   |
| Iron oxide  | 1%-5%     |
| Titania     | 0.5%-1.5% |

Table 2.3

*Physical and chemical properties of phenolic resin*

|                       |                    |
|-----------------------|--------------------|
| Boiling Point         | 98° C              |
| Vapor pressure        | 28 mm of Hg        |
| Vapor density         | 2.1                |
| Spec gravity          | 1.07 - 1.10        |
| pH value              | > 7.9              |
| Viscosity             | 180 -300 cps       |
| Solubility in water   | 100%               |
| Appearance and odor   | Clear amber liquid |
| % Volatiles by volume | 38                 |

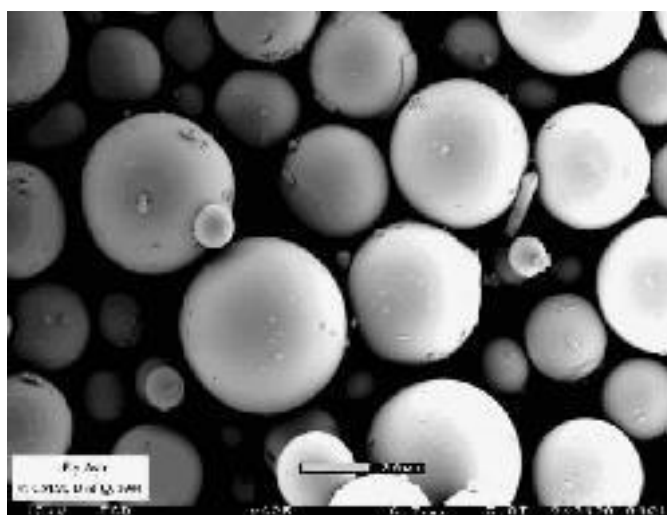


Figure 2.1. Typical microscopic structure of Cenosphere.

## 2.2 Panels Fabrication

Eco-Core mixture was prepared following the procedure explained in the references mentioned before, as well as molding, curing and post curing processes. Eco-Core panels were fabricated in two thicknesses,  $h = 25.4$  mm to prepare static test specimens and  $h = 12.7$  mm to prepare dynamic test specimens. The steps of panels' fabrication followed in this work are listed below:

1. The fly ash (Cenosphere) was treated by the supplier company before delivery to remove lime components by a dilute hydrochloric acid (pH  $\sim 4$ ). The heavier than water fraction of the ash was separated and removed by settling. The lighter floating fraction material was further washed with water approximately 3-4 times and was separated by filtration from the water. The floaters were scooped out and then they were thoroughly dried at  $110^{\circ}\text{C}$  in a convection oven. Subsequently, the treated fly ash was treated with an aminoalkyl triethoxysilane coupling agent. The Cenosphere after saline treatment was dried in an oven to attain a free-flowing material.
2. Resin-alcohol solution was prepared by mixing Isopropanol alcohol with the Phenol-formaldehyde resin at a weight ratio of 1:10. The solution was stirred for about 5 minutes.
3. Treated fly ash was mixed with the resin-alcohol solution at a weight ratio of 5:1. It was mixed in a low-shear planetary motion mixer so that fly ash is uniformly coated with resin. Figure 2.2 shows the mixing bowl with mixture of fly ash and resin. This process was continued for about 12 minutes.
4. The volatile solvents from the fly ash mixture were removed while mixing it in a stream of warm air for about 5 minutes.



*Figure 2.2.* Fly ash-resin mixing process.

5. The volatile fraction for the mixture was calculated by taking three samples (small quantities of the mixture) and weighing them before and after drying for 30 minute at 180° C temperature. The deference in the weight over the original weight represents the volatile fraction. It was calculated for each sample then averaged for the three samples. From knowing the final desired volume and density of the panel and knowing the volatile fraction of the mixture, the quantity of the required mixture can be calculated as:

$$Weight = \frac{density \times volume}{1 - volatile\ fraction} \quad (2.1)$$

Additional amount of about 5% of the calculated mixture weight should be added to compensate for the material lost in the process (bowl, mold and others).

6. The mixture was then charged into compression steel molds. Note that the used steel molds were of two sizes. One of 356 x 356 x 25.4 mm dimensions to produce panels for the static test and the other of 356 x 356 x 12.7 mm to produce panels for the dynamic test. The mixture was distributed uniformly using plastic rollers. Figures 2.3a and b show the mixture in the mold and the distribution by rolling process, respectively.



(a)

(b)

Figure 2.3. (a) Photograph of fly ash-resin mixture in the mold, (b) Distribution process.

7. The mixture was then pre-compacted and preheated in a laboratory hot press at  $82^{\circ}\text{C}$  for about 30 minutes with no pressure (see Figure 2.4).



Figure 2.4. Photograph of preheating of mold and Eco-Core mixture.

8. The preheated panel was then cured at  $163^{\circ}\text{C}$  and 1.55 MPa pressure for about 30 min. The cured Eco-Core panel is shown in Figure 2.5. The time, temperature and pressure cycle used with curing the Eco-Core is shown in Figure 2.6.



Figure 2.5. Photograph of cured Eco-Core panel.

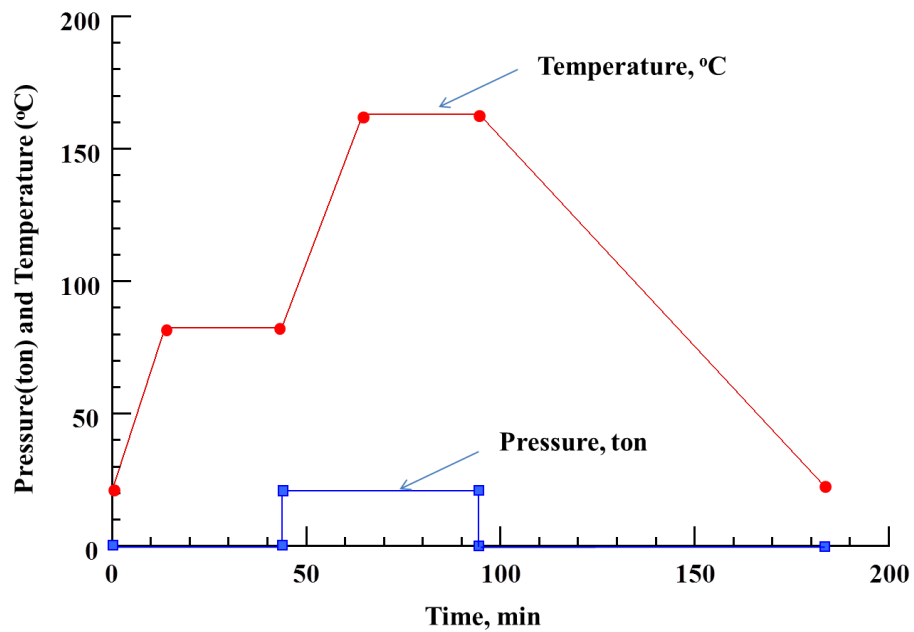


Figure 2.6. Time, temperature and pressure cycle for curing Eco-Core.

9. The Eco-core panels were finally post cured in a circulating air oven at 163° C for 4.5 hours. The temperature cycle for post curing is shown in Figure 2.7. The post cured panel is shown in Figure 2.8.

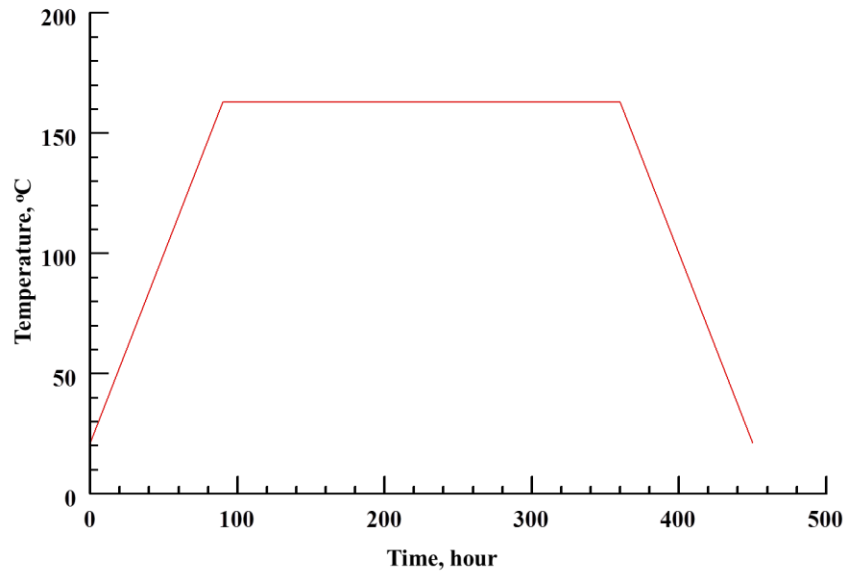


Figure 2.7. Post curing time-temperature cycle.

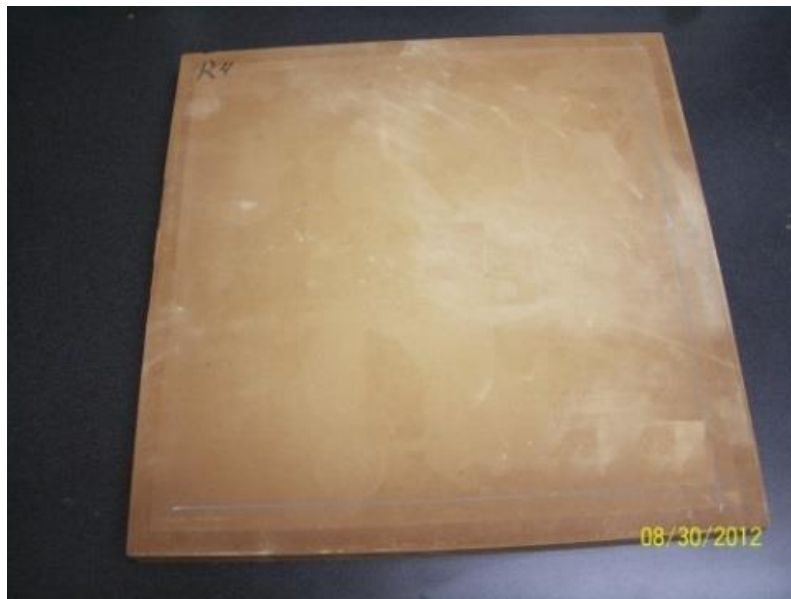


Figure 2.8. Post cured Eco-Core panel.

10. Four panels were fabricated for each size. In order to assess the quality of the fabricated panels, density and dimensional measurements were performed. Each panel was identified and weighed and panel dimensions were measured. Table 2.4 lists the average dimensions, weights and density of the four panels of static test (356 x 356 x 25.4 mm) and Table 2.5 lists the same properties for the four panels of the dynamic test (356 x 356 x 12.7 mm).

Table 2.4

*Properties of static test panels*

| <b>Panel #</b> | <b>Ave length, mm</b> | <b>Ave width, mm</b> | <b>Ave thickness, mm</b> | <b>Weight, g</b> | <b>Bulk density, g/cm<sup>3</sup></b> |
|----------------|-----------------------|----------------------|--------------------------|------------------|---------------------------------------|
| 1              | 304.5                 | 304.6                | 25.6                     | 1157.3           | 0.485                                 |
| 2              | 304.6                 | 304.5                | 25.6                     | 1191.3           | 0.489                                 |
| 3              | 304.7                 | 304.6                | 25.7                     | 1192.4           | 0.501                                 |
| 4              | 304.6                 | 304.7                | 25.7                     | 1238.0           | 0.525                                 |

Table 2.5

*Properties of dynamic test panels*

| <b>Panel #</b> | <b>Ave length, mm</b> | <b>Ave width, mm</b> | <b>Ave thickness, mm</b> | <b>Weight, g</b> | <b>Bulk density, g/cm<sup>3</sup></b> |
|----------------|-----------------------|----------------------|--------------------------|------------------|---------------------------------------|
| 1              | 304.5                 | 304.7                | 12.9                     | 619.0            | 0.519                                 |
| 2              | 304.5                 | 304.5                | 12.9                     | 597.8            | 0.503                                 |
| 3              | 304.7                 | 304.7                | 12.8                     | 586.0            | 0.491                                 |
| 3              | 304.7                 | 304.7                | 12.8                     | 606.6            | 0.510                                 |

The thickness of the panel was quite uniform. Figure 2.9 shows the locations on the panel where measurement of length, width and thickness were taken. These dimensions were averaged and listed in the above tables. Panel number 3 was selected to prepare static test specimens as its density of 0.501 g/cm<sup>3</sup> was the closest to the desired one (0.5 g/cm<sup>3</sup>). For the dynamic test, panel number 2 was selected to prepare the specimens. Its density of 0.503 g/cm<sup>3</sup> was the closest to the first selected panel. Using uniform density of the specimens of the static and dynamic test eliminates the possible variation in the properties according to the density variation. The whole steps of Eco-Core panel fabrication are summarized in Figure 2.10. The SEM microscopic picture of broken piece of Eco-Core material is shown in Figure 2.11 for two magnifications; 250 and 1000 times. This figure shows the sphere to sphere contact structure of the material with very little resin binder.

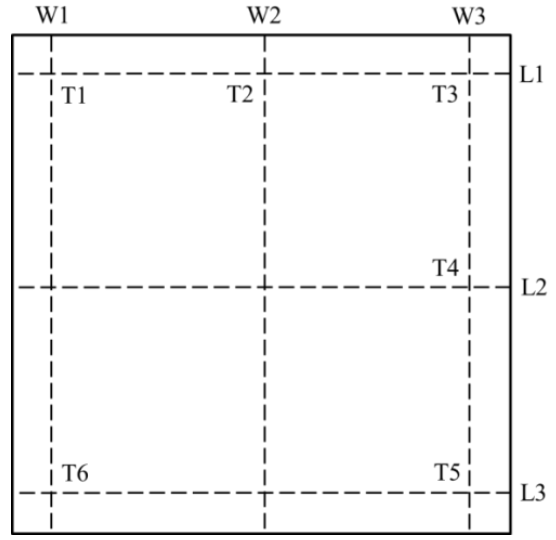


Figure 2.9. Locations of measurements on Eco-Core panel.

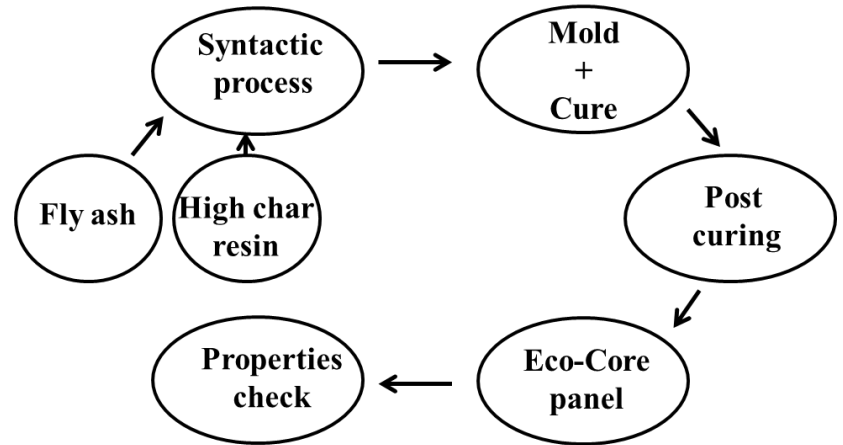


Figure 2.10. Process flow diagram for producing Eco-Core panel.

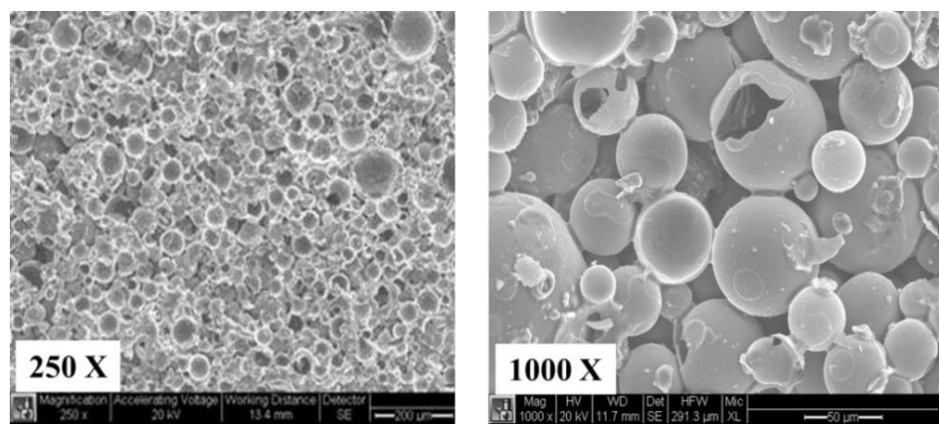


Figure 2.11. SEM micrograph of broken piece of Eco-Core.

## 2.3 Preparation of Test Specimen

The two selected panels of the thicknesses 25.4 mm and 12.7 mm were used to fabricate specimens for the static and dynamic tests, respectively. The fabrication process of the specimen is detailed as below:

**2.3.1 Preparation of static test specimens.** Panel number 3 of the static test panels was selected to perform the fabrication of static test specimens. Thickness and bulk density of the panel were 25.4 mm and  $0.501 \text{ g/cm}^3$ , respectively. The panel was cut into smaller rectangular blocks of 100 mm x 100 mm dimensions to fit in the vise of the drill machine (see Figure 2.12a). Cylindrical specimens were cut from these small panels using a 36 mm inner diameter core cutter (see Figure 2.12b).



(a)



(b)

Figure 2.12. (a) Photograph of cutting of panels, (b) Photograph of core drilling.

At this stage, the diameter of the specimens was about 25% larger than the final diameter. Then specimens were turned on the lathe machine to the final diameter of 28.5 mm and length of 25.4 mm (see Figure 2.13a). The volume and the weight of specimens were measured and the density of each specimen was determined to classify the specimens according to the density. Just the ones within the  $0.5 - 0.52 \text{ g/cm}^3$  density range were chosen to conduct the test. The variation

in the density of specimens was limited to 2%. Table 2.6 lists the geometric configurations and densities of the static test specimens. Figures 2.13a, b and c show turning process, a photograph of the static test specimens and schematic of the specimen, respectively.

Table 2.6

*Dimensions and densities of static test Eco-Core specimens*

| <b>Sleeve type</b> | <b>Specimen number</b> | <b>Length, L<br/>mm</b> | <b>Diameter, d<br/>mm</b> | <b>Weight, w<br/>g</b> | <b>Density, <math>\rho</math><br/>g/cm<sup>3</sup></b> |
|--------------------|------------------------|-------------------------|---------------------------|------------------------|--|
| Rubber             | 1                      | 25.63                   | 28.44                     | 8.21                   | 0.504  |
|                    | 2                      | 25.62                   | 28.44                     | 8.28                   | 0.509  |
|                    | 3                      | 25.63                   | 28.4                      | 8.44                   | 0.520  |
|                    | 4                      | 25.64                   | 28.44                     | 8.34                   | 0.512  |
|                    | 5                      | 25.64                   | 28.44                     | 8.26                   | 0.507  |
|                    | Ave                    | 25.63                   | 28.43                     | 8.31                   | 0.510  |
| Acrylic            | 1                      | 25.62                   | 27.90                     | 7.93                   | 0.506  |
|                    | 2                      | 25.62                   | 27.90                     | 8.10                   | 0.517  |
|                    | 3                      | 25.62                   | 27.90                     | 7.83                   | 0.500  |
|                    | 4                      | 25.62                   | 27.90                     | 7.88                   | 0.503  |
|                    | 5                      | 25.62                   | 27.90                     | 7.97                   | 0.509  |
|                    | Ave                    | 25.62                   | 27.90                     | 7.94                   | 0.507  |
| Aluminum           | 1                      | 25.63                   | 28.40                     | 8.41                   | 0.518  |
|                    | 2                      | 25.63                   | 28.40                     | 8.18                   | 0.504  |
|                    | 3                      | 25.63                   | 28.40                     | 8.33                   | 0.513  |
|                    | 4                      | 25.63                   | 28.40                     | 8.30                   | 0.511  |
|                    | 5                      | 25.63                   | 28.40                     | 8.13                   | 0.501  |
|                    | Ave                    | 25.63                   | 28.40                     | 8.27                   | 0.509  |
| Copper             | 1                      | 25.63                   | 28.37                     | 8.15                   | 0.503  |
|                    | 2                      | 25.63                   | 28.37                     | 8.13                   | 0.502  |
|                    | 3                      | 25.63                   | 28.37                     | 8.28                   | 0.511  |
|                    | 4                      | 25.63                   | 28.37                     | 8.33                   | 0.514  |
|                    | 5                      | 25.63                   | 28.37                     | 8.20                   | 0.506  |
|                    | Ave                    | 25.63                   | 28.37                     | 8.22                   | 0.507  |
| Steel              | 1                      | 25.48                   | 28.58                     | 8.17                   | 0.500  |
|                    | 2                      | 25.63                   | 28.58                     | 8.24                   | 0.501  |
|                    | 3                      | 25.63                   | 28.58                     | 8.35                   | 0.508  |
|                    | 4                      | 25.63                   | 28.58                     | 8.27                   | 0.503  |
|                    | 5                      | 25.63                   | 28.58                     | 8.27                   | 0.503  |
|                    | Ave                    | 25.60                   | 28.58                     | 8.26                   | 0.503  |

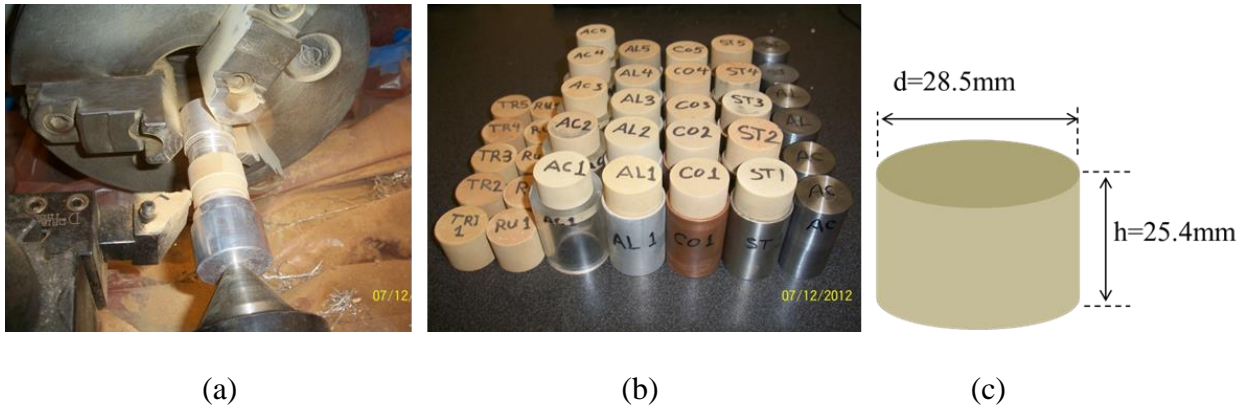


Figure 2.13. (a) Photograph of specimen turning on lathe machine, (b) Photograph of static test specimens, (c) Schematic of static test specimen.

**2.3.2 Preparation of dynamic test specimens.** Panel number 2 of the dynamic test panels was selected to perform the fabrication of dynamic test specimens. Thickness and bulk density of the panel were 12.7 mm and  $0.503 \text{ g/cm}^3$ , respectively. Similar to the previous case, the panel was cut into smaller rectangular blocks of 100 mm x 100 mm dimensions as well. Cylindrical specimens were cut from these small panels using a 16 mm inner diameter core cutter. At this stage, the diameter of the specimen was about 30% larger than the final specimen diameter. Then specimens were turned on the lathe machine to the final diameter of 11 mm.

The 12.7 mm long specimen was cut into two halves each half was placed in the 3.2 mm depth hole of the fixture shown in Figure 2.14. Then it was sanded down by 400-grit sand paper to a final length of 3.2 mm within  $25 \mu\text{m}$  variation. The two surfaces of the specimen were perfectly parallel to minimize the misalignment in the test fixture. Length direction is the axial direction of the test. Dimensions and masses of all specimens were measured and the density was calculated for each specimen and listed in Table 2.7. The density of the selected specimens ranged  $0.5 - 0.52 \text{ g/cm}^3$  with a variation of 2%. A photograph and schematic of the dynamic test specimens are shown in Figures 2.15a and b, respectively.

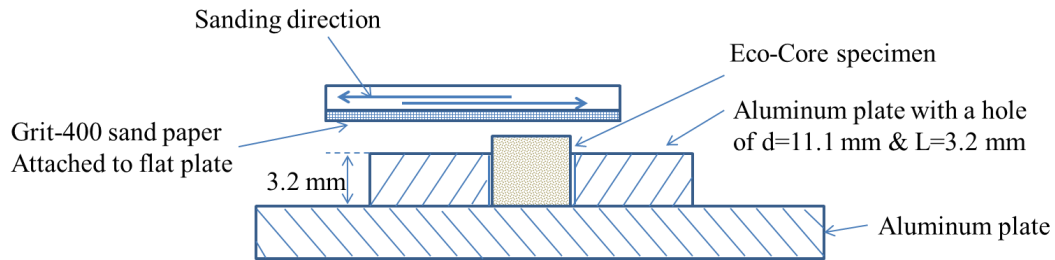
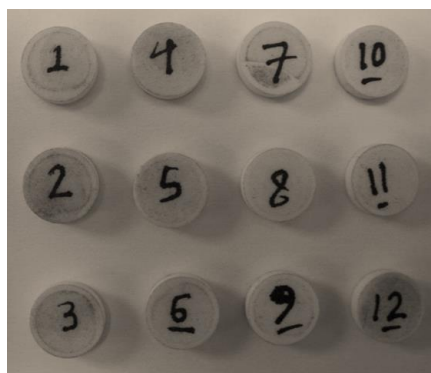


Figure 2.14. Fixture to adjust the length of the dynamic test specimen.

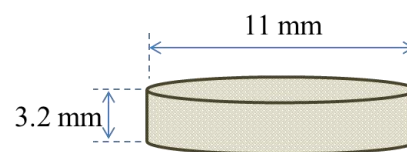
Table 2.7

Dimensions and densities of dynamic test Eco-Core specimens

| SPC # | d, mm | L, mm | w, g  | $\rho$ , g/cm <sup>3</sup> |
|-------|-------|-------|-------|----------------------------|
| 1     | 11.00 | 3.20  | 0.155 | 0.511                      |
| 2     | 11.01 | 3.20  | 0.155 | 0.510                      |
| 3     | 11.00 | 3.21  | 0.153 | 0.500                      |
| 4     | 11.01 | 3.20  | 0.158 | 0.519                      |
| 5     | 10.99 | 3.20  | 0.153 | 0.505                      |
| 6     | 11.00 | 3.20  | 0.155 | 0.509                      |
| 7     | 11.01 | 3.20  | 0.154 | 0.505                      |
| 8     | 11.01 | 3.20  | 0.156 | 0.513                      |
| 9     | 10.99 | 3.19  | 0.152 | 0.502                      |
| 10    | 11.00 | 3.20  | 0.156 | 0.514                      |
| 11    | 11.00 | 3.20  | 0.154 | 0.506                      |
| 12    | 10.99 | 3.19  | 0.156 | 0.516                      |



(a)



(b)

Figure 2.15. (a) Photograph of dynamic test specimens, (b) Schematic of dynamic test specimen.

## 2.4 Summary

Eco-Core panels were molded in two thicknesses, 25.4 mm and 12.7 mm. Then specimens for the static and dynamic tests were prepared. Static test specimen had 25.4 mm length and 28.5 mm diameter. Dynamic test specimen had 3.2 mm length and 11 mm diameter. Total 25 static test and 12 dynamic test specimens were prepared. The density of the static test specimens ranged from 0.500 to 0.520 g/cm<sup>3</sup> with average of 0.507 g/cm<sup>3</sup>. The density of the dynamic test specimens ranged from 0.500 to 0.519 g/cm<sup>3</sup> with average of 0.509 g/cm<sup>3</sup>.

## CHAPTER 3

### Static Confined Compression Tests

This chapter discusses the static confined compression testing of Eco-Core, test results and analysis of results. Then, the results are expressed as net-deviatoric stress versus axial strain response that independent of confinement (lateral) stress using simple assumptions. This response is used to develop a constitutive equation.

#### 3.1 Methodology

The methodology adopted in this study is to measure the axial compression stress-strain response and the confinement stress as it develops in the confinement casing (sleeve) of Eco-Core. Change the confinement sleeve stiffness by changing material and sleeve thickness. From the database of the above test study, develop a comprehensive constitutive equation that includes the confinement stress.

#### 3.2 Confined Compression Testing

Confined compression testing includes two parts: test set up and testing. Note that the static test specimens were used in this test. Preparation and configuration of static test specimen were discussed in Chapter 2.

**3.2.1 Test setup.** The test setup consists of two parts: specimen and test fixture assembly and then compression testing in a universal test machine (MTS 810). The specimen placed inside a sleeve that fits smoothly. Then two (top and bottom) plungers that smoothly fit the sleeve were pushed together to apply compression stress. Three strain gauges were installed on the sleeve to measure Hoop strain as the axial compression stress increases. Four different types of sleeves were used to provide the lateral confinement of the specimens during the compression tests:

acrylic, aluminum, copper and steel. In addition test was conducted with thin rubber sleeve to simulate near zero confinement. The material properties of the sleeves are listed in Table 3.1.

All sleeves had an inner diameter of 28.50 mm, length of 50.80 mm and thickness of 1.65 mm (except acrylic sleeve with 5.00 mm thickness). The three strain gauges were mounted on each sleeve (except on the thin rubber sleeve), they were arranged to be one at the midlevel, and other two at 6.4 mm (0.25 in) from top and bottom of the specimen (see Figure 3.1a). The compression load was applied using steel plungers that snug fit the sleeves (within 25  $\mu\text{m}$  clearance). Schematic of test fixture and the associated induced Hoop strains, Hoop stress, radial stress ( $q$ ) and their calculations based on thin walled cylinder theory are shown in Figures 3.1a and b, respectively.

Table 3.1

*Material properties of sleeves*

| <b>Material</b>    | <b>Modulus<br/>GPa</b> | <b>Strength<br/>MPa</b> | <b>Diameter<br/>mm</b> | <b>Thickness<br/>mm</b> | <b><math>E \times t</math><br/>N/m</b> |
|--------------------|------------------------|-------------------------|------------------------|-------------------------|--|
| Acrylic            | 3.3                    | 55                      | 28.5                   | 5.00                    | $16.5 \times 10^6$                     |
| Aluminum (6061-T6) | 69                     | 255                     | 28.5                   | 1.65                    | $113.9 \times 10^6$                    |
| Copper (122)       | 117                    | 221                     | 28.5                   | 1.65                    | $193.0 \times 10^6$                    |
| Steel (DOM)        | 200                    | 496                     | 28.5                   | 1.65                    | $330.0 \times 10^6$                    |

This arrangement was used to capture maximum deformation or maximum Hoop (circumferential) strain all along the specimen, even if the specimen passed one of the strain gauges. MTS system model 810 was used to conduct the static test (quasi-static). The whole specimen and test fixture assembly was placed in between the two platens of the MTS system. Displacement was applied by the bottom platen of the MTS to simulate compression stress on the specimen. The used displacement rate was 0.02 mm/s over the specimen length of 25.4 mm, which is equivalent to strain rate of  $8.3 \times 10^{-4}$ /s. The three strain gauges and the output of the

MTS machine were all connected to data acquisition system (scanner model 5100). The scanner was connected to a computer that has a STRAIN-SMART software to acquire the data. The test set up in the MTS system including test fixture is showing in Figure 3.2.

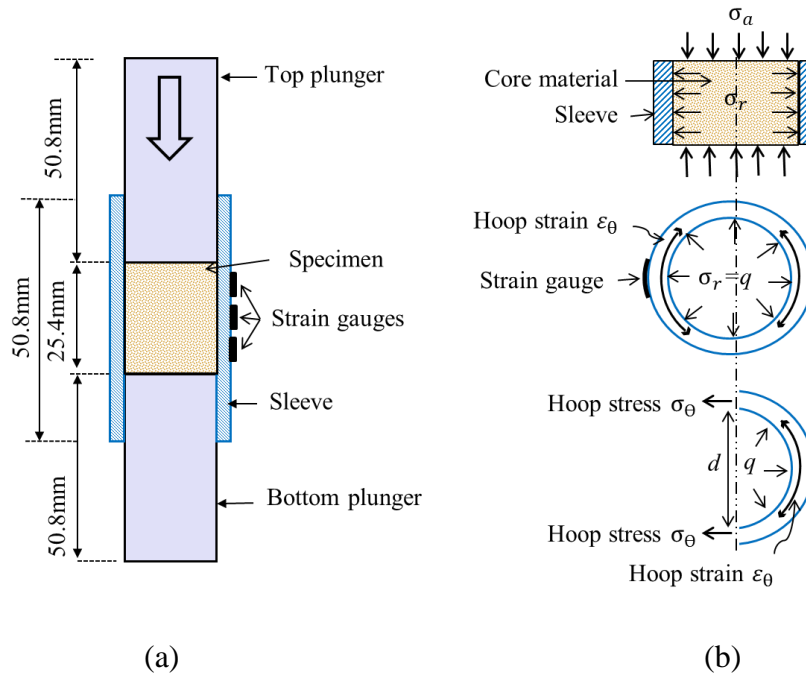


Figure 3.1. (a) Static test fixture, (b) Axial and cross sections of test specimen and sleeve.

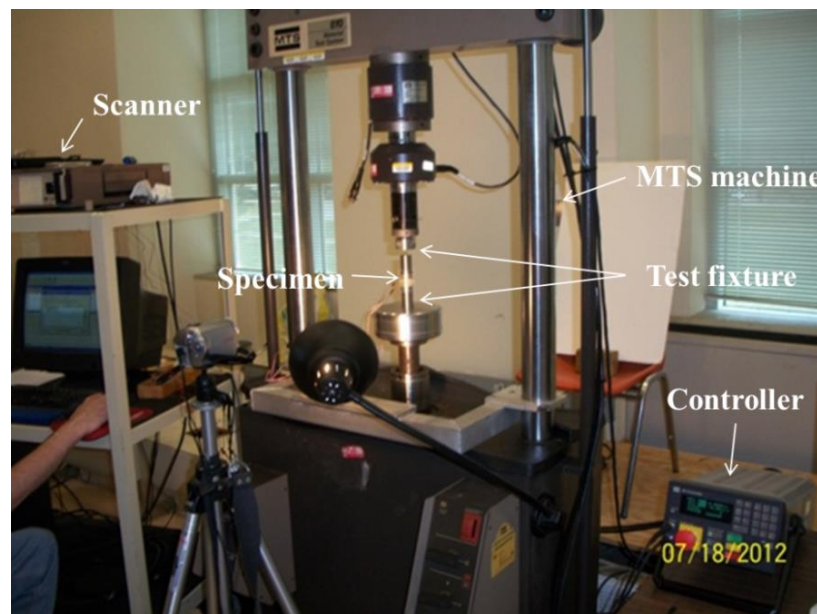


Figure 3.2. Confined compression test setting.

**3.2.2 Testing.** After placing specimen-fixture assembly on the MTS machine and connecting the strain gauges to the data acquisition system, the test was started. The controller of the MTS machine was set to displacement rate of 0.02 mm/s (strain rate of  $8.3 \times 10^{-4}$ /s). The axial displacement ( $\delta$ ) and the force ( $P$ ) from the MTS machine and the three Hoop strains of the sleeve were recorded every 0.02 second. The specimen was compressed to about 60% for stiff sleeves and to about 80% for rubber sleeve. From the raw data, axial stress ( $\sigma_a = P/A_c$ ) and strain ( $\varepsilon_a = \delta/L$ ) were calculated. The cross-sectional area of the specimen is  $A_c = \pi d^2/4$ .

The first maximum load is the failure load ( $P_f$ ) and the corresponding stress and strain are represented as compression strength ( $\sigma_c$ ) and yield strain ( $\varepsilon_c$ ), which is in some references denoted by ( $\varepsilon_y$  or  $\varepsilon_{ys}$ ). The confinement stress ( $q$ ) was calculated from the measured Hoop strain ( $\varepsilon_\theta$ ), by calculating Hoop stress ( $\sigma_\theta = \varepsilon_\theta E_s$ ) and using thin walled cylinder theory (Equation 3.1) [39].

$$q = \frac{2h\sigma_\theta}{d} \quad (3.1)$$

Where  $h$  is the thickness of the sleeve and  $d$  is the diameter of the specimen. Figure 3.1b shows the steps involved in calculating the confinement stress ( $q$ ).

Note that the thin walled cylinder theory to be valid,  $d/h$  of the sleeve has to be more than 10; this requirement is violated in acrylic sleeve. The data is used as a representative value. The test was first conducted using aluminum sleeve confinement then it was repeated for copper, steel and acrylic. In each case five specimens were tested to ensure the repeatability of the test results. The dimensions and test values of  $\sigma_c$  and  $\varepsilon_c$  for all specimens are listed in Table 3.2. The average value for the confined compression strength was 21 MPa, whereas, the unconfined

compression strength ( $\sigma_c$ ) was 20MPa. However, the unconfined strength was used to normalize all data. The average confined at failure (yield) strain was 0.023, whereas, the unconfined yield strain ( $\varepsilon_c$ ) was 0.02. Again, the unconfined yield strain was used to separate the linear and plateau parts of the confined stress-strain curve.

Table 3.2

*Static test results*

| <b>Sleeve type</b> | <b>Specimen number</b> | <b>Length, L<br/>mm</b> | <b>Diameter, d<br/>mm</b> | <b><math>\sigma_c</math><br/>MPa</b> | <b><math>\varepsilon_c</math><br/>m/m</b> |
|--------------------|------------------------|-------------------------|---------------------------|--------------------------------------|---|
| Rubber             | 1                      | 25.63                   | 28.44                     | 20.53                                | 0.023                                     |
|                    | 2                      | 25.62                   | 28.44                     | 20.26                                | 0.019                                     |
|                    | 3                      | 25.63                   | 28.40                     | 18.84                                | 0.027                                     |
|                    | 4                      | 25.64                   | 28.44                     | 21.33                                | 0.020                                     |
|                    | 5                      | 25.64                   | 28.44                     | 21.58                                | 0.022                                     |
| Acrylic            | 1                      | 25.62                   | 27.90                     | 21.48                                | 0.021                                     |
|                    | 2                      | 25.62                   | 27.90                     | 20.49                                | 0.031                                     |
|                    | 3                      | 25.62                   | 27.90                     | 21.41                                | 0.021                                     |
|                    | 4                      | 25.62                   | 27.90                     | 19.94                                | 0.023                                     |
|                    | 5                      | 25.62                   | 27.90                     | 22.18                                | 0.022                                     |
| Aluminum           | 1                      | 25.63                   | 28.40                     | 22.68                                | 0.020                                     |
|                    | 2                      | 25.63                   | 28.40                     | 22.43                                | 0.020                                     |
|                    | 3                      | 25.63                   | 28.40                     | 20.69                                | 0.017                                     |
|                    | 4                      | 25.63                   | 28.40                     | 22.83                                | 0.023                                     |
|                    | 5                      | 25.63                   | 28.40                     | 20.88                                | 0.016                                     |
| Copper             | 1                      | 25.63                   | 28.37                     | 20.52                                | 0.018                                     |
|                    | 2                      | 25.63                   | 28.37                     | 22.21                                | 0.039                                     |
|                    | 3                      | 25.63                   | 28.37                     | 21.31                                | 0.039                                     |
|                    | 4                      | 25.63                   | 28.37                     | 20.45                                | 0.023                                     |
|                    | 5                      | 25.63                   | 28.37                     | 21.72                                | 0.019                                     |
| Steel              | 1                      | 25.48                   | 28.58                     | 21.72                                | 0.034                                     |
|                    | 2                      | 25.63                   | 28.58                     | 22.16                                | 0.020                                     |
|                    | 3                      | 25.63                   | 28.58                     | 19.86                                | 0.019                                     |
|                    | 4                      | 25.63                   | 28.58                     | 21.71                                | 0.023                                     |
|                    | 5                      | 25.63                   | 28.58                     | 20.46                                | 0.029                                     |

### 3.3 Test Results

The results of the tests are presented under three sections according to the type of sleeve confinement: aluminum sleeve, rubber sleeve and other sleeves (copper, steel and acrylic).

**3.3.1 Aluminum sleeve.** The axial stress-strain responses of all five specimens of Eco-Core under aluminum sleeve confinement are plotted in Figure 3.3. All five curves were close to each other's to indicate repeatability of results. The mean value of the five tests was calculated and plotted in Figure 3.4. The curve has three parts: linear part ( $0 \leq \sigma_a \leq \sigma_c$ ), a plateau and then densification curve. The linear part of maximum stress is called the compression strength,  $\sigma_c$  and the corresponding strain is called the yielding strain,  $\varepsilon_c$ . The strain where the densification starts is called densification strain,  $\varepsilon_d$  ( $\varepsilon_d \approx 0.4$ ). The curve between  $\varepsilon_c \leq \varepsilon_a \leq \varepsilon_d$  is called the compressibility of the material and the curve beyond  $\varepsilon_a \geq \varepsilon_d$  is called the densification. Here the axial stress ( $\sigma_a$ ) rises steeply with strain.

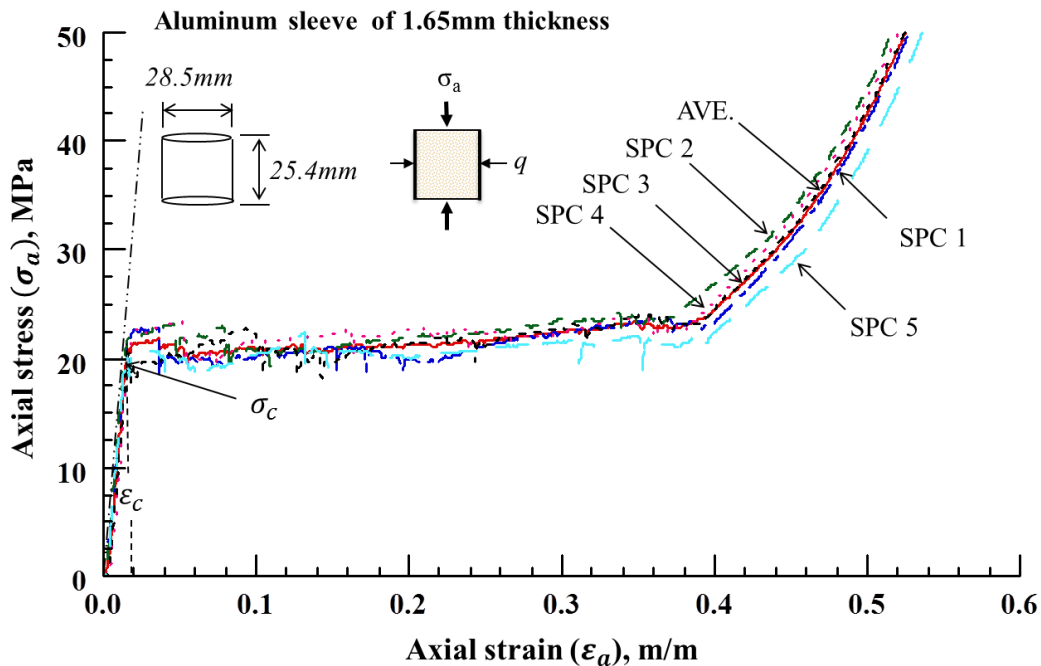


Figure 3.3. Stress-strain response of five Eco-Coe specimens with aluminum sleeve.

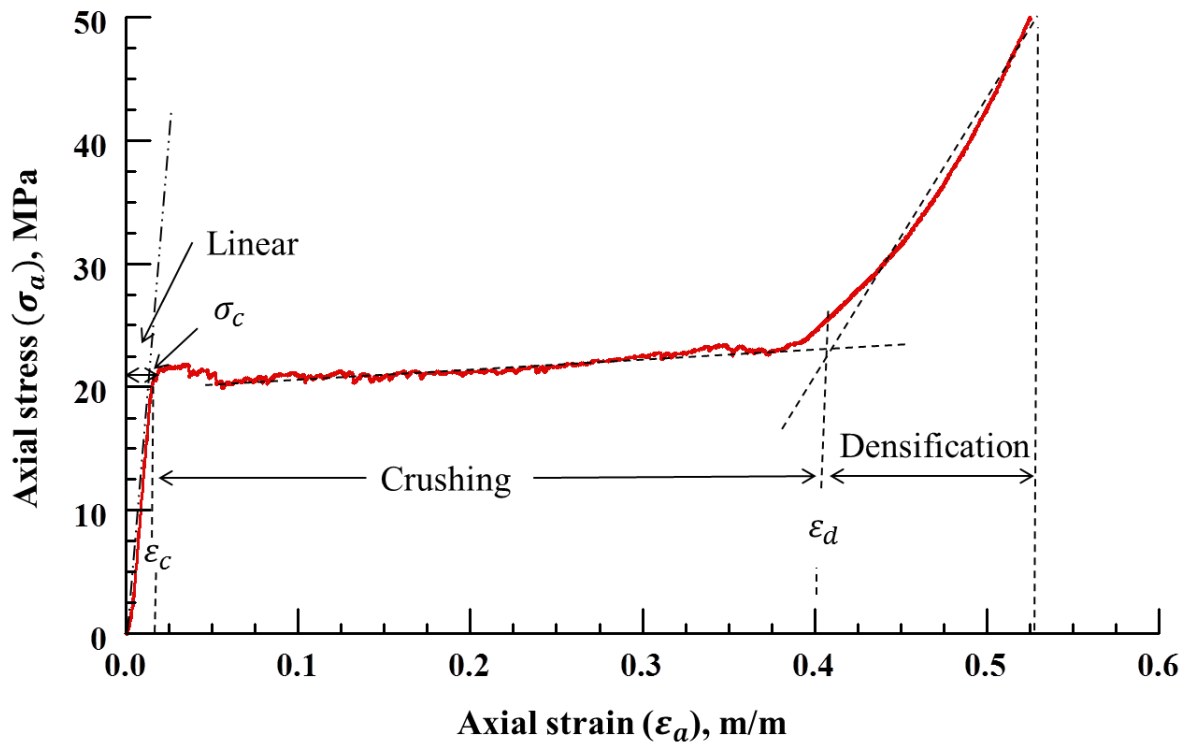


Figure 3.4. Mean stress-strain response of five Eco-Core specimens with aluminum sleeve.

The largest Hoop strain ( $\varepsilon_{\theta}$ ) from the three strain gauges on the sleeve was selected. The mean value of largest Hoop strains of the five sleeves was calculated and plotted against the axial stress in Figure 3.5. This curve has three parts: a linear, nonlinear and the 2nd linear curve. These three represent the linear elastic part, failure onset, crushing and finally densification of Eco-Core of the axial stress-strain response in Figure 3.4. As mentioned previously, the results in Figure 3.5 is average result of five test specimen.

Hoop stress ( $\sigma_{\theta}$ ) of the aluminum sleeve was calculated from Hoop strain ( $\varepsilon_{\theta}$ ) and the aluminum elastic modulus (see Table 3.1). Calculated Hoop stress versus axial stress response is similar to Hoop strain versus axial stress in Figure 3.5, and it is shown in Figure 3.6. The corresponding confinement stress ( $q$ ) acting on the Eco-Core specimen was calculated by Eq. 3.1 and plotted in Figure 3.7 as  $q$  versus  $\sigma_a$ .

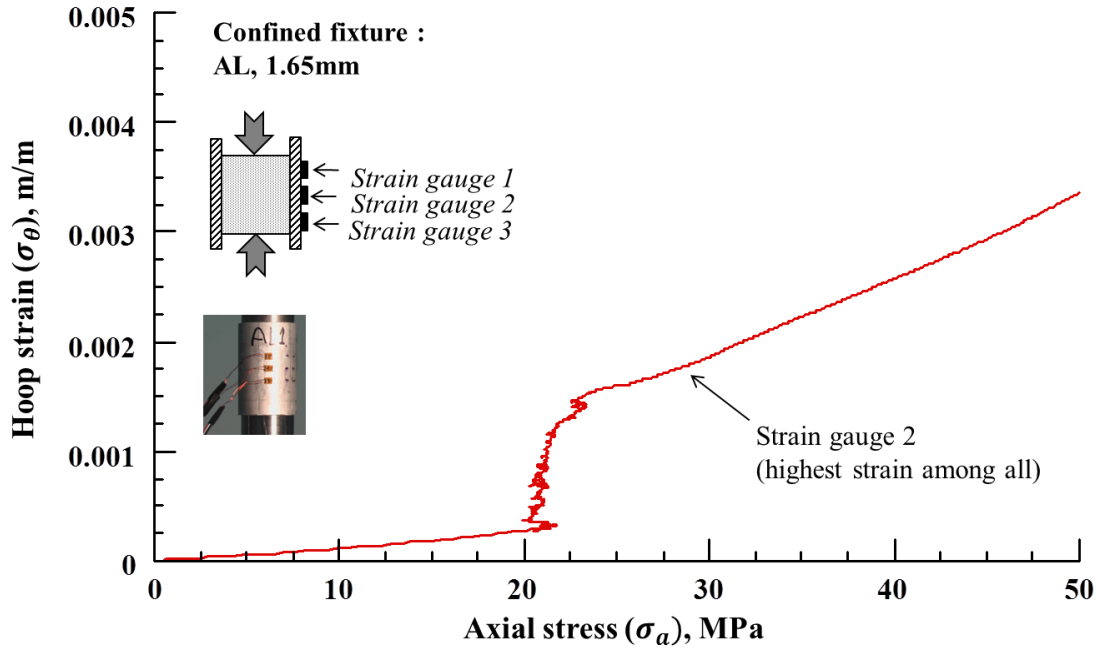


Figure 3.5. Mean Hoop strain versus axial stress of Eco-Core with aluminum sleeve confinement.

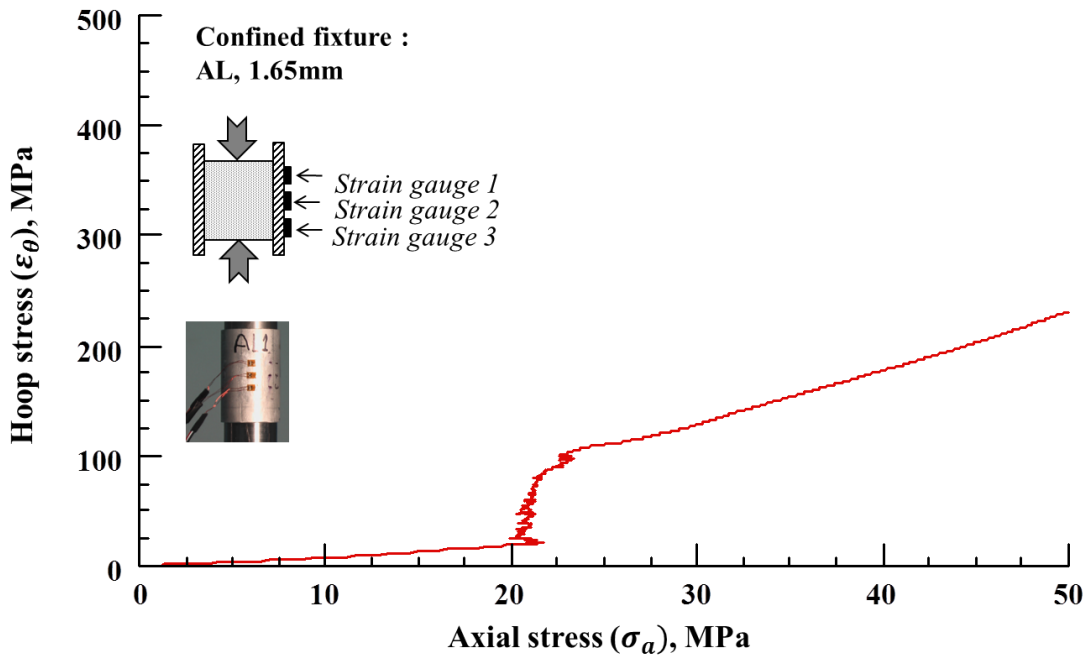


Figure 3.6. Hoop stress versus axial stress of Eco-Core with aluminum sleeve confinement.

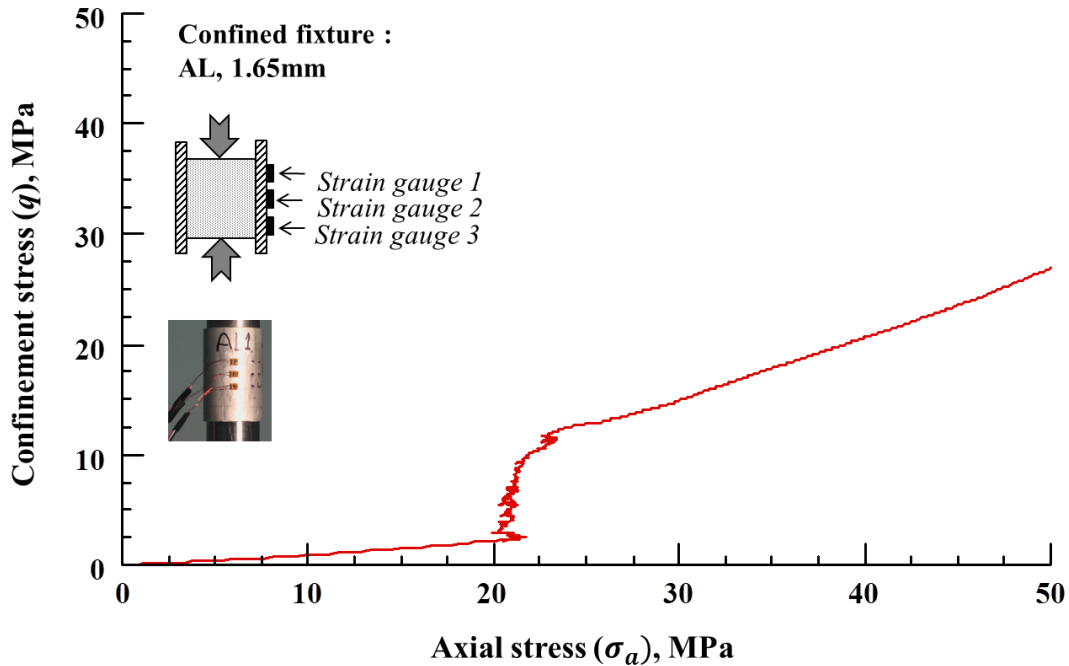


Figure 3.7. Confinement stress versus axial stress of Eco-Core with aluminum sleeve confinement.

**3.3.2 Rubber sleeve.** The thin rubber sleeve of 0.13 mm thickness is barely strong enough to hold the material together all through the test. It was used to represent the unconfined stress-strain response. The axial stress-strain responses for the five specimens of Eco-Core with rubber sleeve were measured and compared to each other's in Figure 3.8. The comparison indicated repeatability of results. The mean value of the five tests was calculated and plotted in Figure 3.9. The curve has three parts as well: linear part identical to that of aluminum sleeve, a concave part that is different from aluminum sleeve (concave stress about 50% of plateau) due to bulging of the material (see Figure 3.9) and then densification curve. The densification strain ( $\varepsilon_d$ ) in this case is extended to about  $\varepsilon_d \approx 0.75$ . No Hoop strain measurement was conducted with this type of confinement due to the difficulty of mounting strain gauges on rubber sleeve and due to the large strains as well.

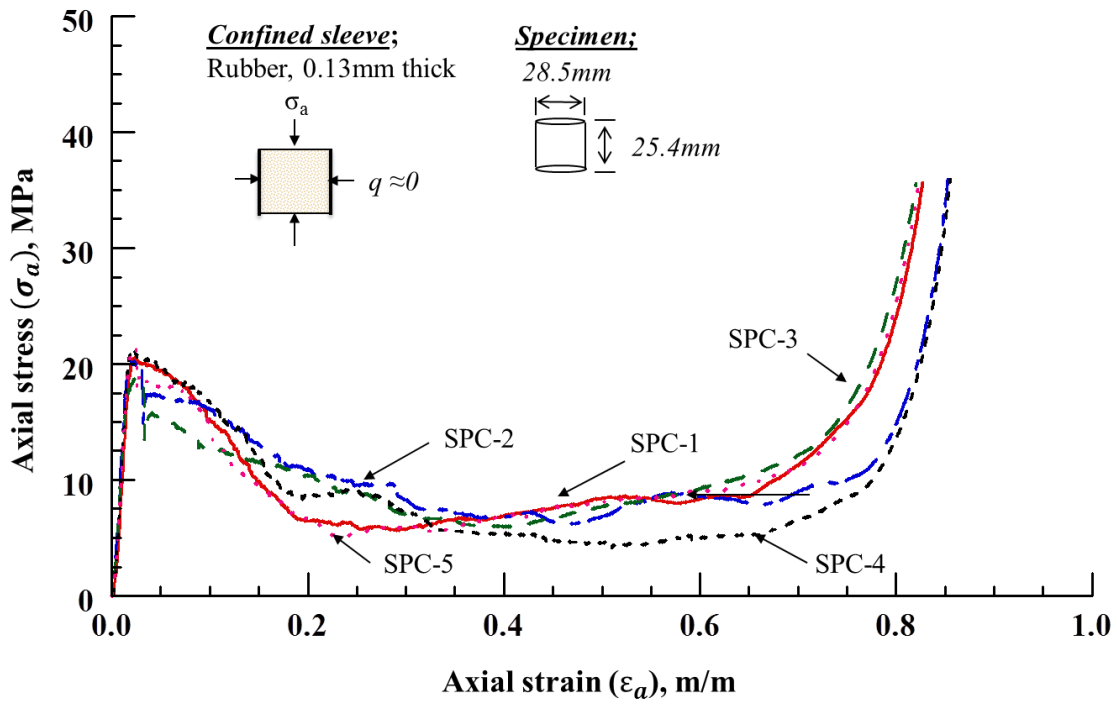


Figure 3.8. Axial stress-strain response for five specimens with rubber confinement.

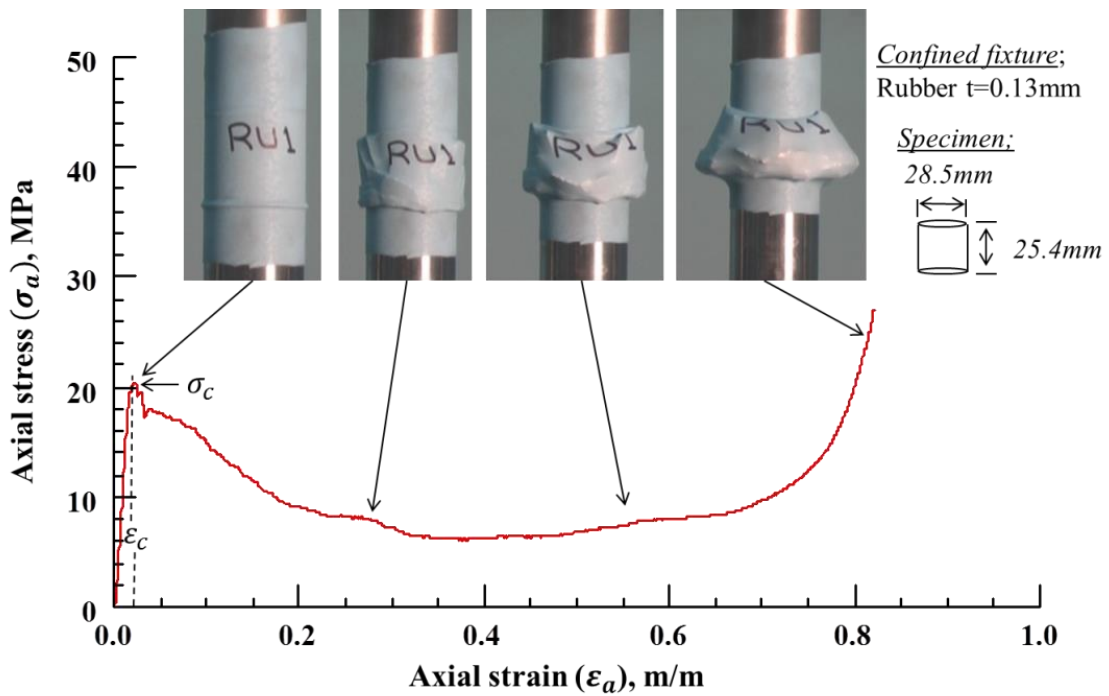


Figure 3.9. Mean stress-strain response of Eco-Core with thin rubber sleeve confinement.

**3.3.3 Effect of sleeve type.** In addition to the aluminum and rubber sleeves, Eco-Core was tested under the confinement of other types of sleeves to check the effect of different confinement. Acrylic sleeve of 5.00 mm thickness, copper sleeve of 1.65 mm thickness and steel sleeve of 1.65 mm thickness were used. Also five specimens were tested with each type of sleeves. Figures 3.10, 3.11 and 3.12 show the response of the five specimens with acrylic, copper and steel sleeves, respectively. The last three figures indicate good repeatability for the results in all three cases.

Axial stress ( $\sigma_a$ ) versus axial strain ( $\epsilon_a$ ) response of Eco-Core under the confinement of the five different sleeves (acrylic, aluminum, copper, steel and rubber) was determined. The different types of material and sleeve thicknesses provided different stiffness level of the sleeves ( $hE$ ). The stiffness was almost zero for rubber sleeve, whereas it is  $16.5 \times 10^6$  N/m for acrylic sleeve,  $113.9 \times 10^6$  N/m for aluminum sleeve,  $193.0 \times 10^6$  N/m for copper sleeve and  $330.0 \times 10^6$  N/m for steel sleeve.

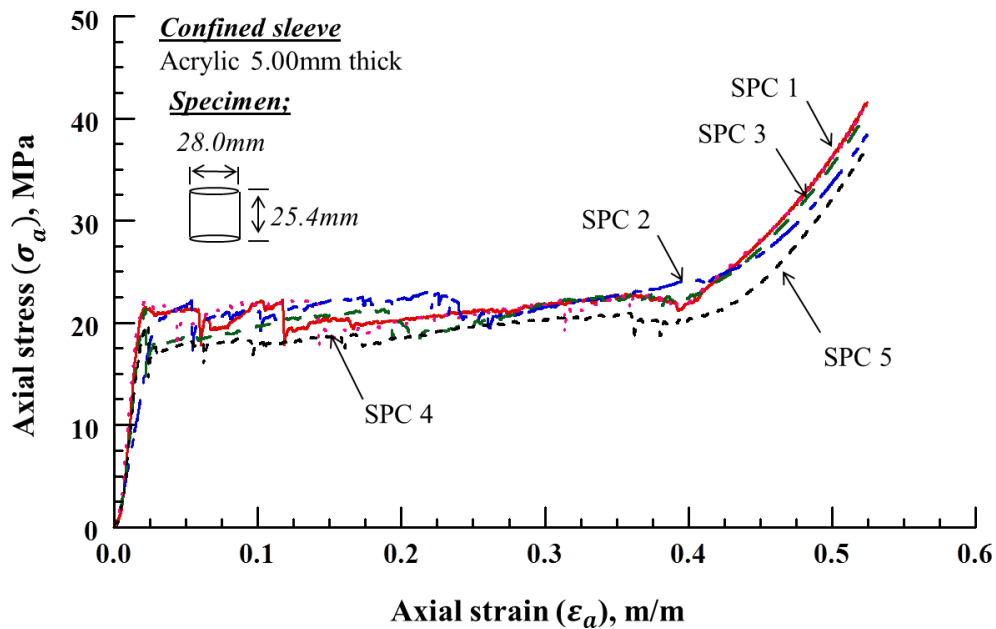


Figure 3.10. Axial stress-strain response for five specimens with acrylic sleeve.

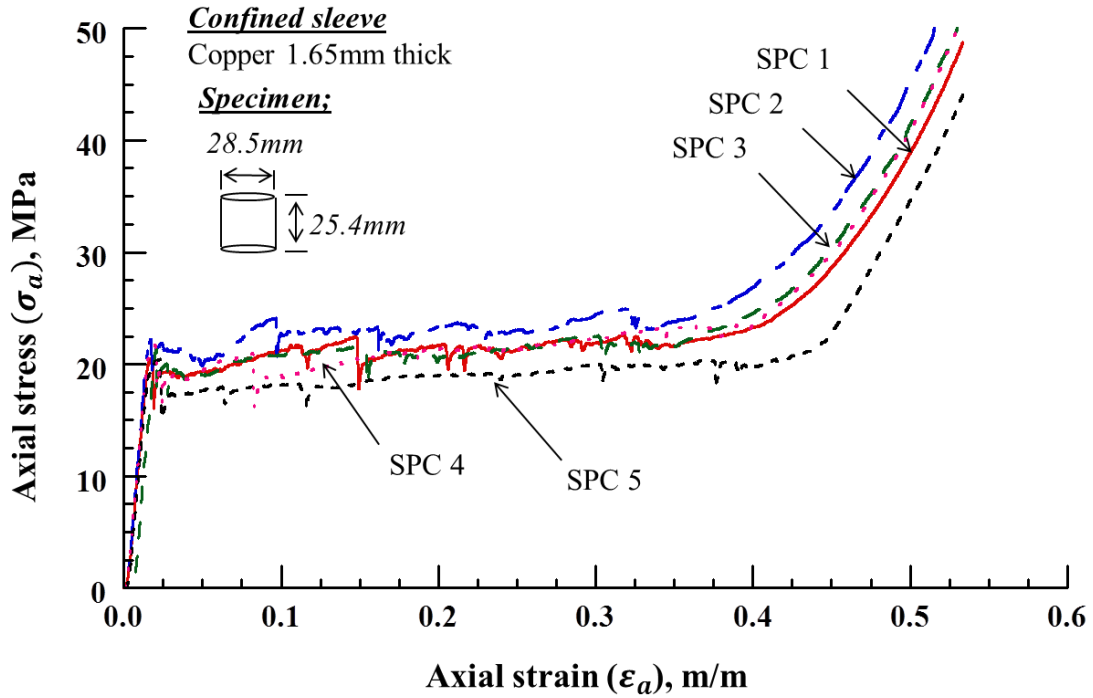


Figure 3.11. Axial stress-strain response for five specimens with copper sleeve.

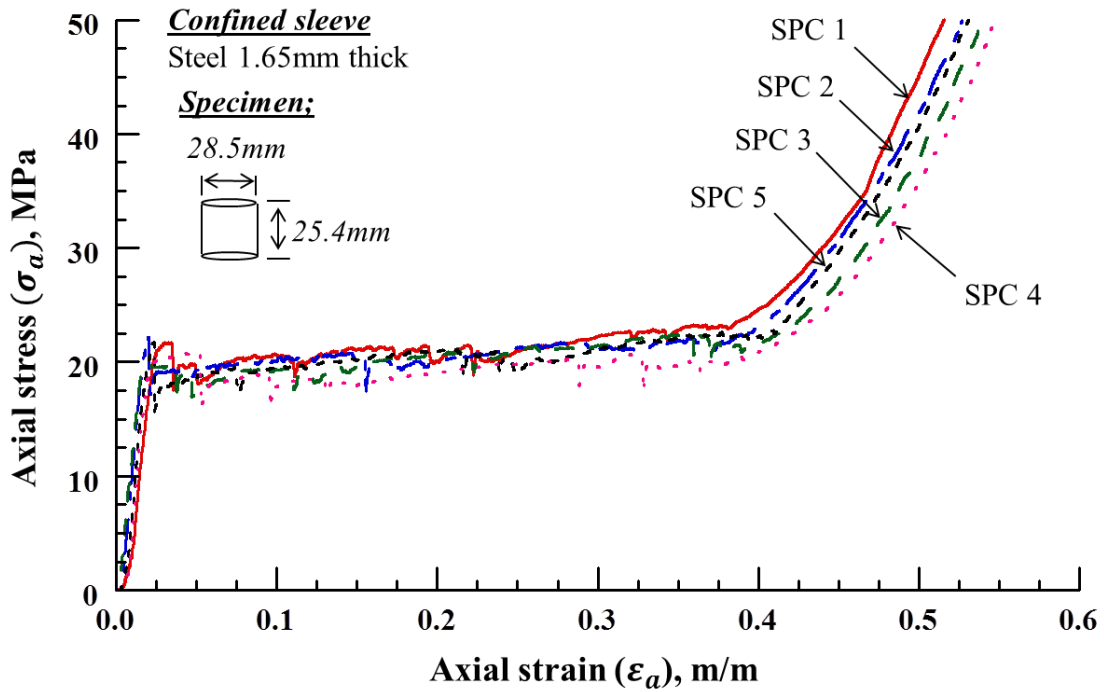


Figure 3.12. Axial stress-strain response for five specimens with steel sleeve.

The average value of axial stress responses under each sleeve type was calculated. The means of the axial stress-strain responses under different sleeves were plotted together as shown in Figure 3.13. Also, average Hoop strains versus axial stress for all sleeve types were plotted together as shown in Figure 3.14. Hoop stresses were calculated from Hoop strains and plotted versus axial stress as shown in Figure 3.15. Note the confinement stress response of all metallic sleeves collapsed as a single curve. However, the acrylic sleeve responded differently because of the violation to the thin walled cylinder theory ( $d/h \geq 10$ ). The confinement stresses of the metallic sleeves were all plotted versus axial stresses as shown in Figure 3.16. The last figure showed that the confinement stress was independent of sleeve type or sleeve stiffness ( $hE$ ).

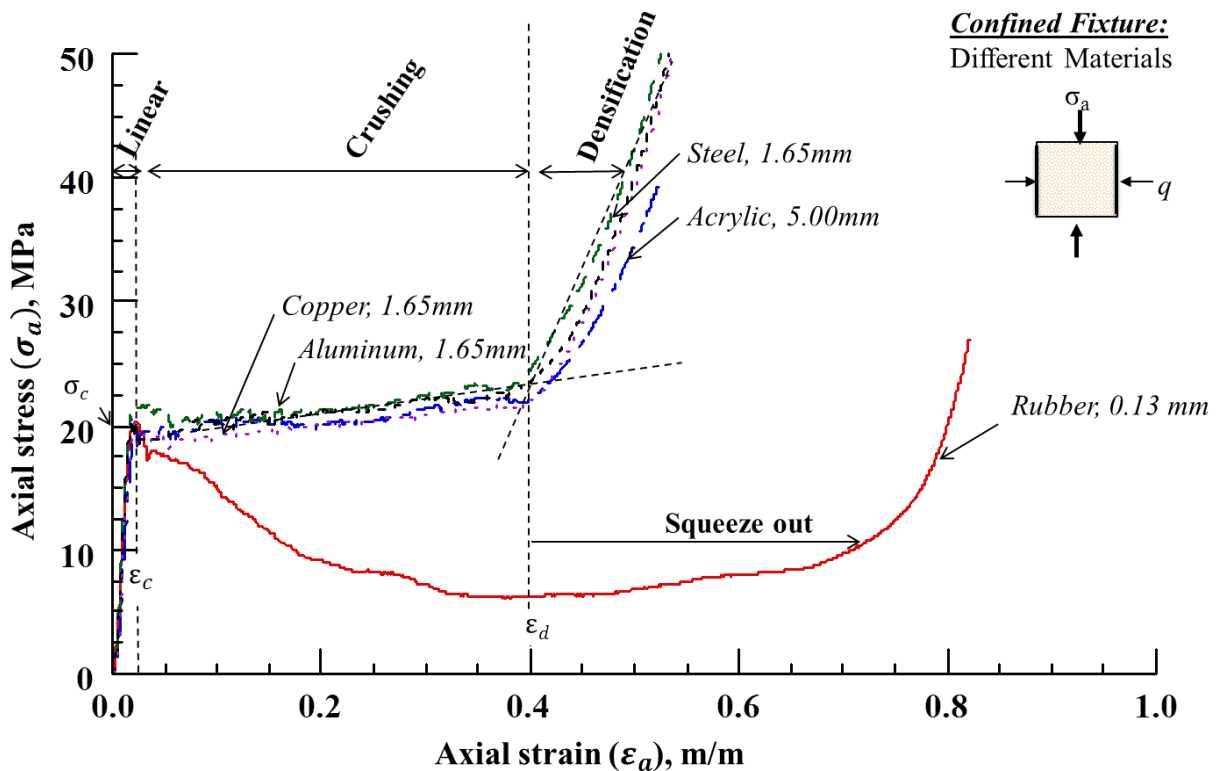


Figure 3.13. Stress-strain response of Eco-Core under different types of sleeve confinement.

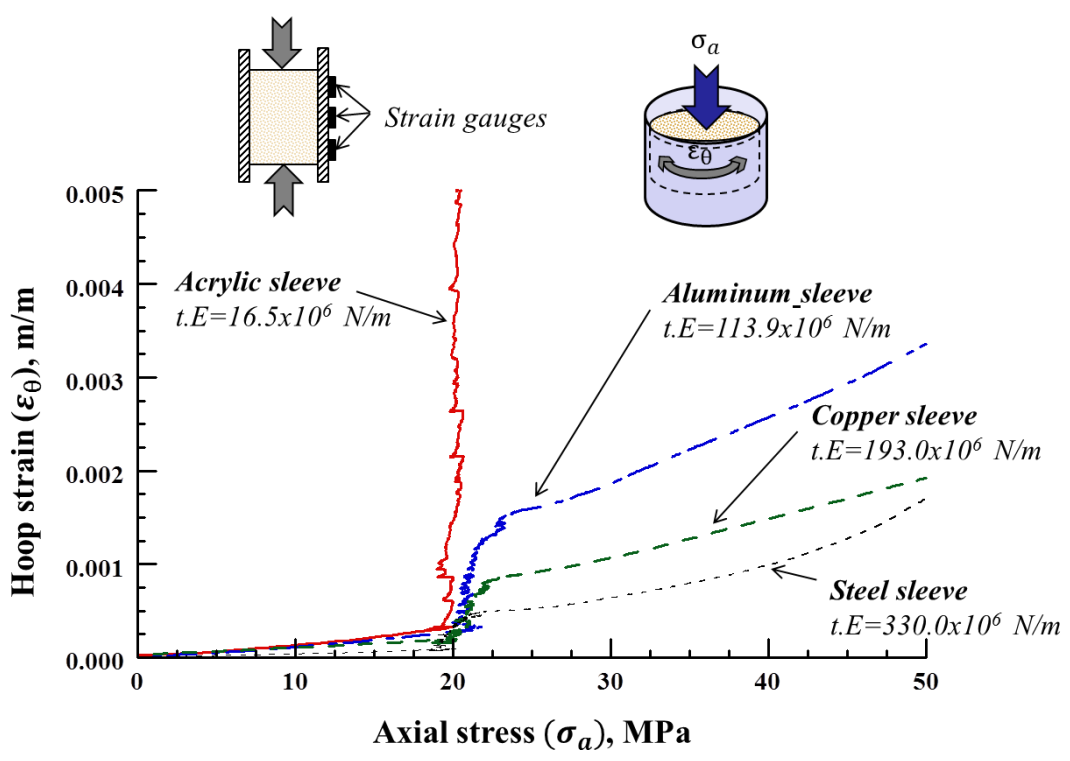


Figure 3.14. Mean Hoop strain of different sleeves versus axial stress of Eco-Core.

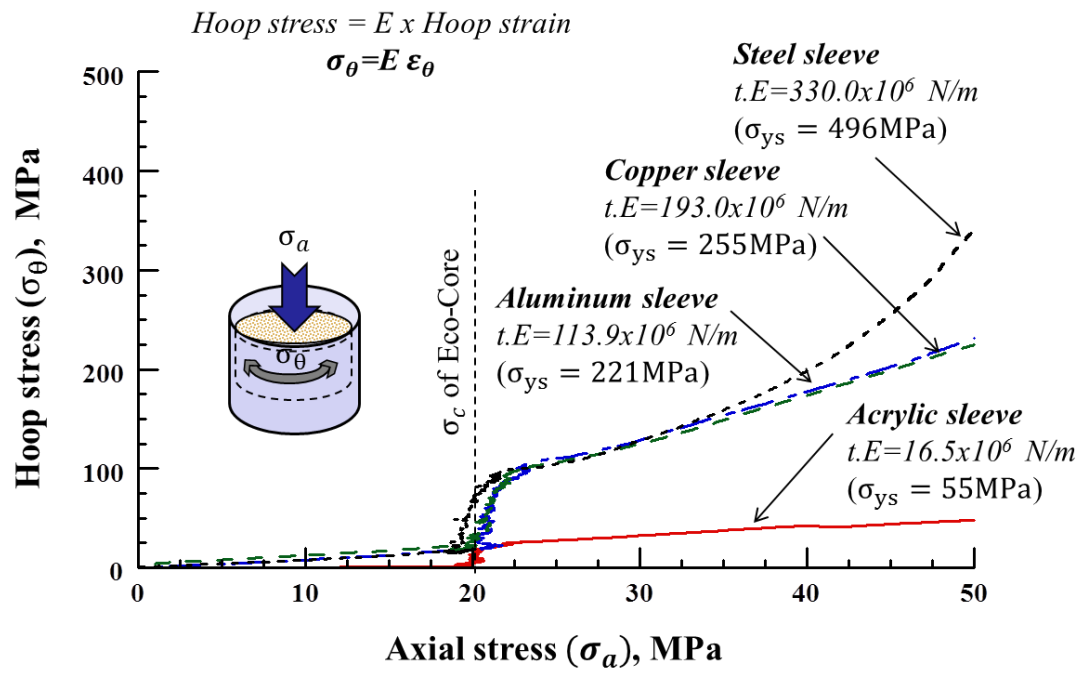


Figure 3.15. Hoop stress of different sleeves versus axial stress of Eco-Core.

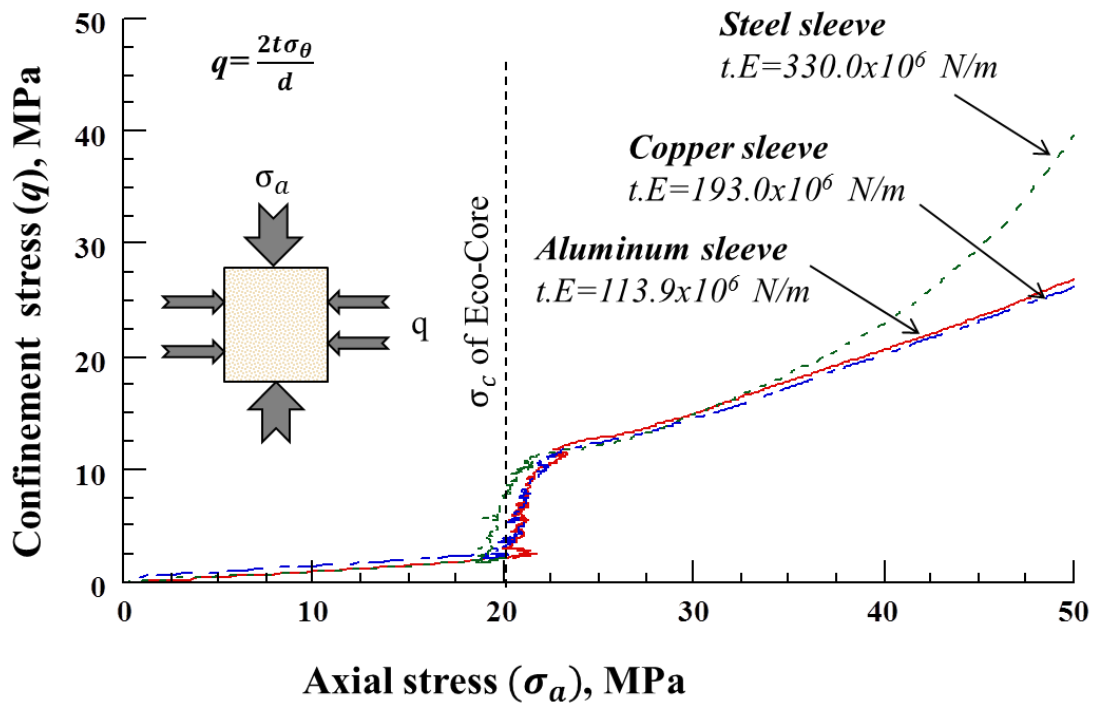


Figure 3.16. Confinement stress versus axial stress of Eco-Core under different sleeves confinement.

### 3.4 Development of Static Constitutive Equation

The stress state acting on confined test specimen is shown in Figure 3.17a. This includes axial stress ( $\sigma_a$ ), radial compressive stress ( $q$ ) and the friction shear between the specimen and the sleeve ( $\tau_\mu$ ). To derive a constitutive equation, the following assumptions were made:

- The friction shear between the specimen and the sleeve ( $\tau_\mu$ ) is replaced by an equivalent axial frictional stress ( $\sigma_\mu$ ).
- Then the principal axial stress is  $\sigma_a - \sigma_\mu$ .
- The axisymmetric principal lateral stress is  $q$ .

From these assumptions, an effective net-deviatoric stress-strain relation was derived as the one that controls the failure of Eco-Core.

**3.4.1 Frictional stress ( $\sigma_\mu$ ).** In all previous studies, friction force between the specimen and the sleeve was either ignored or estimated by numerical or analytical simulation. Our experimental observations showed that friction effect is significant and must be included. Therefore, friction effect was considered in this work. Static coefficient of friction between Eco-Core and the sleeve material was measured as detailed in Appendix A. The coefficient of static friction ( $\mu$ ) for all sleeves was found to be about 0.18.

The equivalent force in the axial direction due to the shear friction between Eco-Core and sleeve was denoted by  $F_\mu$  (see Figure 3.17a). Dividing this force by the cross section area of the specimen ( $A_c = \pi d^2/4$ ) results in an equivalent friction stress in the axial direction called  $\sigma_\mu$  and it can be derived as:

$$\sigma_\mu = 4q\mu\left(\frac{l}{d}\right)(1 - \varepsilon_a) \quad (3.2)$$

Where  $\mu$  is the static coefficient of friction and  $l$  and  $d$  are the length and the diameter of the specimen, respectively. This equation accounts for axial contraction ( $\varepsilon_a$ ) of the specimen due to crushing. From the superposition of  $\sigma_\mu$  on the axial stress (Figure 3.17b), we get the principal frictional axial stress ( $\sigma_a - \sigma_\mu$ ).

**3.4.2 Net-deviatoric stress ( $\sigma_{d-\mu}$ ).** The difference between the maximum and minimum principal stresses acting on a body is called deviatoric stress ( $\sigma_d$ ).

$$\sigma_d = \sigma_1 - \sigma_3 \quad (3.3)$$

Where  $\sigma_1$  and  $\sigma_3$  are maximum and minimum principal stresses, respectively. In this case, the axial principal stress is the difference between the axial stress ( $\sigma_a$ ) and the equivalent frictional

stress in the axial direction ( $\sigma_\mu$ ), it is referred to by principal frictional axial stress ( $\sigma_a - \sigma_\mu$ ).

The asymmetric (cylindrical specimen) lateral principal stress is the hydrostatic stress ( $q$ ). The

deviatoric stress is referred to by the net-deviatoric stress ( $\sigma_{\mu-d}$ ) in this study to indicate that it

includes the frictional effects. The net-deviatoric stress is determined by using the superposition

of ( $q$ ) on the principal axial stress ( $\sigma_a - \sigma_\mu$ ) of Figure 3.17b, as shown in Figure 3.17c. Similar

approach of the superposition was used for metals by Rittle, Hanina and Ravichandran [24].

Mathematically, the net-deviatoric stress ( $\sigma_{\mu-d}$ ) is derived as:

$$\sigma_{d-\mu} = \sigma_a - q \left[ 1 + 4\mu \left( \frac{l}{d} \right) \right] (1 - \varepsilon_a) \tag{3.4}$$

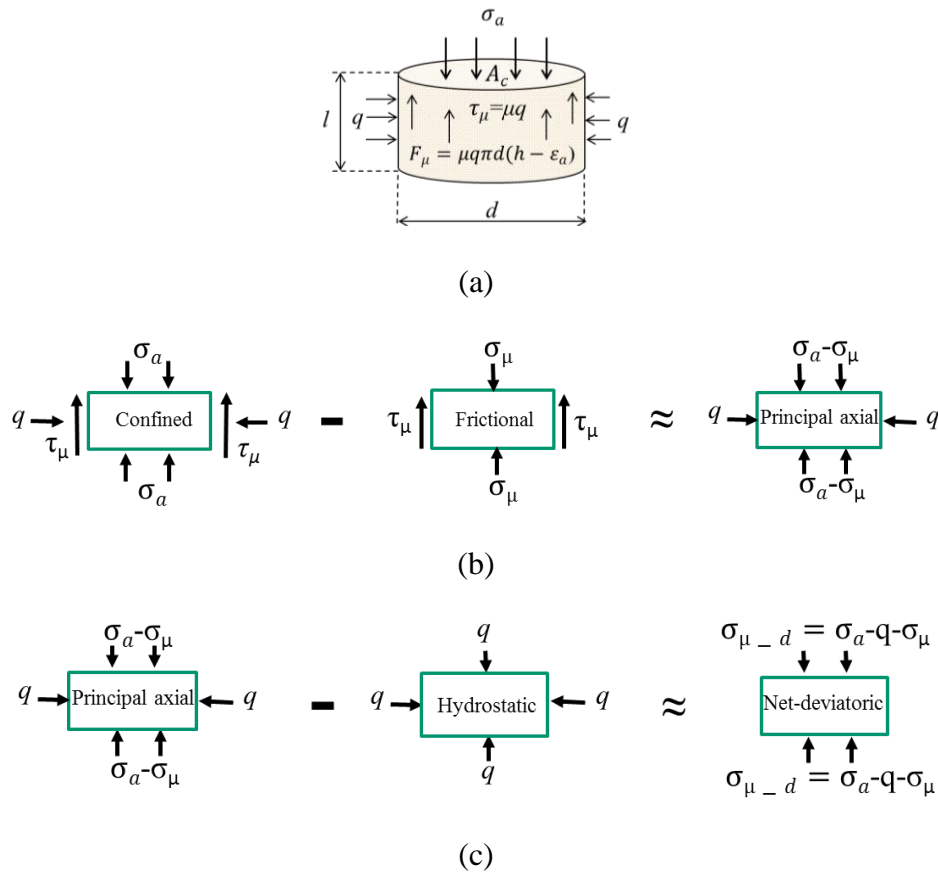


Figure 3.17. (a) Stress state on Eco-Core specimen confined by sleeve, (b) Derivation of principal axial stress, (c) Derivation of net-deviatoric stress.

The plot of  $\sigma_{\mu-d}$  versus  $\varepsilon_a$  for aluminum, copper, steel and rubber sleeves are shown in Figure 3.18. All four curves collapsed into a single curve until the Eco-Core started to densify. Therefore, the net-deviatoric stress ( $\sigma_{\mu-d}$ ) versus axial strain ( $\varepsilon_a$ ) is considered to be unique and that controls the failure response of Eco-Core until reaches or near solid state. Once it reaches the solid state, Eco-Core follows the Gibson and Ashby's model [21].

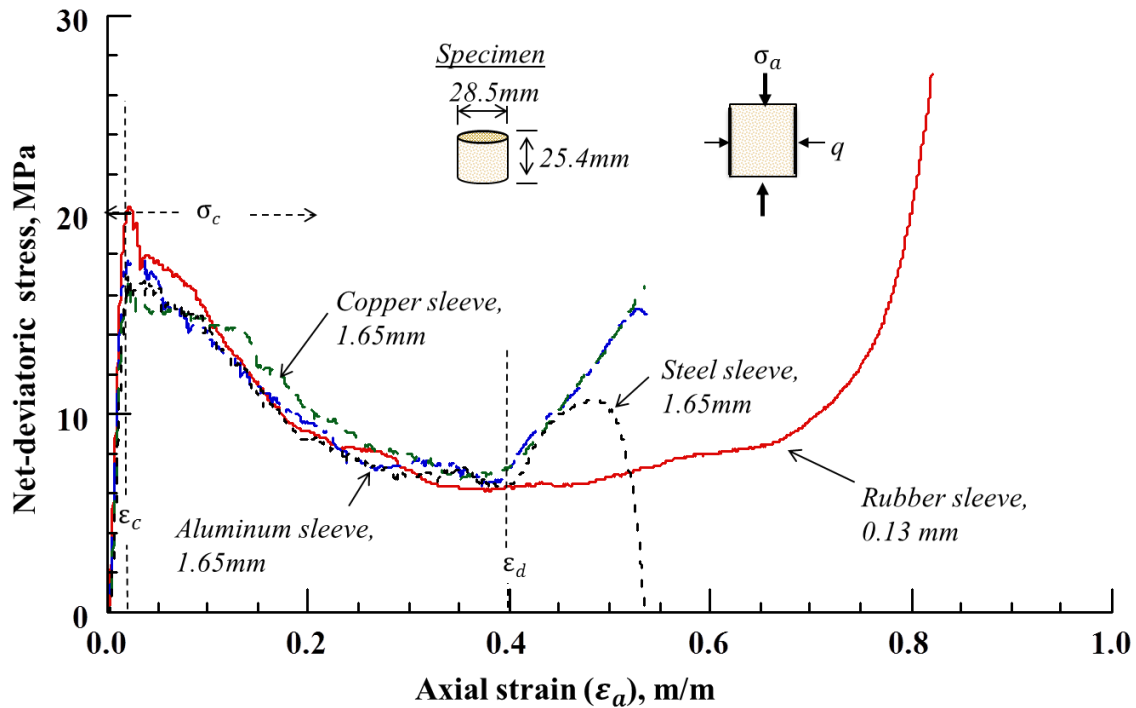


Figure 3.18. Net-deviatoric stress of Eco-Core under different types of sleeve confinement.

**3.4.3 Development of constitutive equation.** The net-deviatoric stress-axial strain response of Eco-Core under aluminum sleeve confinement was chosen to develop the constitutive equation. The normalized net-deviatoric stress ( $\sigma_{\mu-d}/\sigma_c$ ) versus axial strain ( $\varepsilon_a$ ) response from the mean experimental data was used for curve fitting. The response is divided into two regions: up to crushing strain ( $\varepsilon_c$ ) which is  $\varepsilon_c = 0.02$ , and beyond crushing strain

( $\varepsilon_a > \varepsilon_c$ ). Least Squares Curve fitting method was used to fit both parts of the response with two parts equation as:

$$\frac{\sigma_{d-\mu}}{\sigma_c} = \begin{cases} 50\varepsilon_a - (15\varepsilon_a)^2 & \text{for } \varepsilon_a \leq \varepsilon_c \\ 0.05(5.5\varepsilon_a)^{2.5} + 1.05e^{-5\varepsilon_a} & \text{for } \varepsilon_a > \varepsilon_c \end{cases} \quad (3.5)$$

Figure 3.19 shows the comparison of Equation 3.5 with the experimental data In terms of net-deviatoric stress.

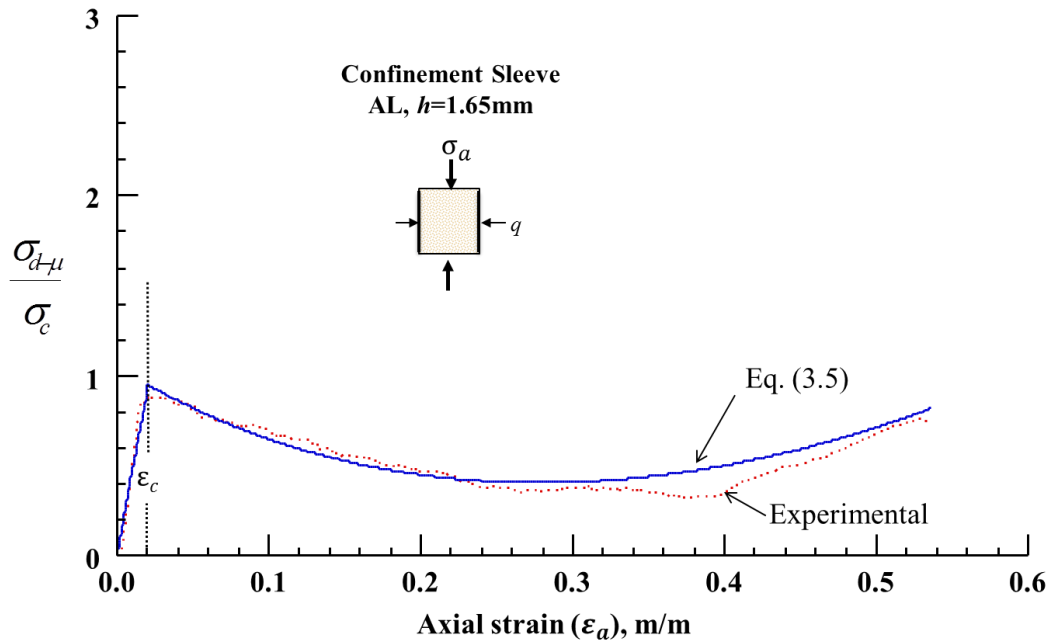


Figure 3.19. Comparison of curve fitting equation (3.5) and experiment.

Equation 3.5 is rewritten in terms of normalized axial stress and axial strain by adding the confinement and equivalent friction stresses for both sides of the equation as follows:

$$\frac{\sigma_a}{\sigma_c} = \begin{cases} 50\varepsilon_a - (15\varepsilon_a)^2 + \frac{q}{\sigma_c} \left[ 1 + 4\mu \left( \frac{h}{d} \right) (1 - \varepsilon_a) \right] & \text{for } \varepsilon_a \leq 0.02 \\ 0.05(5.5\varepsilon_a)^{2.5} + 1.05e^{-5\varepsilon_a} + \frac{q}{\sigma_c} \left[ 1 + 4\mu \left( \frac{h}{d} \right) (1 - \varepsilon_a) \right] & \text{for } \varepsilon_a > 0.02 \end{cases} \quad (3.6)$$

Equation 3.6 represents the multi-axial stress constitutive equation of Eco-Core. This equation expresses the axial stress as a function of axial strain, confinement stress and average friction effect. The response of the constitutive equation 3.6 is compared against the experimental data (axial stress versus axial strain) in Figure 3.20 for Eco-Core with aluminum sleeve confinement. The average difference between Equation 3.6 and experiment is limited to 4.1% and maximum error of 12%.

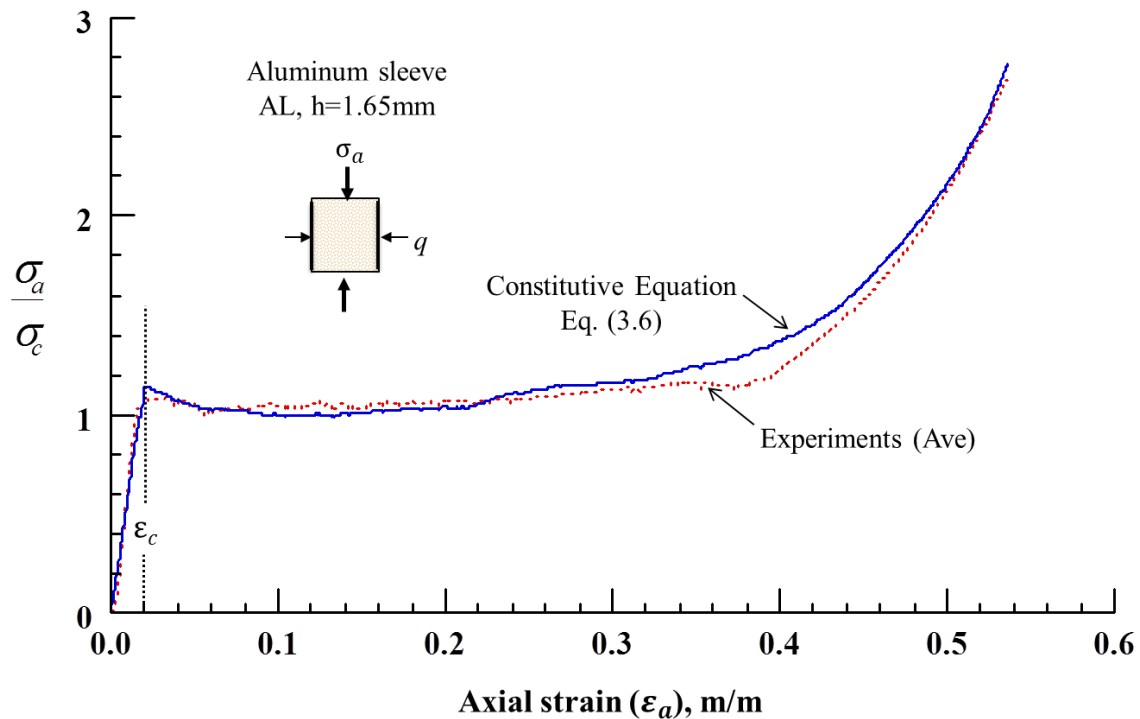


Figure 3.20. Comparison between constitutive equation and experimental data (aluminum sleeve).

The developed constitutive equation was compared with the experimental data of the two other metallic sleeves, copper and steel sleeves. Figures 3.21 and 3.22 show the comparison for the copper sleeve and steel sleeve, respectively. In both cases the average error was about 6%, the maximum error for copper sleeve was about 10% and the maximum error for steel sleeve was about 14%.

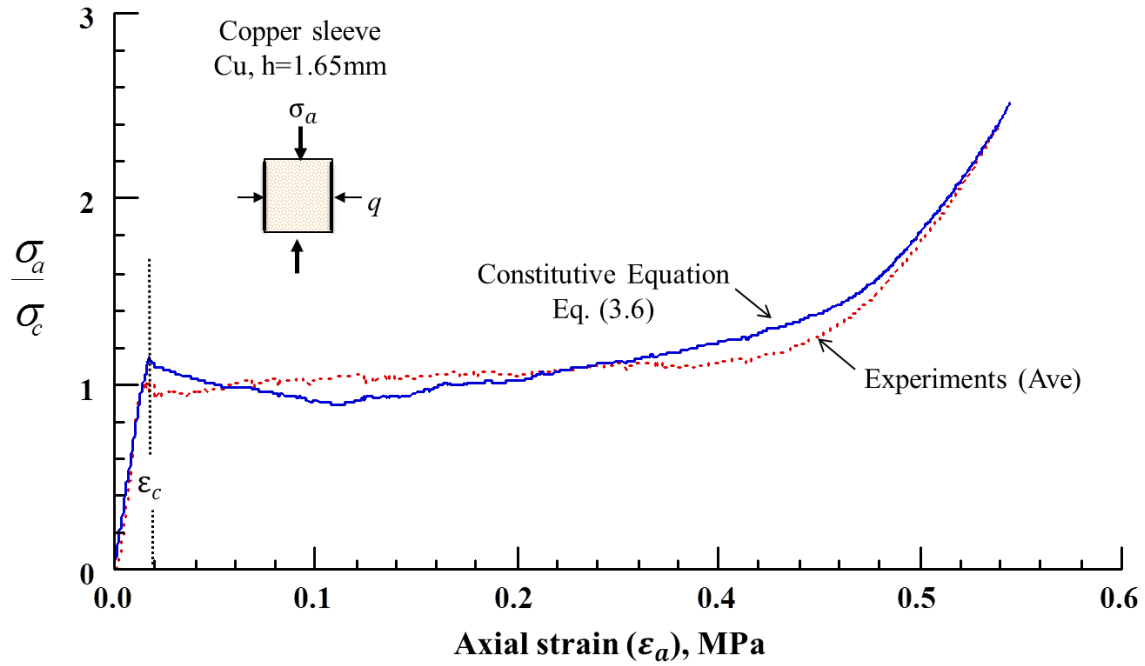


Figure 3.21. Comparison between constitutive equation and experiments (copper sleeve).

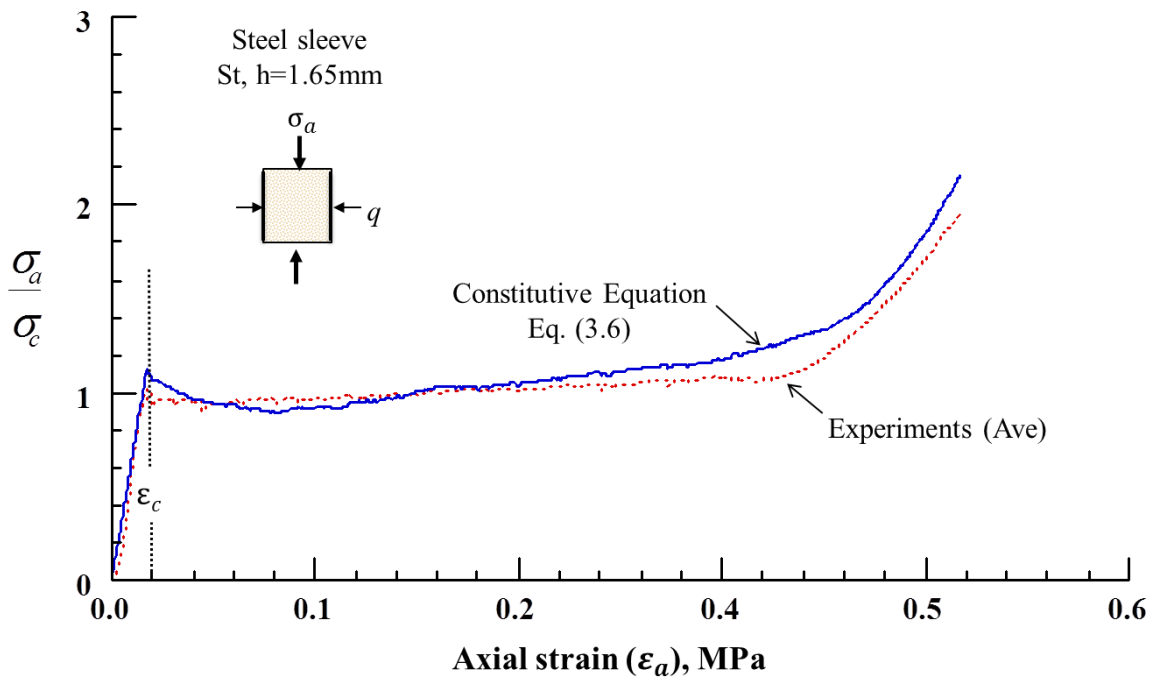


Figure 3.22. Comparison between constitutive equation and experiments (steel sleeve).

### 3.5 Summary

Static confined compression test of Eco-Core was conducted using different sleeves (acrylic, aluminum, copper, steel and rubber) to simulate different confinement stress. The confinement stress was calculated from the measured Hoop strain at the sleeve. The axial stress, radial confinement stress and the friction between the specimen and the sleeve were reduced to net-deviatoric stress (net-deviatoric stress = axial stress – friction equivalent stress – confinement stress). The net-deviatoric stress versus axial strain was found to be unique and independent of confinement stress. From these results, a general axial stress-strain constitutive equation was developed for Eco-Core under a multi-axial stress state. The equation was validated by experiment.

## CHAPTER 4

### Dynamic Confined Compression Tests

This chapter discusses the dynamic (high strain rate) confined compression study of Eco-Core material. The chapter includes development of test fixture and methodology, Split Hopkinson Pressure Bar (SHPB) high strain testing and analysis of results, also it includes the modification and validation of SHPB apparatus and design of test specimen. Based on the test results a dynamic constitutive equation was developed in this chapter.

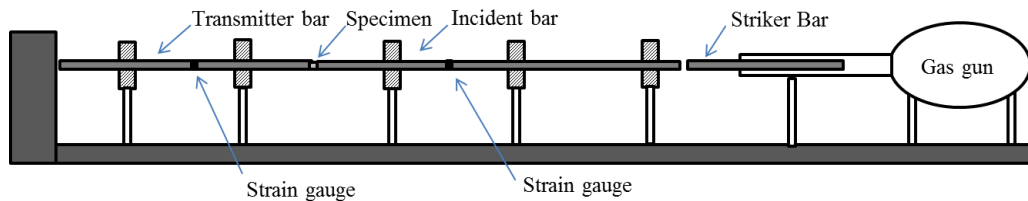
#### 4.1 High Strain Rate Testing

High strain rate test was conducted using the SHPB test apparatus and using a specially designed test fixture. The SHPB test apparatus was independently validated for solid specimens tested in literature. Then the apparatus was used to test Eco-Core using the specially designed fixture. Note that preparation of dynamic test specimens was explained in Chapter 2.

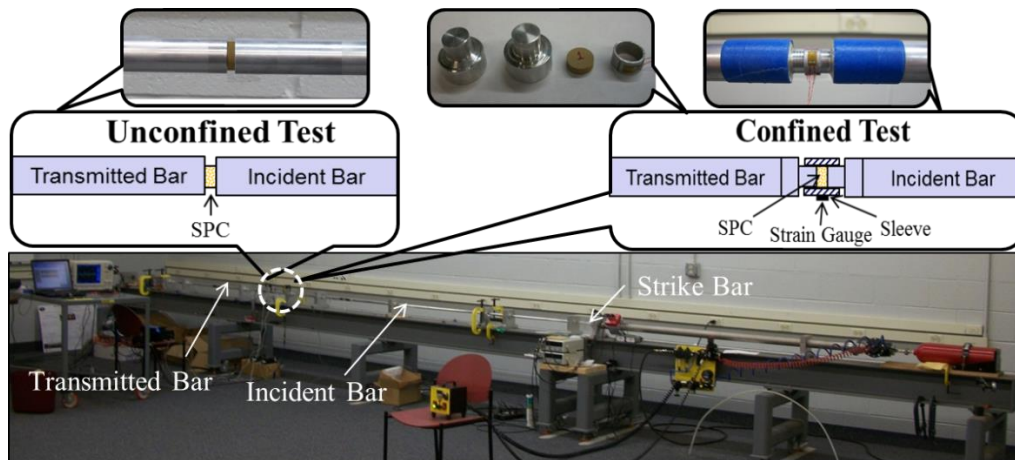
**4.1.1 SHPB test apparatus and analysis.** The Split Hopkinson Pressure Bar test apparatus is used for high strain rate testing of materials. It was designed and developed at NC A&T State University. Details of the apparatus are given in references [15, 16]. A schematic and photograph of SHPB apparatus are shown in Figures 4.1a and b, respectively. For testing with the SHPB, a cylindrical solid specimen (in this study) is sandwiched between the incident bar and the transmitter bar.

A compressive stress/strain pulse is produced by the impact of a striker bar on the impact end of the incident bar passes through the whole assembly. A one-dimensional wave propagation model of the setup is shown in Figure 4.2. The pulse propagates through the incident bar toward the specimen, which is called incident pulse,  $\varepsilon_i(t)$ . When the pulse reaches the specimen-incident bar interference, part of the pulse passes through the specimen and then into the

transmitter bar, which is called transmitted pulse,  $\varepsilon_t(t)$ . The other part of the incident pulse reflects back to the incident bar as a tensile pulse, which is called reflected pulse,  $\varepsilon_r(t)$ . The incident and reflected pulses are measured by the strain gauge installed on the incident bar at a distance of 0.9 m from the specimen-incident bar interference. The transmitted pulse is measured by a strain gauge installed on the transmitter bar at a distance of 0.9 m from the specimen-transmitter bar interference.



(a)



(b)

Figure 4.1. (a) Schematic of SHPB testing, (b) Photograph of SHPB testing.

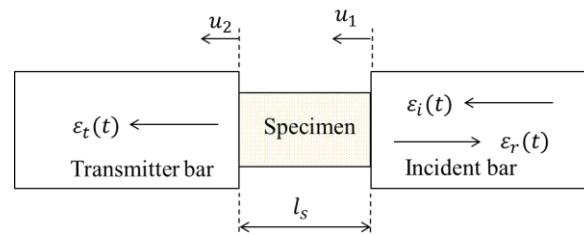


Figure 4.2. A one-dimensional strain/stress wave propagation analysis.

During the test, the specimen undergoes deformation until it reaches the dynamic limit; while the stress wave propagates through the specimen. The signals of the two strain gauges are acquired by a high speed digital oscilloscope. The waveform signal is processed by Xviewer software to get strain rate, strain and stress versus time from the reflected and transmitted pulse signals. The strain rate in the specimen is calculated from the reflected wave signal,  $\varepsilon_r(t)$  by the equation below:

$$\dot{\varepsilon}_s(t) = \frac{2c_b \varepsilon_r(t)}{l} \quad (4.1)$$

Where  $c_b$  is the speed of sound in the bars (5051m/s),  $l$  is the specimen length (3.2 mm). The strain is calculated by integrating the strain rate (Eq. 4.1) with respect to time as:

$$\varepsilon_s(t) = \frac{2c_b}{l} \int_0^t \varepsilon_r(t) dt \quad (4.2)$$

The axial stress in the specimen as a function of time is calculated from transmitted wave signal,  $\varepsilon_t(t)$  as:

$$\sigma_s(t) = \frac{A_b E_b}{A_s} \varepsilon_t(t) \quad (4.3)$$

Where  $A_b$  is the cross-section area of Incident/Transmitter bar (285 mm<sup>2</sup>),  $A_s$  is the cross-section area of the specimen (95 mm<sup>2</sup>) and  $E_b$  is the elastic modulus of bar material (71.7 GPa).

The stress-strain response of the specimen is obtained by Equations 4.2 and 4.3. This method of computation is given in number of text books on impact, for example [42] and in many references, for example [15, 16]. Note that the parts of SHPB could be made of different material like steel, magnesium or polymer. However, the concept and the calculations are the same and only the bars' properties are different.

**4.1.2 Calibration of strain rate versus gas gun pressure.** This section establishes the relation between the pressure of the gas gun of SHPB apparatus and specimen strain rate. Although the relation can be established through analysis, but experiment approach is found to be simpler and accurate. SHPB tests on Eco-Core specimens confined in aluminum sleeve were conducted for gas gun pressures of 55 kPa to 124 kPa (8 psi to 18 psi). Strain rate in the specimen was determined for each pressure. The resulting strain rate against pressure was found to be linear, see Figure 4.3.

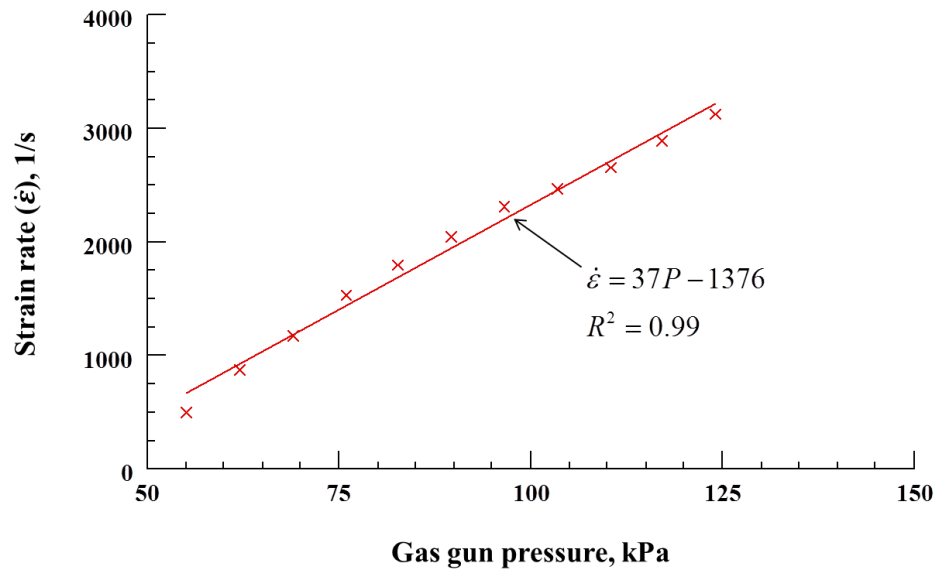


Figure 4.3. Calibration of strain rate of confined Eco-Core versus pressure of gas gun.

The data followed Eq. 4.4 below with mean square root error of 0.99.

$$\dot{\epsilon} = 37P - 1376 \quad (4.4)$$

The pressure ( $P$ ) is expressed in kPa and strain rate ( $\dot{\epsilon}$ ) in 1/s. Eq. 4.4 was used to calculate pressures for required strain rates. For planned strain rates around 500/s, 1500, 2225 and 3250/s, corresponding pressures were 55 kPa, 76 kPa, 97 kPa and 124 kPa, respectively. The same approach of calibration was used for polycarbonate and nylon 6/6 specimens of 6.35 mm

diameter and 6.35 mm length. To test polycarbonate specimen at 1200/s and nylon 6/6 specimen at 1250/s strain rates, gas gun pressures were found to be 97 kPa and 103 kPa, respectively.

**4.1.3 Validation of SHPB apparatus.** Before modifying SHPB apparatus for confined compression tests of Eco-Core, the original SHPB apparatus was validated for polycarbonate and nylon 6/6 specimens at 1200/s and 1250 strain rates, respectively. Measured responses were compared with the results of Salisbury [43] and Chou, Robertson and Rainey [44], respectively. Note that the used specimens were cylindrical shape with 6.35 mm diameter and 6.3 mm length, to match the reference results. In addition, the unconfined compression test of Eco-Core at different strain rates up to 3132/s were conducted and results were compared with references [15, 16]. Figure 4.4 Shows the axial stress-strain response of polycarbonate specimen at strain rate ranging from 1160/s to 1290/s with the results of Salisbury [23] for strain rate of 1200/s. The present results bounds Salisbury's results, four results agreed very well with each other's.

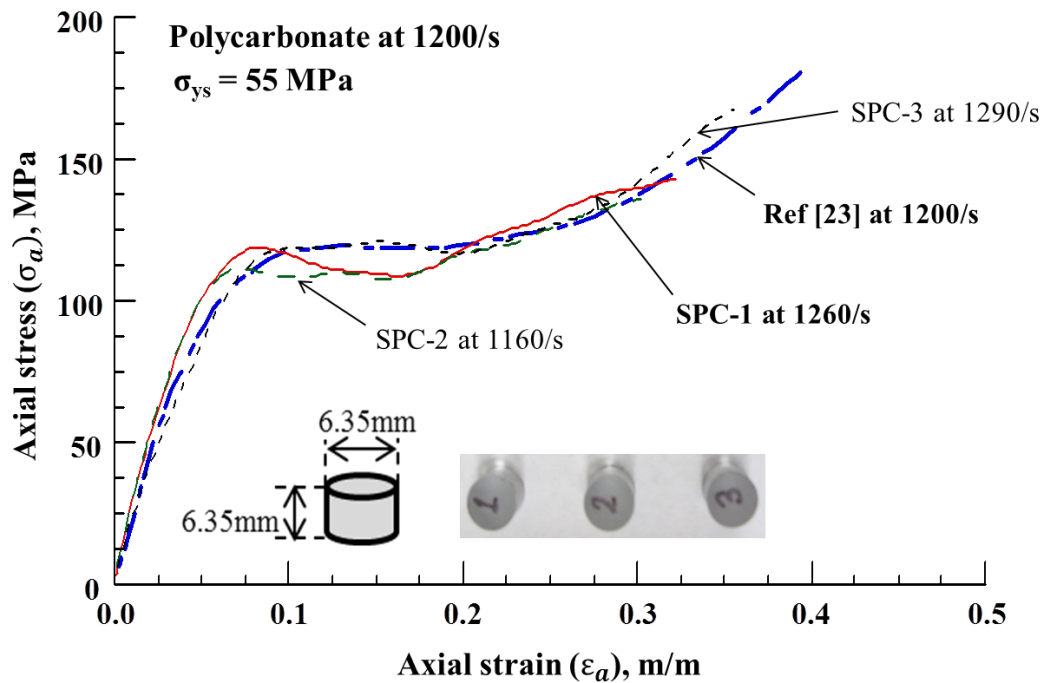


Figure 4.4. Axial stress-strain response of polycarbonate at about 1200/s strain rate.

Figure 4.5 shows the stress-strain responses of nylon 6/6 specimen. Present results are for strain rates ranged from 1157/s to 1250/s whereas; Chou, Robertson and Rainey [24] result is for 1250/s strain rate. Present results of 1157/s and 1250/s bounded and agreed well with Chou's et al result [24]. The above results validate fidelity of our SHPB test apparatus, accuracy of instrumentations and data analysis.

Repeatability of the Eco-Core testing was demonstrated by performing unconfined tests in the range of 500/s to 3132/s strain rates. Dynamic axial stress-strain response of unconfined Eco-Core is shown in Figure 4.6. Present results of six strain rates are plotted and compared with Panduranga's results [16]. The results showed a weak or no effect of strain rate on the stress-strain response of Eco-Core, which is same as that concluded by Panduranga and presented in Chapter 1 of this work as Eq 1.2. The present results for 3132/s strain rate agreed well with Panduranga's result [16] for 3150/s. Panduranga's result was produced for 12.7 mm diameter and 3.2 mm thick specimen whereas the present results were for 11 mm specimen diameter.

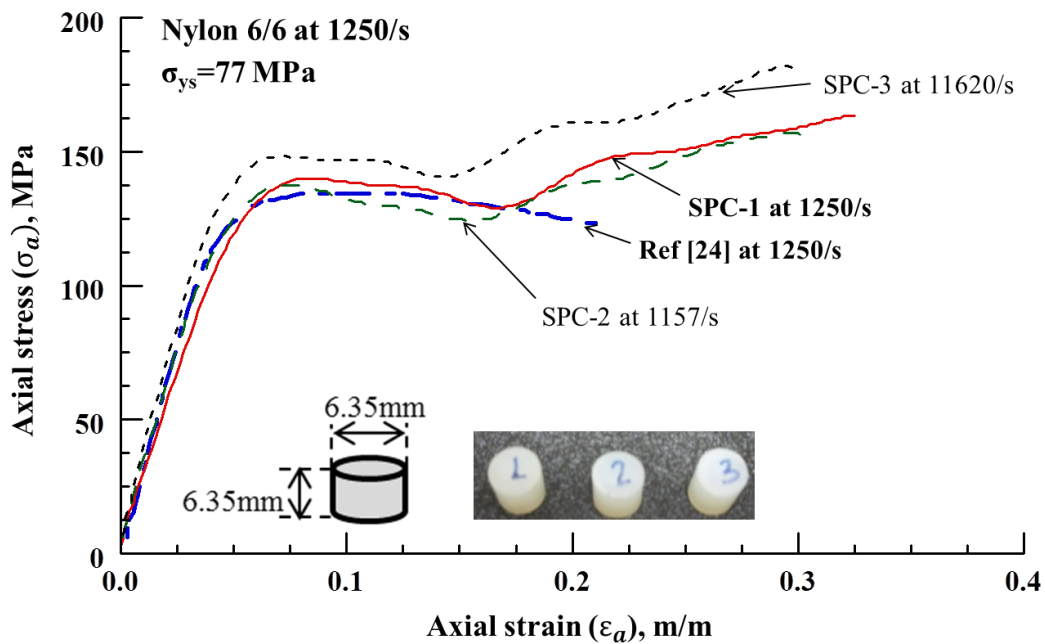


Figure 4.5. Axial stress-strain response of nylon 6/6 at about 1250/s strain rate.

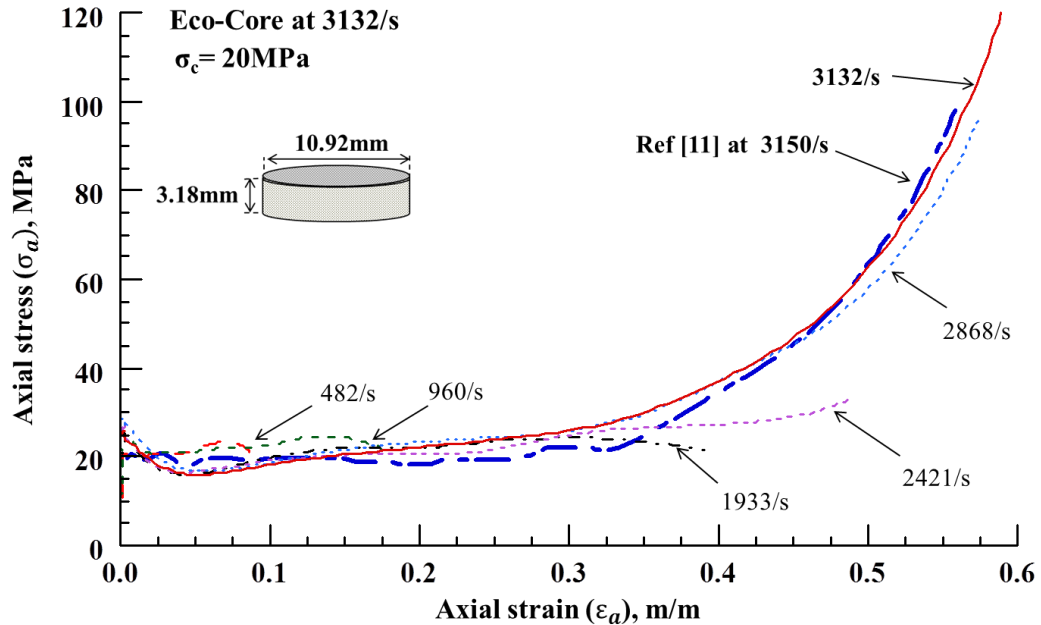


Figure 4.6. Axial stress-strain response of unconfined Eco-Core at different strain rates.

## 4.2 High Strain Rate Testing of Confined Eco-Core

High strain rate testing of Eco-Core specimen under lateral confinement consists of three major tasks as:

**4.2.1 Design of specimen.** High strain rate testing of foams under confined conditions is a challenge as there are no straight forward steps to perform such test. It is even more challenging, when the lateral confinement stress history needs to be measured. Considerable amount of trials were conducted to select sleeve material (steel, copper or aluminum) and dimensions. Among the three sleeve materials, aluminum was selected to maintain material compatibility with other parts. It had the lowest stiffness ( $h.E = 62 \times 10^6 \text{ N/m}$ ) among the three sleeves.

Many preliminary experiments were performed on different diameter sleeves and were found that  $8.4 \text{ mm} \leq d \leq 15.9 \text{ mm}$  (Based on the available standard sizes) worked very well and gave consistent results. Therefore, 11 mm diameter, 0.9 mm thickness and 6 mm long sleeve was

selected. The sleeve thickness ( $h=0.9$  mm) was chosen, so that  $h/d$  ratio matches with the one used in static confined test (Chapter 3). Accordingly, specimen diameter was determined to be 11 mm to fit the inner diameter of the sleeve within 25  $\mu\text{m}$  clearance.

To establish specimen length, number of SHPB tests were conducted for specimens of lengths ranged from 1 to 13 mm. Typical static stress-strain response of Eco-Core is shown in Figure 4.7a. It consists of linear response ( $\epsilon_c$ ), crushing response ( $\epsilon_{crush}$ ) and densification ( $\epsilon_d$ ) parts. In dynamic tests on short specimens, the linear stress-strain response ( $\epsilon_c$ ) was very difficult to measure. On the other hand, for long specimens the densification response ( $\epsilon_d$ ) was very difficult to attain as well as high strain rate values ( $\dot{\epsilon} > 3000/s$ ). The best compromising specimen length was found to be 3.2 mm to acquire all three parts of the stress-strain response (linear, crushing and densification) and to achieve high strain rate tests ( $\dot{\epsilon} > 3000/s$ ) as well. Figure 4.7b shows the strain versus specimen length for two regions (linear,  $\epsilon_c$  and densification,  $\epsilon_d$ ) of axial stress-strain response. The two curves intersect at 3.2 mm, which was chosen as the specimen length. The aspect ratio of the specimen ( $l/d$ ) is 2.9, which is within the recommended range for testing soft material [41].

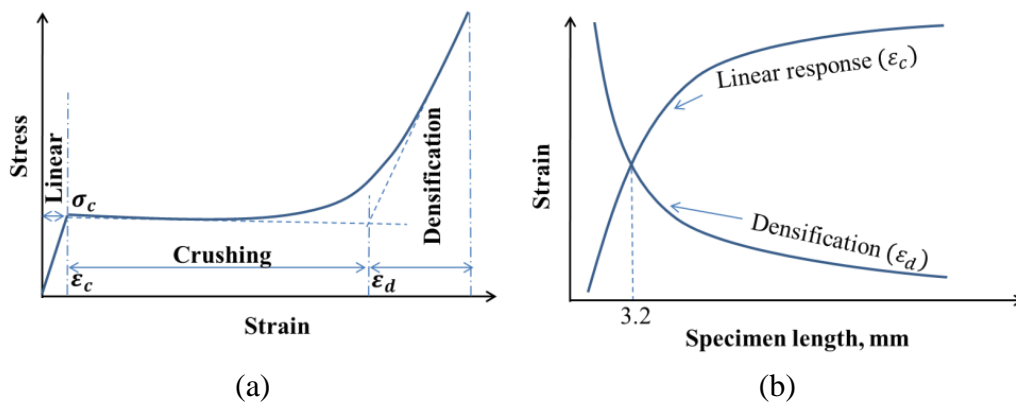


Figure 4.7. (a) Typical compression response of foam, (b) Effect of Eco-Core specimen length on response.

**4.2.2 Confined compression test fixture.** Test fixture consists of two plugs, sleeve and the strain gauge attached to the sleeve. Plugs were made of aluminum 7075/T6 to match the impedance of the SHPB bars. Figure 4.8a shows the assembled test fixture with the specimen. The left plug butts against the specimen and the transmission bar and the right plug butts against the specimen and the incident bar. Dimensions of the identical plugs are shown in Figure 4.8a. The specimen snug fits to the sleeve within  $25\mu\text{m}$  clearance and the two plugs slide into the sleeve within  $50\mu\text{m}$ . The length of the sleeve was taken to be 6 mm (as mention before) to encase the specimen and the ends of the two plugs. A small gage (1 mm size) strain gauge of 350 Ohm resistance supplied by Micro-Measurements Company was mounted on the mid-length of the sleeve to measure Hoop strain as the specimen undergoes axial compression during the test. Photograph of plugs, specimen and the sleeve are shown in Figure 4.8b.

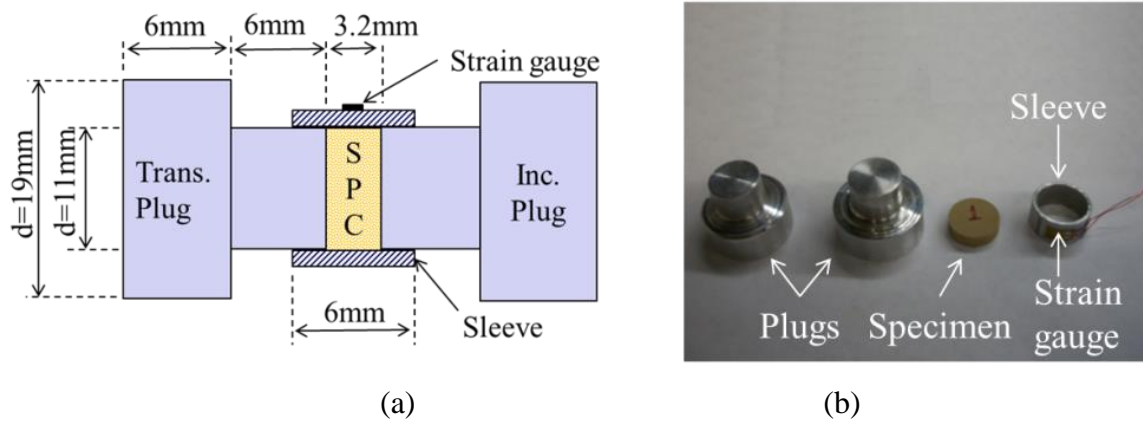


Figure 4.8. (a) Schematic of dynamic test fixture, (b) Photograph of dynamic text fixture.

**4.2.3 Testing of confined Eco-Core.** After SHPB apparatus was validated, confined compression test of Eco-Core was conducted. Specimen of  $d=11$  mm and  $l=3.2$  mm was inserted gently inside the aluminum sleeve. Specimen location was adjusted carefully to be in the mid-length of the sleeve, which is the same as strain gauge location on the outer surface of the sleeve. Arrangement is shown in Figure 4.8a. The whole fixture was placed in between the incident and

transmitter bars. The center of the incident plug was aligned to the center line of the incident bar and they were taped together without leaving any gap between them. The same process was repeated on the transmitter side of the specimen.

The strain gauge of the sleeve was connected to the same oscilloscope that the incident and transmitter strain gauges were connected to. The gas gun of the apparatus was charged to the desired pressure (55 kPa, 76 kPa, 97 kPa and 124 kPa). The trigger of the oscilloscope was turned on standby position. Then the system was fired, the striker bar impacts the incident bar. The stress wave was generated at the impact site, traveled along the incident bar, specimen and then to the transmitter bar. The data acquisition system acquired the strain gauge signals from the incident and transmitter bars and the sleeve (Hoop strain) at a rate of 0.5 MHz. The original waveform signals were filtered to reduce the noise using the Xviewer software. The signals were saved and reduced to strain rate, axial strain and axial stress, using Equations 4.1, 4.2 and 4.3. The parameters used in calculations were:  $A_b = 285 \text{ mm}^2$ ,  $A_s = 95 \text{ mm}^2$ ,  $E_b = 71.7 \text{ GPa}$ ,  $c_b = 5051 \text{ m/s}$  and  $l = 3.2 \text{ mm}$

From the acquired Hoop strain data of the sleeve,  $\varepsilon_\theta(t)$ ; Hoop stress,  $\sigma_\theta(t)$  was calculated using Eq. 4.5.

$$\sigma_\theta(t) = E\varepsilon_\theta(t) \quad (4.5)$$

Where  $E$  is the elastic modulus of the sleeve material (69 MPa). Then the radial stress or the lateral confinement stress acting on the specimen  $q(t)$  was calculated by using Eq. 4.6.

$$q(t) = \frac{2h\sigma_\theta}{d} \quad (4.6)$$

Where  $h$  is the thickness of sleeve (0.9 mm) and  $d$  is the diameter of the specimen (11 mm). The effective friction stress between the specimen and the sleeve was expressed as an equivalent

stress in the axial direction ( $\sigma_\mu$ ) in Chapter 3 on static confined compression test of Eco-Core.

In this chapter, the equivalent friction stress,  $\sigma_\mu$  can be expressed in term of time as in Eq. 4.7.

$$\sigma_\mu(t) = 4\mu q(t) \left( \frac{l}{d} \right) (1 - \varepsilon_a(t)) \quad (4.7)$$

Where  $\mu$  is the coefficient of friction between Eco-Core and the aluminum sleeve (0.18), see Appendix A for details. The superposition of data calculated from Equations 4.1, 4.2, 4.3 and 4.7 gave the transient multi-axial stress-strain response of Eco-Core at different strain rates.

### 4.3 Test Results of Confined Eco-Core

The test results presented in two parts, typical stress-strain response of confined Eco-Core at 3120/s strain rate and results at different strain rates. The first part expresses in details the basic results of the wave form and the reduction of these results to a final stress-strain response. The second part presents the final stress-strain results for different stain rates.

**4.3.1 Typical stress-strain response.** A typical time history of strain pulse signals for dynamic confined compression test is shown in Figure 4.9. The figure shows the three strain/stress pulses of the bars (incident, transmitted and reflected pulses), in addition to the fourth pulse of the Hoop strain gauge. The duration of the incident pulse ( $T/2$ ) was about 415  $\mu\text{s}$  (1135 - 720  $\mu\text{s}$ ) and the frequency ( $f=1/T$ ) was 1.2 kHz. Calculation of pulse frequency helps to select the suitable sampling rate of the data acquisition system (Oscilloscope), which is 0.5 MHz in this present case.

Note that selecting higher sampling rate results in oscillatory data due to high frequency noise whereas lower sampling rate will result in missing important phenomenons like peak strains/stress. Figure 4.9 also shows that Hoop strain signal leads the transmitted/reflected signals by about 175  $\mu\text{s}$ . That is because Hoop strain signal was measured at the specimen location, but

the transmitted/reflected signals were measured by the transmitter/incident strain gauges at 0.9 m from the specimen location. The time of the intersection point between the transmitted and reflected pulses (1135  $\mu\text{s}$ ) was selected as a reference and Hoop strain pulse was shifted to synchronize with other pulses.

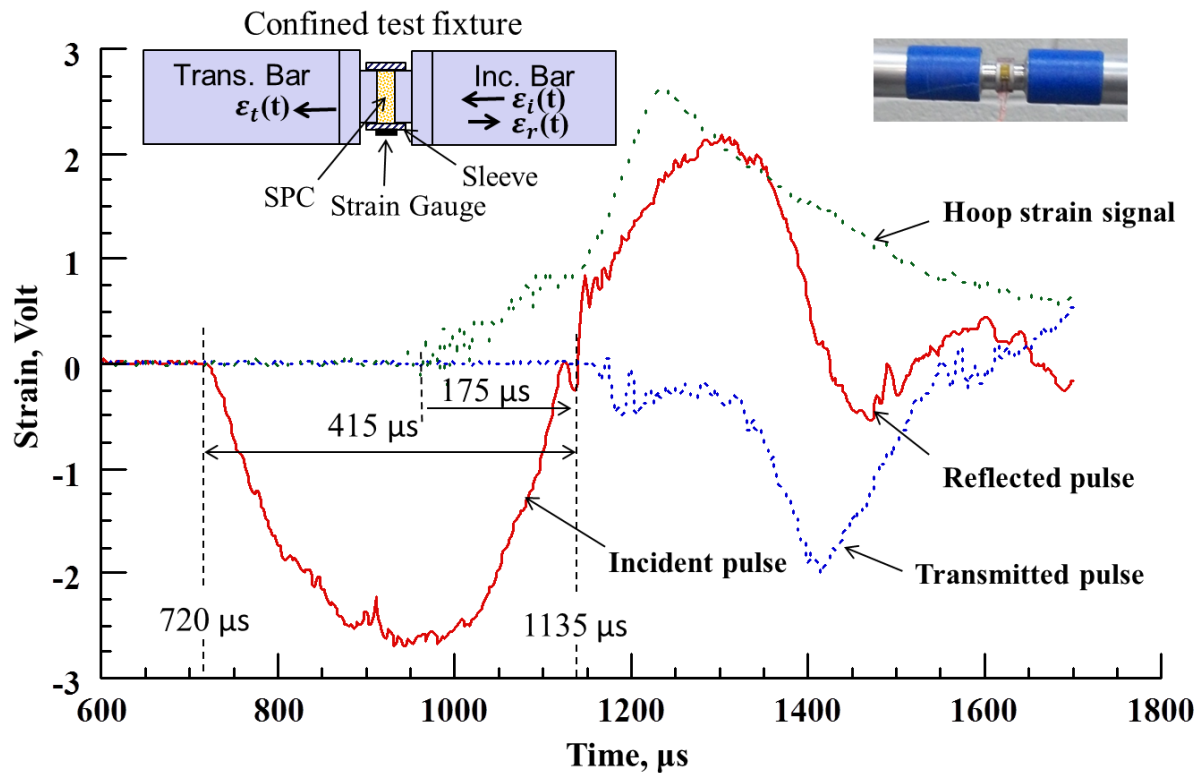


Figure 4.9. Typical time history of strain pulses of confined compression test at 3120/s.

The dynamic equilibrium of the specimen during the entire test period was verified by comparing the incident pulse to the sum of transmitted and reflected pulses. The pulses time history in Figure 4.10 shows that the two values were close to each other's. It indicates that the strains of the bars on both sides of the specimen were almost equal. Since the bars have the same area and modulus of elasticity, then the stresses on both sides of the specimen were equal as well. That verified the confined specimen was under dynamic equilibrium over the entire period of the test.

The strain rate, axial strain and axial stress results were derived from the time history of the reflected pulse,  $\varepsilon_r(t)$  and transmitted pulses,  $\varepsilon_t(t)$ . Strain rate response was calculated by Eq.4.1 and plotted versus time in Figure 4.11a. Axial strain response was calculated by Eq.4.2 and plotted versus time in Figure 4.11b. The average strain rate was calculated by the slope of the strain versus time response and was found to be about 3120/s. The axial stress response was calculated by Eq.4.3 and plotted versus time in Figure 4.11c.

The final axial stress-strain response was derived for the strain versus time response (Figure 4.11.b) and the stress versus time response (Figure 4.11c). The derived axial stress-strain response at 3120/s strain rate is plotted in Figure 4.11d. Using the same procedure and calculations the stress-strain responses of Eco-Core specimens at different strain rates were determined as explained in details in the next section.

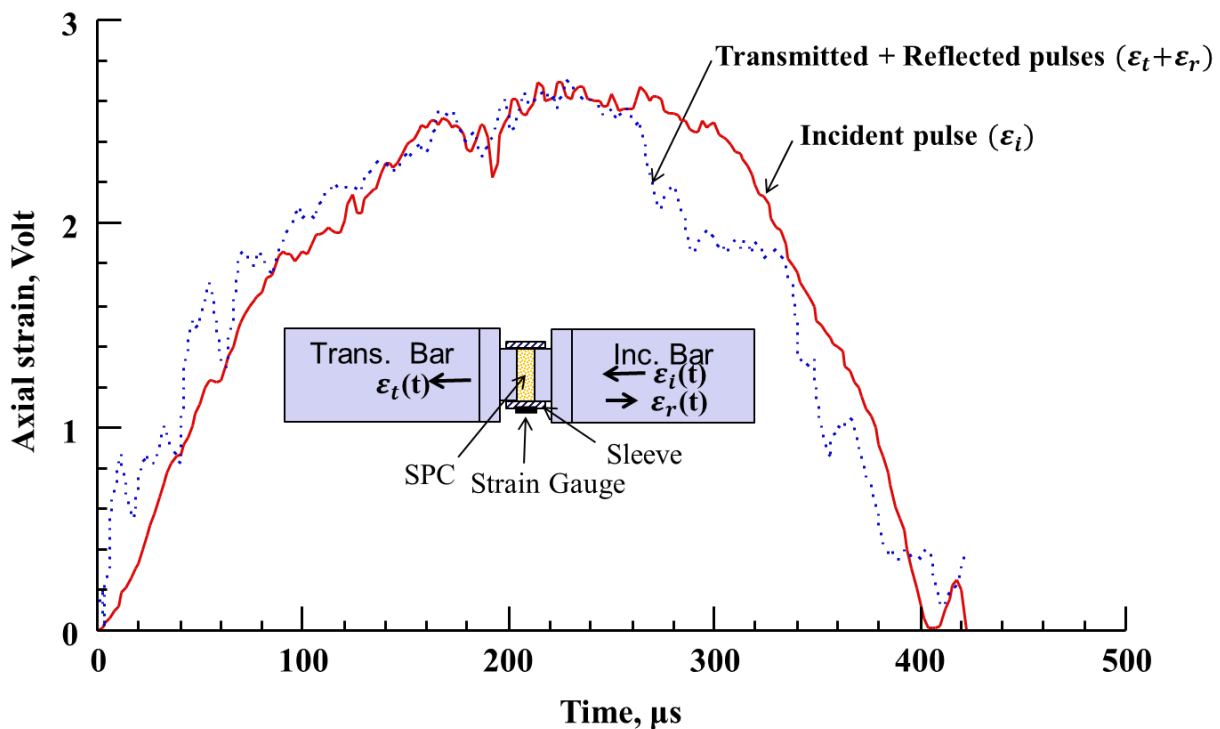


Figure 4.10. Dynamic balance response of SHPB.

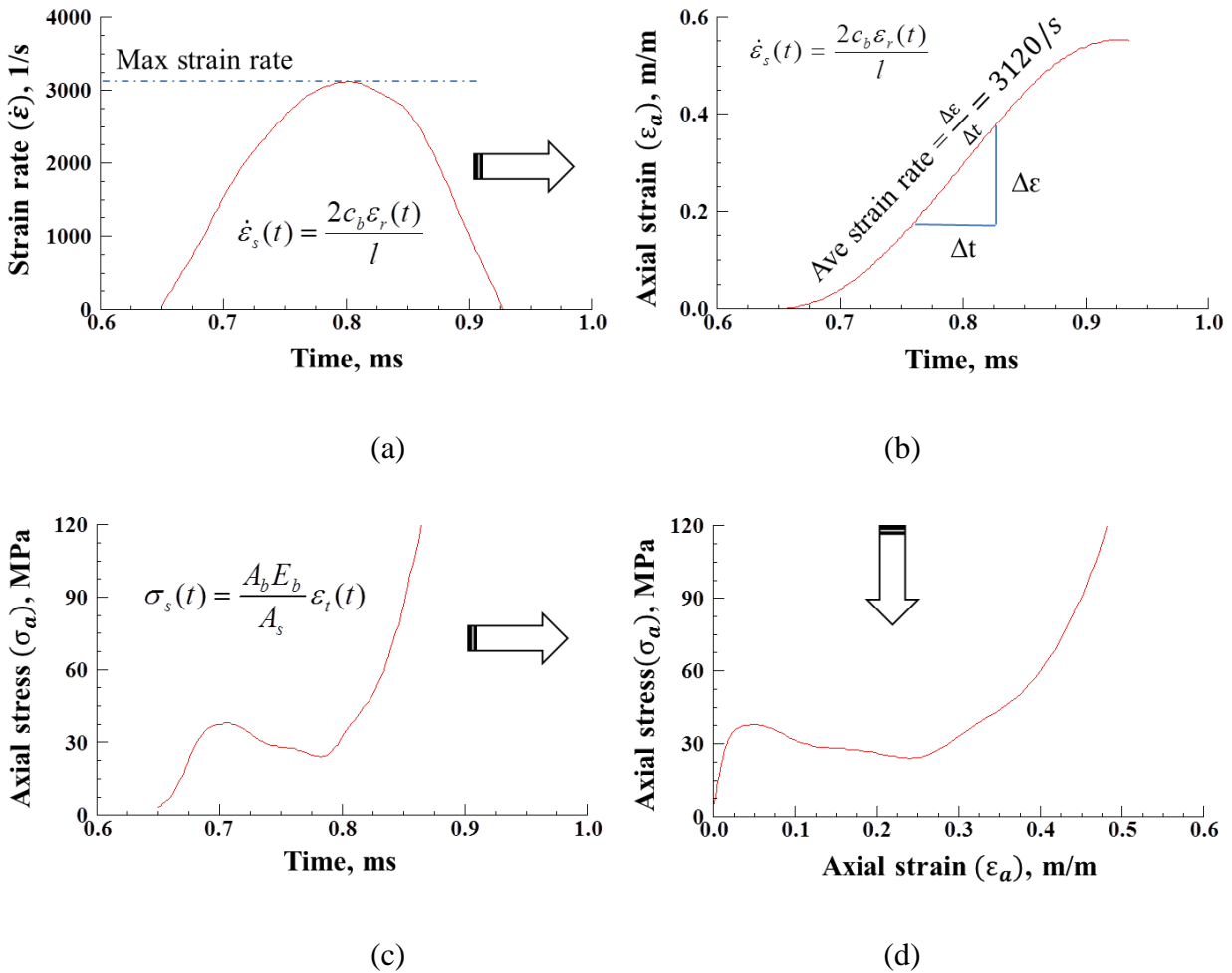


Figure 4.11. (a) strain rate versus time response, (b) axial strain versus time response, (c) Axial stress versus time response, (d) Axial stress-strain response at 3120/s strain rate.

**4.3.2 Results for different strain rates.** Test was conducted at different strain rates around 500/s, 1574/s, 2220/s and 3120/s. At each strain rate three specimens were tested. The strain rate of the three specimens of each case ranged as: 431/s to 568/s, 1474/s to 1577/s, 2208/s to 2303 and 3111/s to 3158/s, respectively. The middle curves (500/s, 1574/s, 2220/s and 3120/s) were taken to assess the strain rate effect. The axial stress-strain responses were determined, as before, and the confinement stresses were calculated from Hoop strains as in Eq. 4.7. Figures 4.12, 4.13, 4.14 and 4.15 show the responses of the three specimens at 500/s, 1574/s, 2220/s and

3120/s strain rates, respectively. The last four figures indicate good repeatability of the results at the mentioned strain rates.

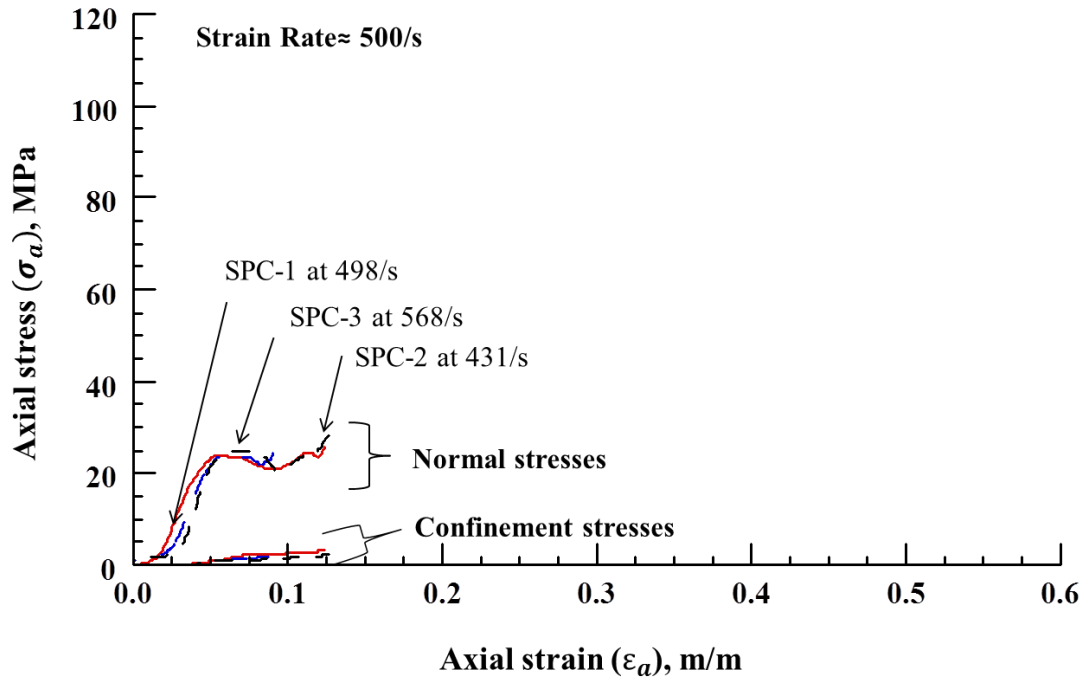


Figure 4.12. Axial and confinement stresses versus axial strain at 500/s strain rate.

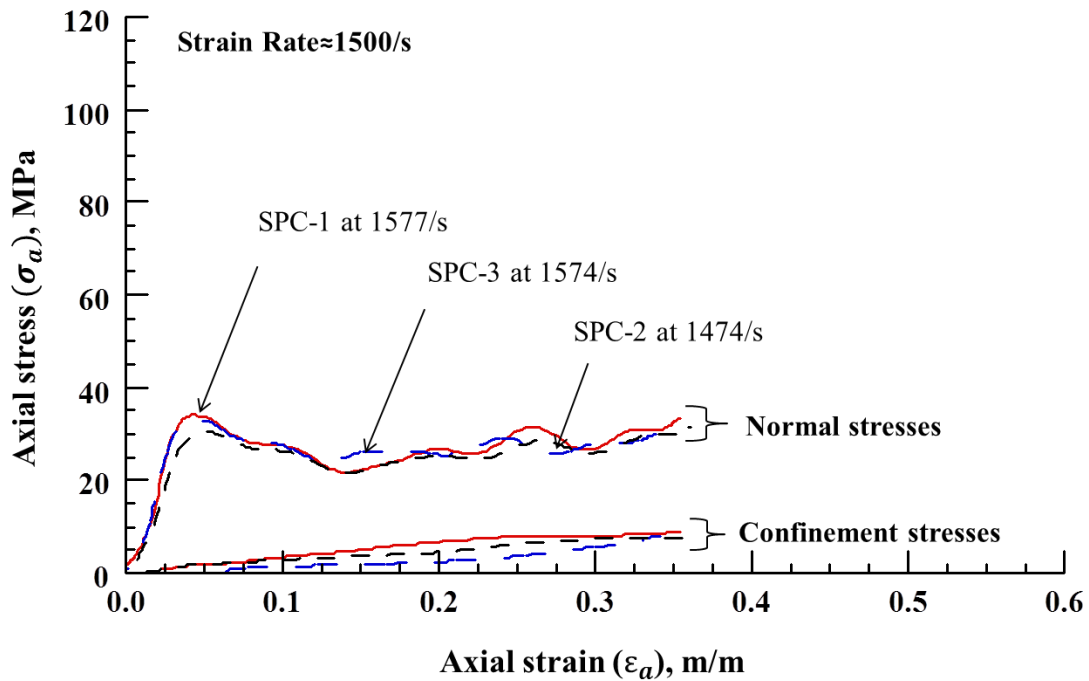


Figure 4.13. Axial and confinement stresses versus axial strain at 1574/s strain rate.

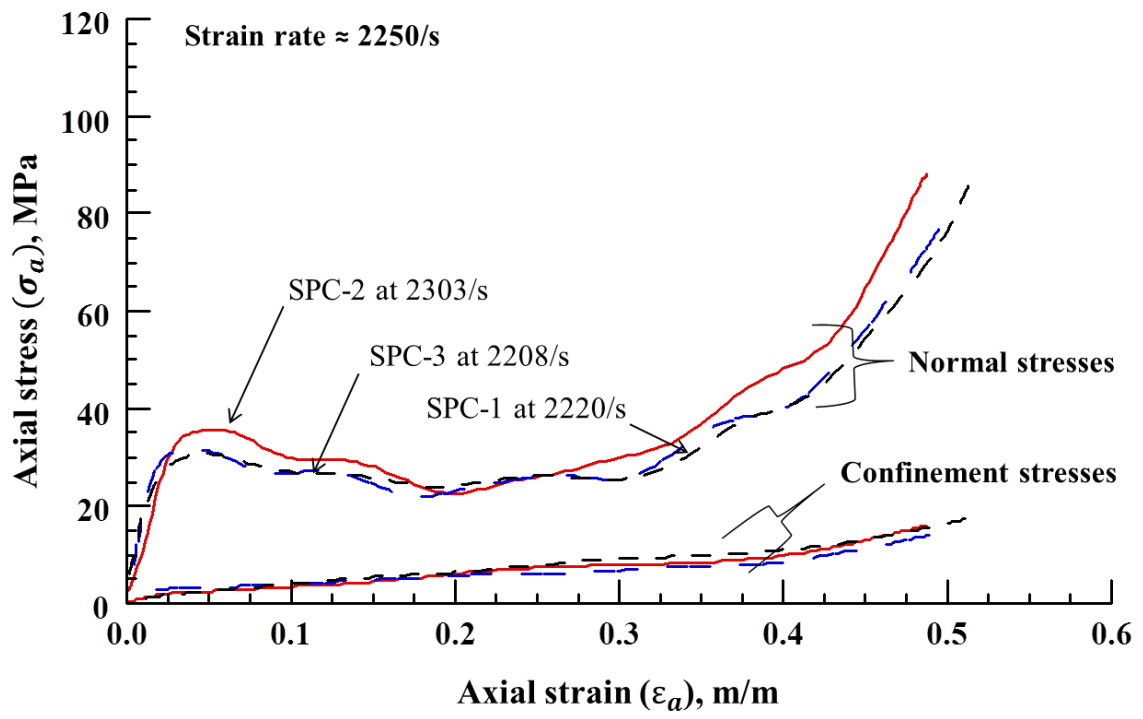


Figure 4.14. Axial and confinement stresses versus axial strain at 2220/s strain rate.

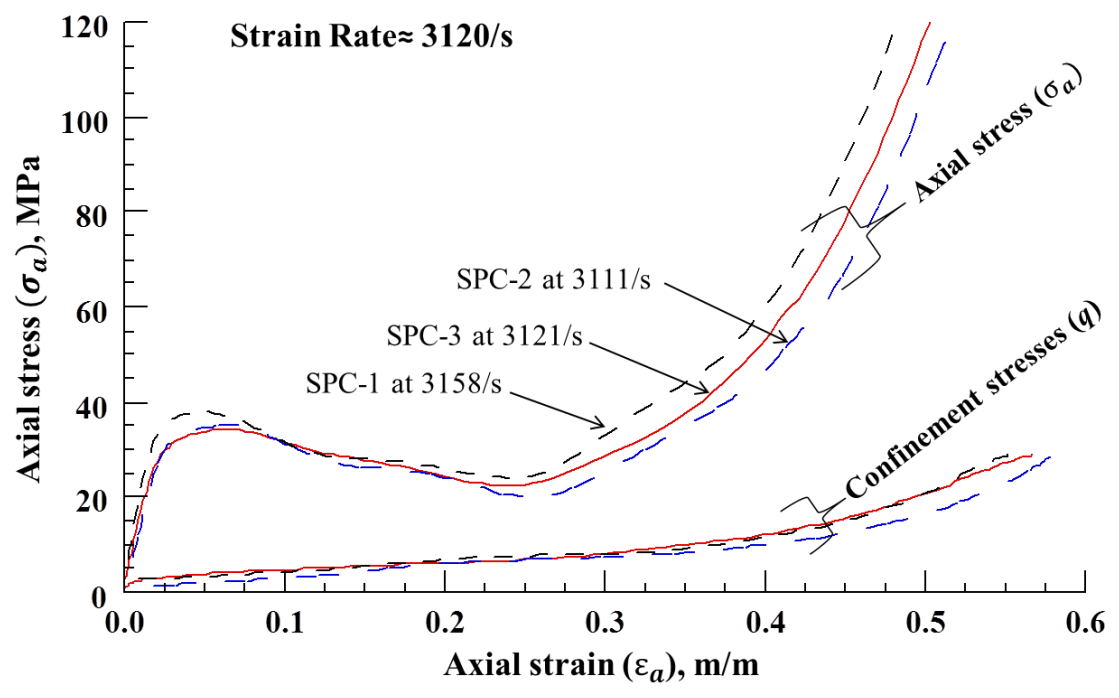


Figure 4.15. Axial and confinement stresses versus axial strain at 3120/s strain rate.

The axial stress-strain response of Eco-Core at 500/s, 1574/s, 2220/s and 3120/s were compared with each other's and with the static test results in Figure 4.16. The test results showed that Eco-Core under confinement becomes a strain rate sensitive. The compressive strength increased with increasing strain rate and was almost doubled when the strain rate changed from static to 3120/s (see Table 4.1).

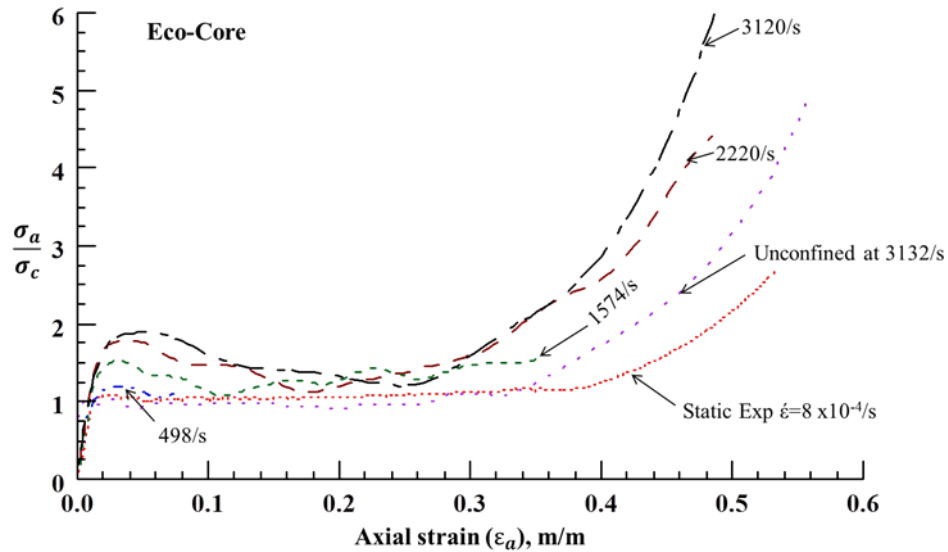


Figure 4.16. Axial stress-strain response at different strain rates.

Table 4.1

*Strain rates and compression strengths of Eco-Core specimens*

| SPC # | Strain rate ( $\dot{\epsilon}$ ), 1/s | Comp. strength ( $\epsilon_c$ ), MPa |
|-------|---------------------------------------|--------------------------------------|
| 1     | 498                                   | 24.00                                |
| 2     | 431                                   | 24.06                                |
| 3     | 568                                   | 24.80                                |
| 4     | 1537                                  | 33.60                                |
| 5     | 1474                                  | 33.03                                |
| 6     | 1574                                  | 30.44                                |
| 7     | 2220                                  | 35.66                                |
| 8     | 2303                                  | 32.45                                |
| 9     | 2408                                  | 31.01                                |
| 10    | 3158                                  | 34.05                                |
| 11    | 3111                                  | 35.22                                |
| 12    | 3121                                  | 37.83                                |

#### 4.4 Derivation of Dynamic Constitutive Equation

Confinement stresses versus axial strain for different strain rates were plotted in Figure 4.17. The figure shows that confinement stress,  $q(t)$  is insensitive to strain rate. Confinement stress followed the same response as that of axial stress. At higher strain rates, which contain higher impact energy, the limit of confinement stress increased. The confinement stress limit ( $q/\sigma_c$ ) was 0.15 at  $\dot{\epsilon}=500/s$  and it increased to 0.45 at  $\dot{\epsilon}=3120/s$ .

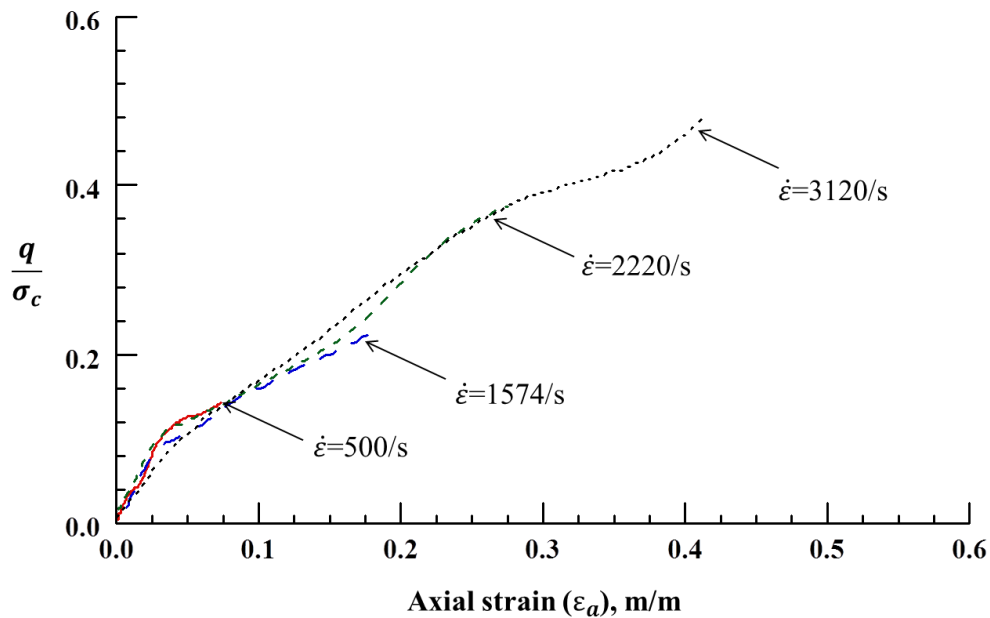


Figure 4.17. Confinement stress versus axial strain at different strain rates.

To include the lateral confinement stress in the axial stress-strain responses, the deviatoric stress was introduced (which refers to the difference between the axial stress and the lateral confinement stress). The frictional effect between the specimen and the sleeve was determined to be important as discussed in Chapter 3. Therefore, an equivalent axial friction stress,  $\sigma_\mu(t)$  was calculated by Eq. 4.7. The equivalent friction stress,  $\sigma_\mu(t)$  versus axial strain response is a function of,  $q(t)$ . Thus, it is also independent of strain rate. To account for both; friction effect and lateral stress, the net-deviatoric stress was introduced and determined as:

$$\sigma_{d-\mu}(t) = \sigma_a(t) - q(t) - \sigma_\mu(t) \quad (4.8)$$

Where  $\sigma_a(t)$  is the axial stress,  $q(t)$  is the confinement stress and  $\sigma_\mu(t)$  is the equivalent friction stress in the axial direction.

All the stresses were normalized to compression strength to express the Equation in a non-dimensional form. The net-deviatoric stress versus axial strain for different dynamic strain rates (500/s, 1574/s, 2220/s and 3120/s) was determined by Eq.4.8. The static ( $8 \times 10^{-4}$ /s) net-deviatoric stress was determined in Chapter 3. The static and dynamic net-deviatoric stresses at different strain rates were plotted versus axial strain in Figure 4.18. The figure shows that the net-deviatoric stress is sensitive to strain rate where the compression strength of the material increased with increasing strain rate. The figure also shows that the net-deviatoric stress-axial strain response consists of two parts: Linear (semi-linear) response continues until the failure of the material ( $\varepsilon_a \leq \varepsilon_c$ ) and non-linear response starts after the failure of the material ( $\varepsilon > \varepsilon_c$ ) and consists of crushing and densification of the material.

A multi-variable Least Squares Curve Fitting was performed on the linear and nonlinear parts of the response. The two parts of the fitted equation are given by:

$$\frac{\sigma_{d-\mu}}{\sigma_c} = \begin{cases} 50 + ((25 \times 10^{-3})\dot{\varepsilon})\varepsilon_a - ((15 + 0.1\dot{\varepsilon})\varepsilon_a)^2 & \text{for } \varepsilon_a \leq \varepsilon_c \\ 0.05(5.5\varepsilon_a)^{(2.5+7 \times 10^{-4}\dot{\varepsilon})} + (1.05 + 28 \times 10^{-5}\dot{\varepsilon})e^{-5\varepsilon_a} & \text{for } \varepsilon_a > \varepsilon_c \end{cases} \quad (4.9)$$

Where  $\sigma_c$  is the compression strength (20MPa) and  $\varepsilon_c$  is the compression yield strain (0.02).

Figure 4.19 shows that the response of the fitted Eq. 4.9 agreed reasonably with experimental results of net-deviatoric stress. Alternatively, Eq. 4.9 was expressed in terms of axial stress by adding confinement and friction stresses to both sides of the equation, that resulted in:

$$\frac{\sigma_a}{\sigma_c} = \begin{cases} 50 + ((25 \times 10^{-3})\dot{\epsilon})\epsilon_a - ((15 + 0.1\dot{\epsilon})\epsilon_a)^2 + \frac{q}{\sigma_c} \left[ 1 + 4\mu\left(\frac{h}{d}\right)(1 - \epsilon_a) \right] & \text{for } \epsilon_a \leq \epsilon_c \\ 0.05(5.5\epsilon_a)^{(2.5+7 \times 10^{-4}\dot{\epsilon})} + (1.05 + 28 \times 10^{-5}\dot{\epsilon})e^{-5\epsilon_a} + \frac{q}{\sigma_c} \left[ 1 + 4\mu\left(\frac{h}{d}\right)(1 - \epsilon_a) \right] & \text{for } \epsilon_a > \epsilon_c \end{cases} \quad (4.10)$$

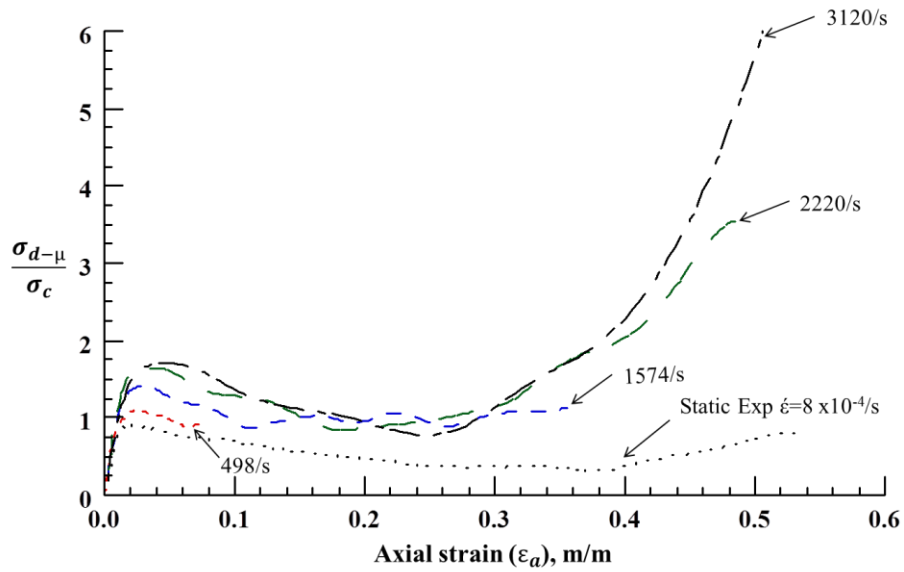


Figure 4.18. Net-deviatoric stress-strain response at different strain rates.

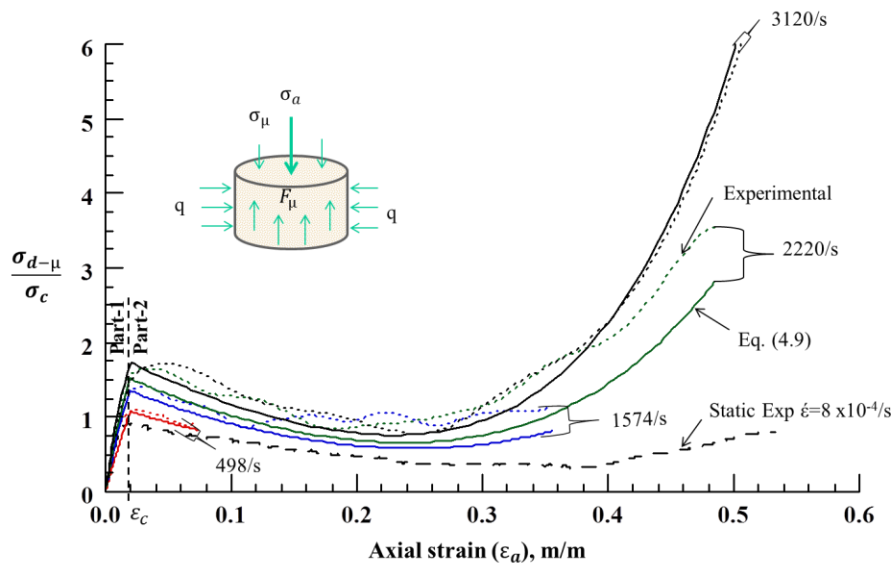


Figure 4.19. Comparison of Eq. 4.9 and experimental net-deviatoric stress versus axial strain at different strain rates.

The response of Eq. 4.10 was validated by the experimental data for strain rates ranged from static ( $\dot{\epsilon} = 8 \times 10^{-4} / s$ ) to 3120/s as shown in Figure 4.20. The experimental response is represented by dotted lines and Eq. 4.10 response is presented by solid lines. The two responses agreed well with each other.

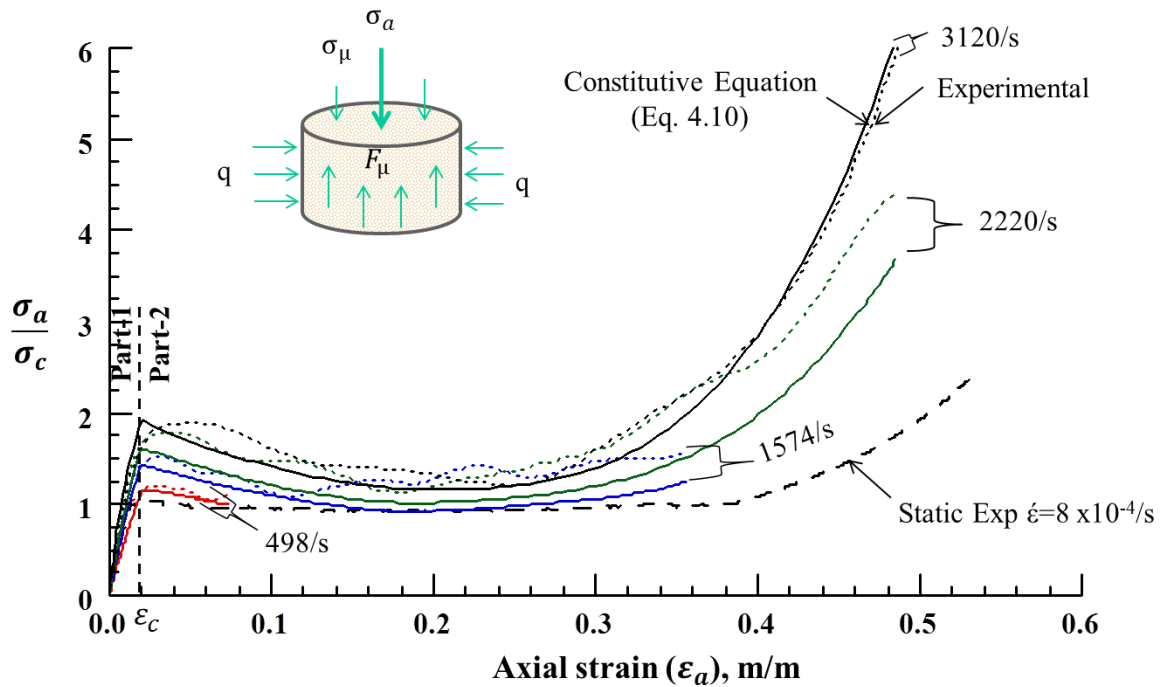


Figure 4.20. Validation of constitutive equation (Eq. 4.10) by experiments.

#### 4.5 Energy Absorption

Energy absorption of Eco-Core was compared with other commercial core materials such as PVC foam, Balsa wood and Rohacell R-71. Dynamic tests were conducted at a strain rate of about 3500/s. Tested core material and their corresponding densities are: Eco-Core ( $500\text{kg/m}^3$ ), PVC foam ( $100\text{kg/m}^3$ ), Balsa Wood ( $202\text{kg/m}^3$ ) and Rohacell-A ( $75\text{kg/m}^3$ ). All the materials were tested under the same exact conditions. The specimen size was 11 mm diameter and 3.2 mm length. Aluminum sleeve of 11 mm inner diameter and 0.9 mm thickness was used for confinement. Test strain rate was almost the same in all cases that ranged from 3120/s to 3490/s.

Energy absorption per unit volume of a material is determined by the area under the compression stress-strain curve within the densification limit. The densification limit strain was estimated for each material by the intersection of the two tangent lines, one from the densification curve and another from the crushing curve (see Figure 4.21). The area under the shaded region gave the energy absorption per unit volume. This can also be calculated by integration of Eq.4.10 for axial strain limits of 0 to  $\varepsilon_d$ .

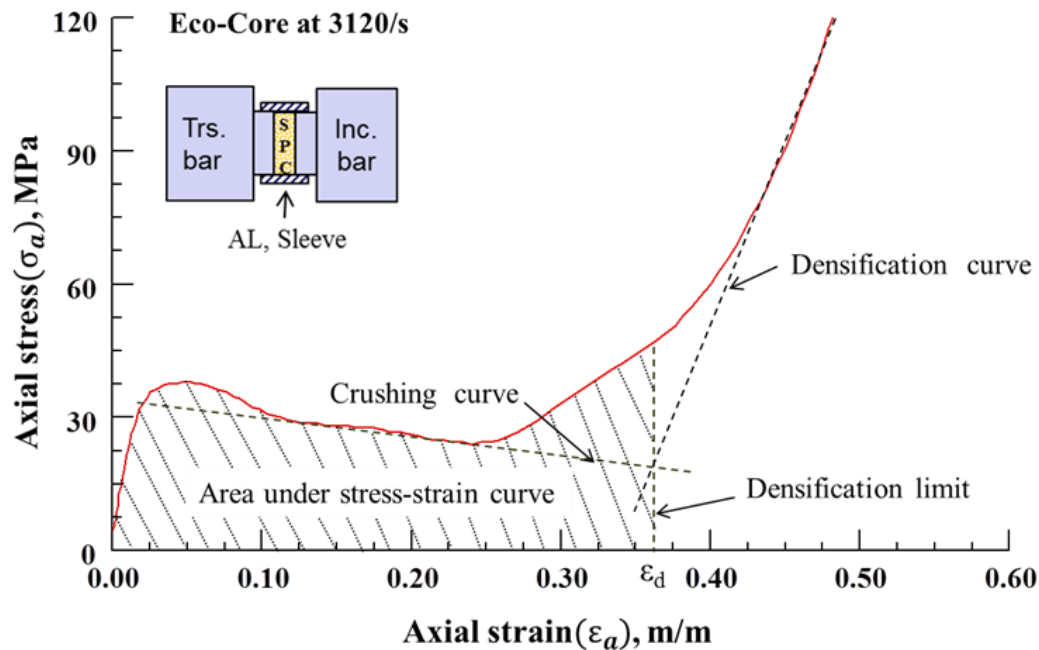
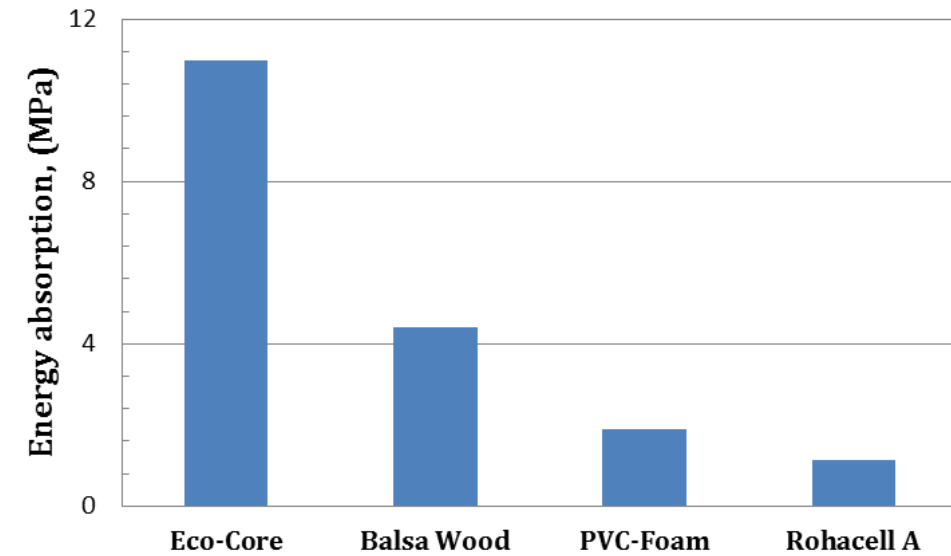


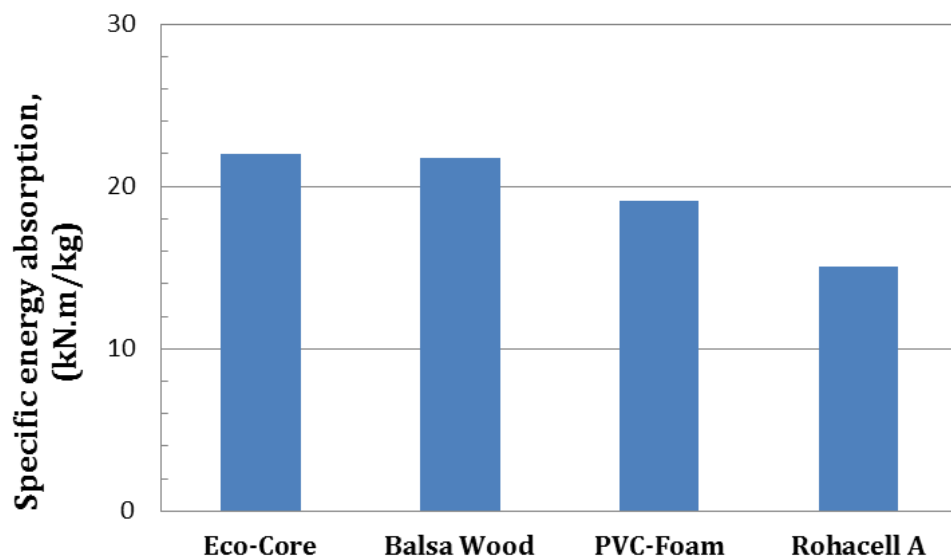
Figure 4.21. Stress-strain curve of Eco-Core for energy absorption at 3120/s.

Eco-core absorbs energy through four phases: breaking of bonds between micro-balloons, translation of micro-balloons, crushing of hollow micro-balloons and final densification. Energy absorption per unit mass or specific energy absorption of the material can be determined by dividing the energy absorption per unit volume by the density of the material. Energy absorptions per unit volume and per unit mass were determined for Eco-Core and other commercial core materials. Results of all are compared with each other's as shown in Figure 4.22. The energy absorption per unit volume of Eco-Core is more than twice that of the nearest

material (Balsa wood). Both PVC foam and Rohacell-A foam have lowest volumetric energy absorption capability. The energy absorption per unit mass of Eco-Core is still better than all other core materials but the difference is less dramatic.



(a)



(b)

Figure 4.22. (a) Energy absorption per unit volume of different core materials, (b) Energy absorption per unit mass of different core materials.

## 4.6 Summary

High strain rate confined compression testing of Eco-Core material was conducted for a strain rate ranged from 500/s to 3120/s using a confined compression test fixture in a SHPB apparatus. A special test fixture was developed to apply and measure both radial and axial stresses simultaneously. The designed specimen had 11 mm diameter and 3.2 mm length. The test instrumentation and data analysis were validated by comparing the measured stress-strain response of polycarbonate, nylon 6/6 and Eco-Core materials with data in literature. Test results showed that, like unconfined test results, the stress-strain response consists of three domains: linear (semi-linear), nonlinear or plateau (crushing) and densification. Unlike unconfined test, the stress-strain response is dependent on strain rate and confined compression strength of Eco-Core increased with the increasing strain rate.

An empirical stress-strain equation for Eco-Core was developed. The equation has two parts: One for initial linear part ( $\varepsilon_a \leq \varepsilon_c$ , strain at compression strength) and nonlinear part for  $\varepsilon_a > \varepsilon_c$ . The developed stress-strain equation was verified by experiments. The energy absorption per unit volume of Eco-Core was found far superior than Balsa wood (more than 2 times) and other commercial polymer foams. The energy absorption per unit mass of Eco-Core is marginally better than other commercial materials.

## CHAPTER 5

### Simulation by LS-DYNA

This Chapter presents the finite element simulation of the static and the dynamic tests by using LS-DYNA code. A user defined material model was used in the simulation. The problem was modeled as an axisymmetric problem. The simulation was performed for both static and dynamic conditions at different strain rates and simulation results were compared with experiments.

#### 5.1 Background

LS-DYNA is a general purpose finite element program developed by the Livermore Software Technology Corporation (LSTC) for simulating complex problems. It uses explicit time integration to solve nonlinear, transient dynamic finite element analysis. Nonlinearity refers to any of the following: Changing any of the boundary conditions over time like contacts among parts, large deformations like crashing and nonlinear material behavior like thermoplastic materials. Transition refers to analyzing high speed, short duration events where inertial forces are important. LS-DYNA is one of the most flexible finite element analysis software used by the industries of automobile, aerospace, construction, military, manufacturing, and bioengineering [45].

The most important factor in any successful analytical simulation including LS-DYNA is the right selection of material model involved in the simulation. LS-DYNA is provided with many material models classified under different categories as shown in Figure 5.1. In the literature, many studies were found about simulation of dynamic tests. Several material models were used in those reviewed cases of study like: modified Drucker Prager model and concrete model to simulate concrete [46, 47], Johnson Holmquist concrete model to simulate ultra-high

performance cement based composites (UHPCC) used in defense works [48], linear elastic isotropic material model to simulate PMMA [49] and to simulate adhesive joints [50], Johnson–Cook and power law plasticity models to simulate steel [51], isotropic hardening plasticity model to simulate SFRC [52], Johnson Cook model to simulate copper [53] and aluminum 6061 [54], crushable foam and Deshpande and Fleck foam models to simulate light weight metal foam [55].

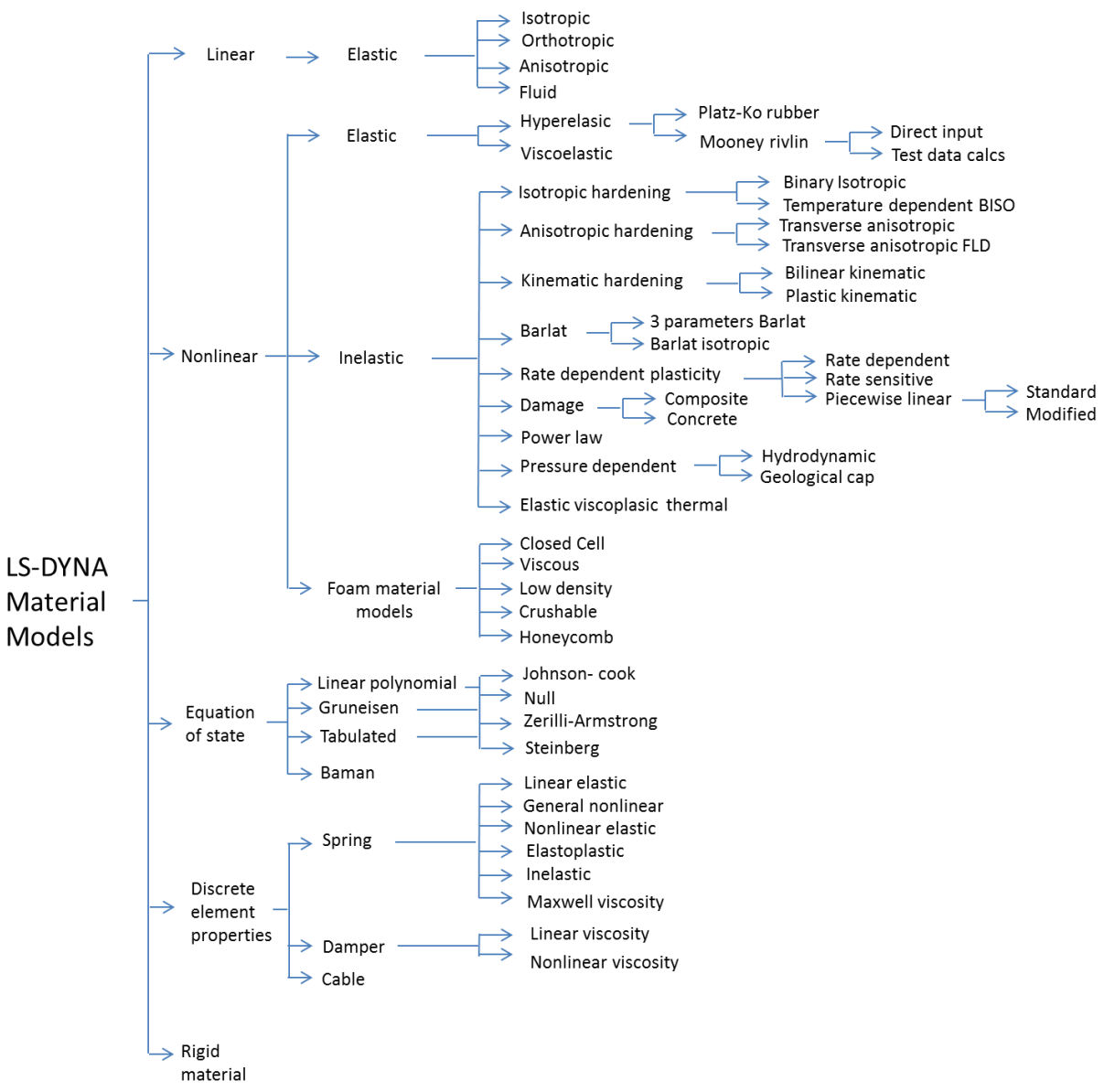


Figure 5.1. LS-DYNA material models.

From the dynamic study in chapter 4, it was found that the lateral confinement and its measurement are limited by the geometry and dimensions of both specimen and sleeve. Therefore, simulation of these tests especially dynamic one saves considerable amount of time, cost and efforts. Besides, it opens the door for flexible analysis of the effects of different parameters like specimen dimensions (long specimen) and impact velocity (very high strain rates), which are experimentally infeasible. This chapter focuses on this subject for Eco-Core. The problem approached by using the previously developed constitutive equation of Eco-Core in Chapters 4 as a material model in LS-DYNA simulation code.

## **5.2 Challenges**

The simulation of high strain rate testing of foams in general under lateral confinement is scarce in the literature. In addition, no material model is available in particular for syntactic foam in the analysis codes like LS-DYNA. Although, some models are defined by experimental stress-strain data as a multi-linear response, still they are all 1- dimensional and mostly strain rate insensitive. That makes them invalid for dynamic multi-axial problems. Therefore, simulating Eco-Core under multi-axial stress state requires special modifications for the available material models.

## **5.3 Material Model**

The process of development of material model for Eco-Core consists of two major parts; selection of suitable model available in LS-DYNA and modifying the model to fit Eco-Core.

**5.3.1 Selection of LS-DYNA material model.** The development of material model for Eco-Core in LS-DYNA code starts with the determination of the best available model can be used to represent the material. Most of the material models provided with LS-DYNA as listed in Figure5.1 (all except foam models) are incompressible and rely on the plasticity theory in their

response. That means volume of the material is constant and only the shape changes when it deforms plastically. Dimensions change according to Poisson's ratio which increases up to about 0.5 while the volumetric change is constant at zero. That leads to a very high axial stress response when the material is under lateral constraint. As that is not the case in syntactic foams like Eco-Core, those models are eliminated from the selection.

Foam models in general are compressible and rely on volumetric change in case of reversible deformation like padded foams (urethane) or irreversible deformation or crushing like PVC foam. Therefore, the selection of material model to simulate Eco-Core as a crushable material with volumetric change is limited within the Foam Material Models. Only Low Density Foam Model and Crushable Foam Model allow for defining of material response by experimental stress-strain data as a multi-linear response. Then the rest of the foam material models are eliminated from the selection.

Crushable Foam Model exhibited discontinuity in response when used for simulating Eco-Core. It is believed because the model assumes sudden drop in the stress followed by sudden raise to the previous stress level when crushing. This model is eliminated from selection because real response of Eco-Core does not exhibit discontinuity. Then Low Density Foam Model was the most suitable among all; therefore it was selected to simulate Eco-Core.

**5.3.2 Modification of material model by constitutive equation.** After the selection of Low Density Foam Model, it needed to be modified to simulate Eco-Core material. The properties of the original model can be listed as:

- It is 1-dimensional and requires the experimental stress-strain curve information to be defined as multiple points (stress, strain), that makes it a multi-linear curve.
- It assumes Poisson's ratio = 0, that means no lateral expansion while deforming axially.

- It is strain rate insensitive, that means strain rate has no effects on the response.
- It also requires additional material properties like density, modulus, strength and others.

Eco-Core differs from the model as; it expands laterally while deforms axially and it is a strain rate sensitive when it is confined. The approach to overcome these issues and modify the model to simulate Eco-Core is explained below:

- From the static response study in Chapter 3, it was found that the correlation between the confined and unconfined response of Eco-Core is:

$$\sigma_{conf} = \sigma_{unconf} + q + \sigma_{\mu} \quad (5.1)$$

Where  $\sigma_{conf}$  is the confined axial stress response,  $\sigma_{unconf}$  is the unconfined axial stress response,  $q$  is the lateral confinement stress and  $\sigma_{\mu}$  is the equivalent friction stress between specimen and the sleeve in the axial direction.

- The constitutive equation in Chapter 4 (Eq. 4.10) is used to identify the experimental curve information for the material model.
- By approximating first part of Eq. 4.10 to a linear response and expressing second part in form of Eq. 5.1, Eq. 4.10 can be rewritten in Pascal stress units in the following form:

$$\sigma_a = \begin{cases} 50 \times 10^6 \varepsilon_a & \text{for } \varepsilon_a \leq 0.02 \\ \left[ (5.5 \varepsilon_a)^{(2.5 + 7 \times 10^{-4} \dot{\varepsilon})} + (21 + 65 \times 10^{-4} \dot{\varepsilon}) e^{-5 \varepsilon_a} \right] \times 10^6 + (q + \sigma_{\mu}) & \text{for } \varepsilon_a > 0.02 \end{cases} \quad (5.2)$$

Where  $(q + \sigma_{\mu})$  is the lateral stress and friction stress added together in Pascal units.

- The response of  $(q + \sigma_{\mu})$  is a strain rate insensitive. The correlation between  $(q + \sigma_{\mu})$  and  $\varepsilon_a$  is explained in details In Appendix B. For the used aluminum sleeve of  $d=11$  mm and

$h=0.9$  mm, the experimental  $(q + \sigma_\mu)$  as a function of  $\varepsilon_a$  for  $\varepsilon_a > 0.02$  is represented by the fourth order polynomial equation denoted by Eq. 5.3 below:

$$(q + \sigma_\mu) = 4.2 - 21.5\varepsilon_a + 709.3\varepsilon_a^2 - 2621.2\varepsilon_a^3 + 2973.7\varepsilon_a^4 \quad (5.3)$$

- From Equations 5.2 and 5.3, the multi-axial stress response can be expressed as a function of axial strain ( $\varepsilon_a$ ) and strain rate ( $\dot{\varepsilon}$ ).
- The expression for the strain rate ( $\dot{\varepsilon}$ ) as a function of impact velocity ( $V$ ) and specimen length ( $l$ ) was derived in details in Appendix C. The derived equation denoted by the following Eq. 5.4:

$$\dot{\varepsilon} = (299V - 480) \times \frac{0.0032}{l} \quad (5.4)$$

Where  $V$  is the velocity of impact in m/s and  $l$  is the specimen length in m.

- From Equations 5.2, 5.3 and 5.4, the axial stress ( $\sigma_a$ ) of Eco-Core under multi-axial stress state, can be determined as a function of  $\varepsilon_a$ ,  $V$  and  $l$ .
- Initial values for  $\varepsilon_a$ ,  $\sigma_a$  and  $(q + \sigma_\mu)$  were all set to zero.
- A loop was created for a variable named  $I$  in the LS-DYNA code.  $I$  increased from 2 to 51 with step of 1.
- Inside the loop a value of  $\varepsilon_a$  was created for each value of  $I$  as:  $\varepsilon_a = (I - 1) \times 0.02$ . Thereby  $\varepsilon_a$  increased from 0.02 to 1 with step of 0.02.
- Also inside the loop a value of  $(q + \sigma_\mu)$  was calculated for each  $\varepsilon_a$  by Eq. 5.3.
- Again inside the same loop a value for  $\sigma_a$  was calculated for each  $\varepsilon_a$  by Equations 5.2, 5.3 and 5.4 considering the corresponding value of strain rate.

- Since the initial value of  $\sigma_a$  was set to zero and next value (at  $\varepsilon_a = 0.02$ ) was calculated by Eq. 5.2, then  $\sigma_a$  for  $\varepsilon_a \leq 0.02$  became a linear response determined by the two values of  $\sigma_a$  (at  $\varepsilon_a = 0$  and 0.02) . Whereas, for  $\varepsilon_a > 0.02$  ,  $\sigma_a$  is determined only by Eq. 5.2.
- A multi-linear material curve was defined by the calculated 50 stress-strain points of the loop.
- The material curve besides other required data like density, modulus and strength were used to define and modify the Low Density Foam model to simulate Eco-Core.

#### 5.4 Simulation of Static Test

The developed material model was used in simulating the static confined compression test of Eco-Core. The simulation process included the development of finite element model, extracting the simulation results from the model and verification of simulation results by experiments.

**5.4.1 Finite element model of static test.** The static test fixture shown in Figure 5.2a was simulated in 2-dimentional mechanical model as a symmetric problem along the x-axis and axisymmetric along Y-axis as shown in Figure 5.2b. Element type PLANE162 was used with all components of the model. The element is defined by four nodes having six degrees of freedom at each node: translations, velocities, and accelerations in the nodal x and y directions. Key option 3 of the element type was used to indicate the axisymmetric.

The modified Low Density Foam model was used for Eco-Core. In the static range (up to 100/s), the strain rate has no significant effect on the response. Therefore, it was ignored and the material model was reduced by eliminating all the terms of the strain rate. A Linear Elastic Isotropic material model was used with the other components in the model. Area mesh was performed. Boundary conditions were imposed on the model represented by constraining the

displacement in the Y-direction for all nodes at the bottom of the specimen ( $Y=0$ ). The 2-dimensional Automatic Surface to Surface contact was chosen to identify the contacts among all components.

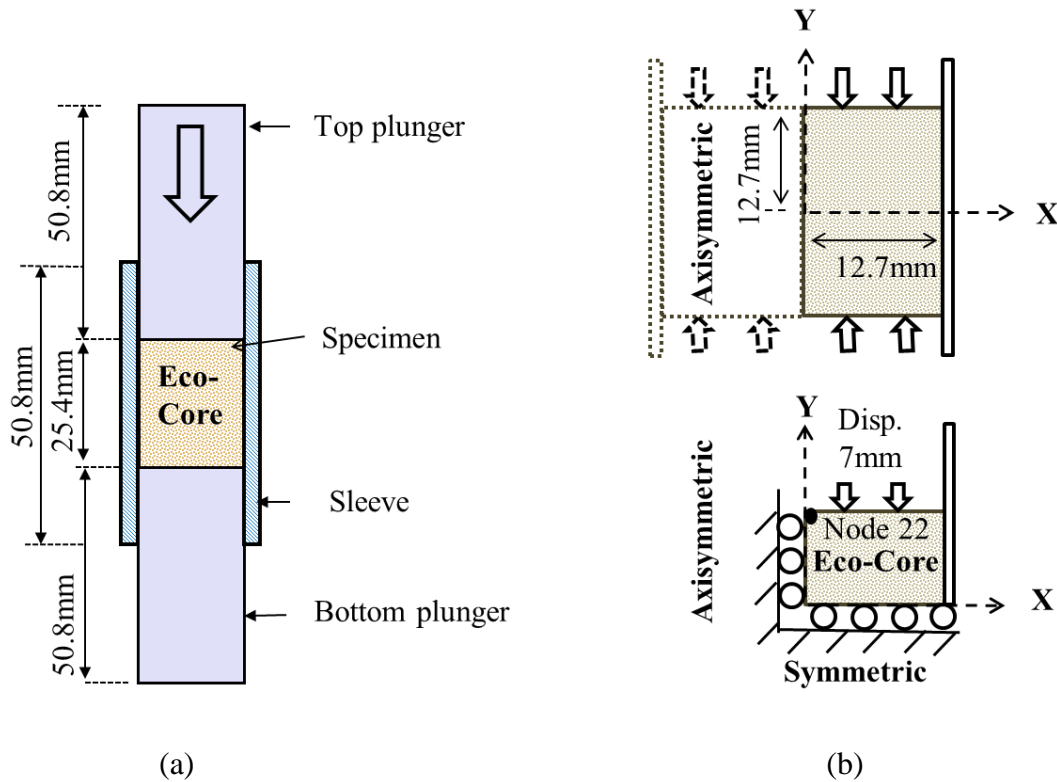


Figure 5.2. (a) Static test setup, (b) A 2-d axisymmetric model of static test setup.

The load was applied in the form of displacement imposed on the plunger in the Y-direction. Displacement value of -7 mm and duration time of 10 second were chosen. With knowing the length of the specimen is 12.7 mm, Approximated maximum resultant strain and strain rate were expected to be 0.55 and  $5.5 \times 10^{-2}/s$ , respectively. Then the duration time was reduced from 10 to 0.1 second to reduce the computational time. The results did not change since the model has become a strain rate insensitive in the static range. The finite element model is shown in Figure 5.3.

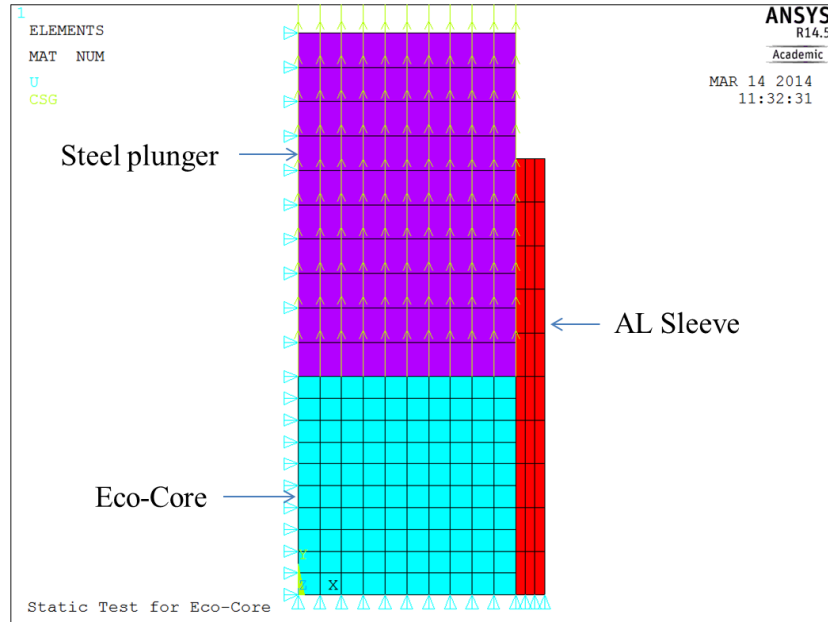


Figure 5.3. Finite element model of static test.

**5.4.2 Results of static test simulation.** Nodes at different location of the specimen were selected to acquire the simulation results. They were located at top/inner side, midlevel/center and bottom/outer side of the specimen, namely noted by Nodes, 22, 81, and 11, respectively. Also, two other nodes were selected on the inner side at the bottom of the specimen (Node 1) and other one at the bottom of the plunger (Node 122). Figure 5.4 shows nodes locations.

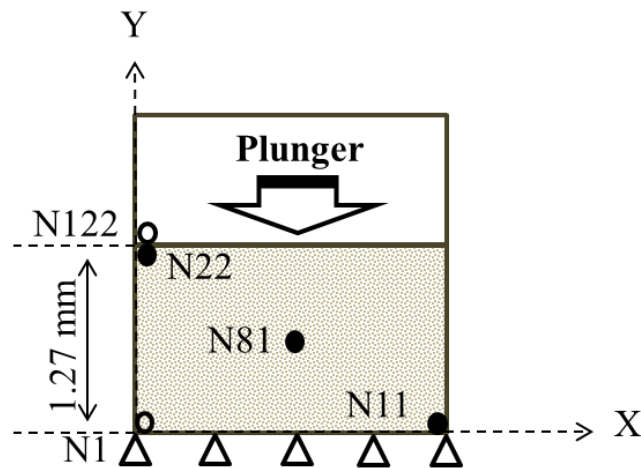


Figure 5.4. Nodal selection for monitoring stress and strain.

The strain response was not possible to be acquired directly by LS-DYNA. It is believed that is because the program was enabling to recognize the elastic strain and plastic strain from the information provided by the Modified Low Density Foam. Average total mechanical strain for the specimen was derived from displacement response of Nodes 1 and 122 at top and bottoms of the specimen. Figure 5.5a shows the displacement response of the two nodes versus time. From the displacement difference and specimen length, strain versus time response shown in Figure 5.5b was calculated. The axial stress versus time response for Nodes 22, 81 and 11 was acquired directly and plotted in Figure 5.5c. It indicates a uniform axial stress all over the specimen. From the last two figures, the axial stress-strain response was determined and plotted in Figure 5.5d.

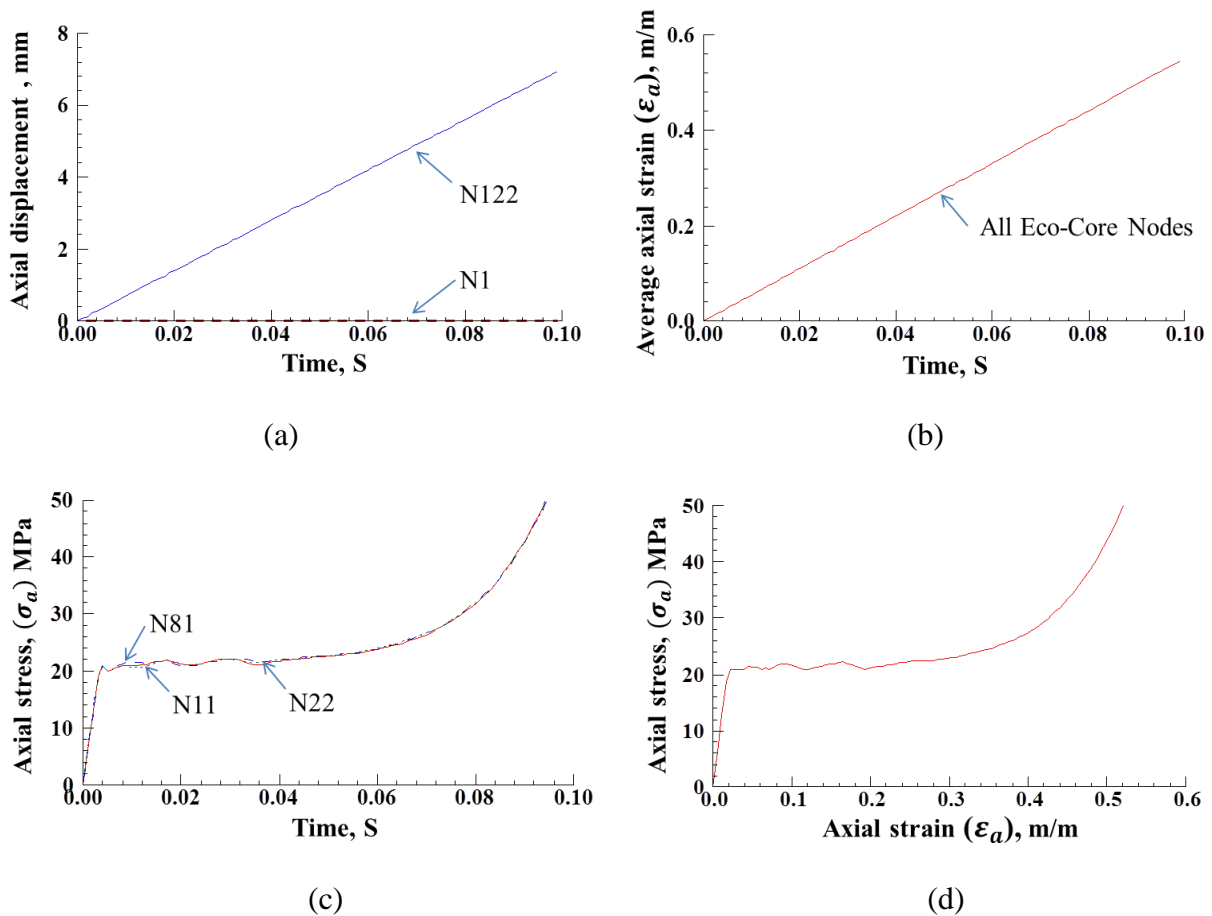


Figure 5.5. (a) Disp. response, (b) Strain response, (c) Stress response (d) Stress-strain response.

LS-DYNA Plot results for the stress and displacement of the model at the last sub-step of the loading step are shown in Figures 5.6a and b, respectively. The whole static test simulation steps in the form of ANSYS Parametric Design Language format (APDL-Code) are listed in the code presented in Appendix D.

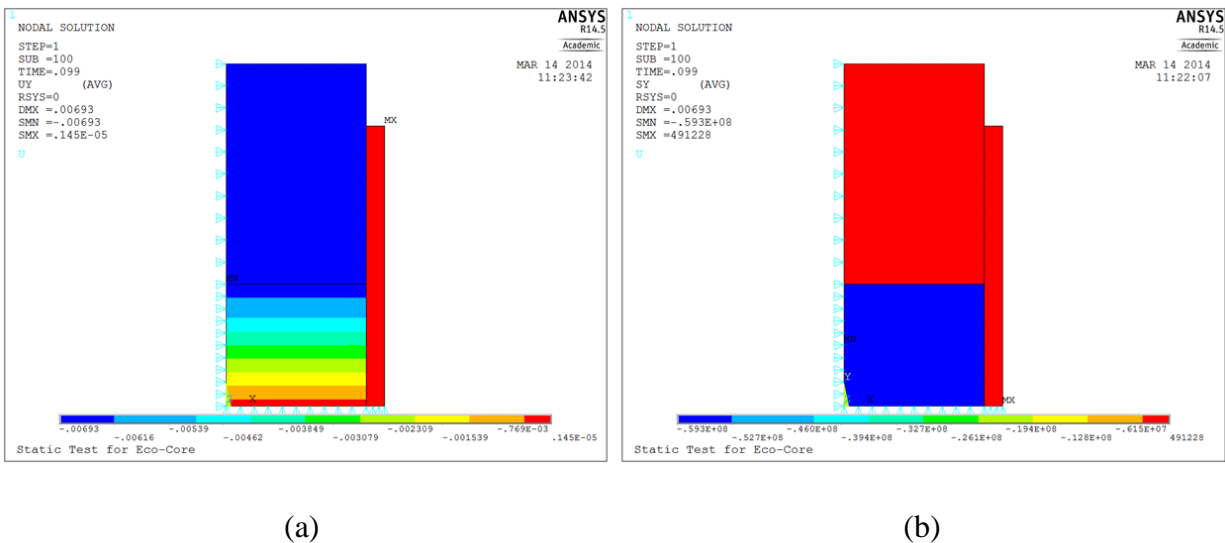


Figure 5.6. (a) Displacement response of Node 22, (b) Stress response of Node 22.

**5.4.3 Validation of static test simulation results.** The stress-strain response obtained from LS-DYNA simulation of the static test was compared to the experimental response and the developed constitutive equation as well in Figure 5.7. The last figure shows a very reasonable agreement among all. It indicates that the developed LS-DYNA model simulated the static test very reasonably.

## 5.5 Simulation of Dynamic Test

**5.5.1 Finite element model of dynamic test.** The dynamic test apparatus, Split Hopkinson Pressure Bar (SHPB) including the test fixture-specimen assembly was simulated. The schematic of SHPB is shown in Figure 5.8. A 2-dimensional mechanical model with axisymmetric along Y-axis (in horizontal level) is shown in Figure 5.9. It is important to mention here that LS-DYNA does not recognize the axisymmetric unless along the Y-axis.

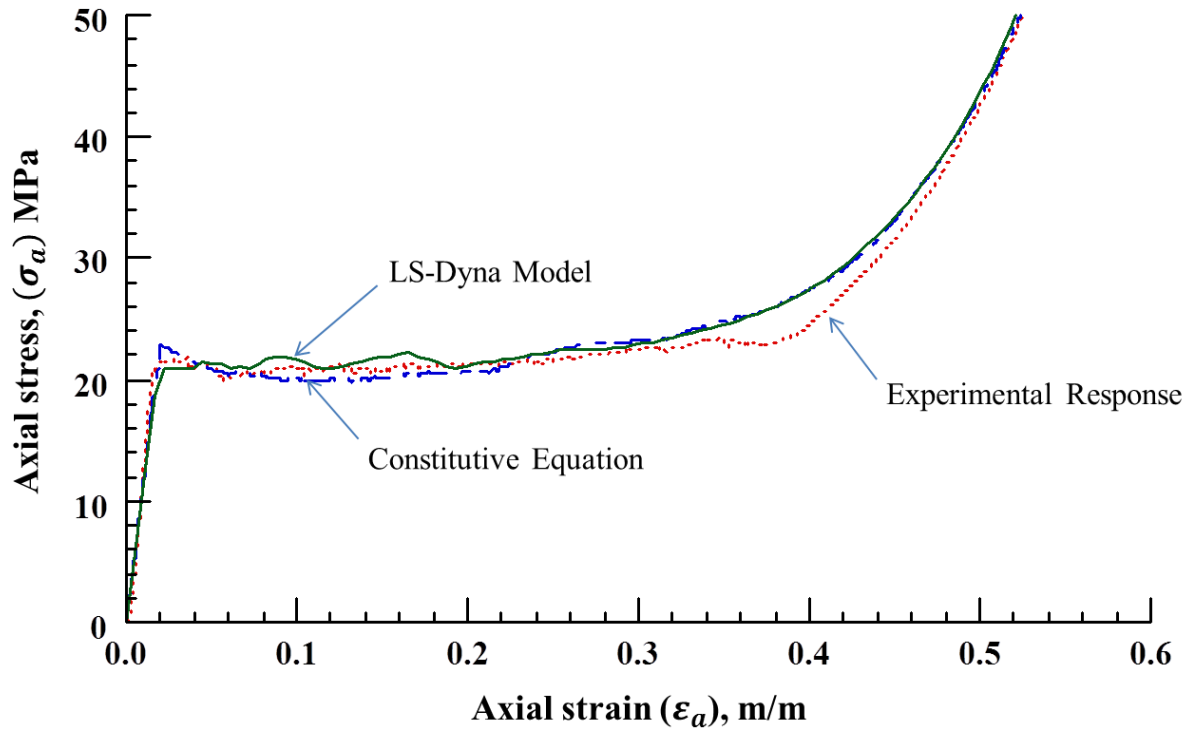


Figure 5.7. Comparison of LS-DYNA and experimental results for static test.

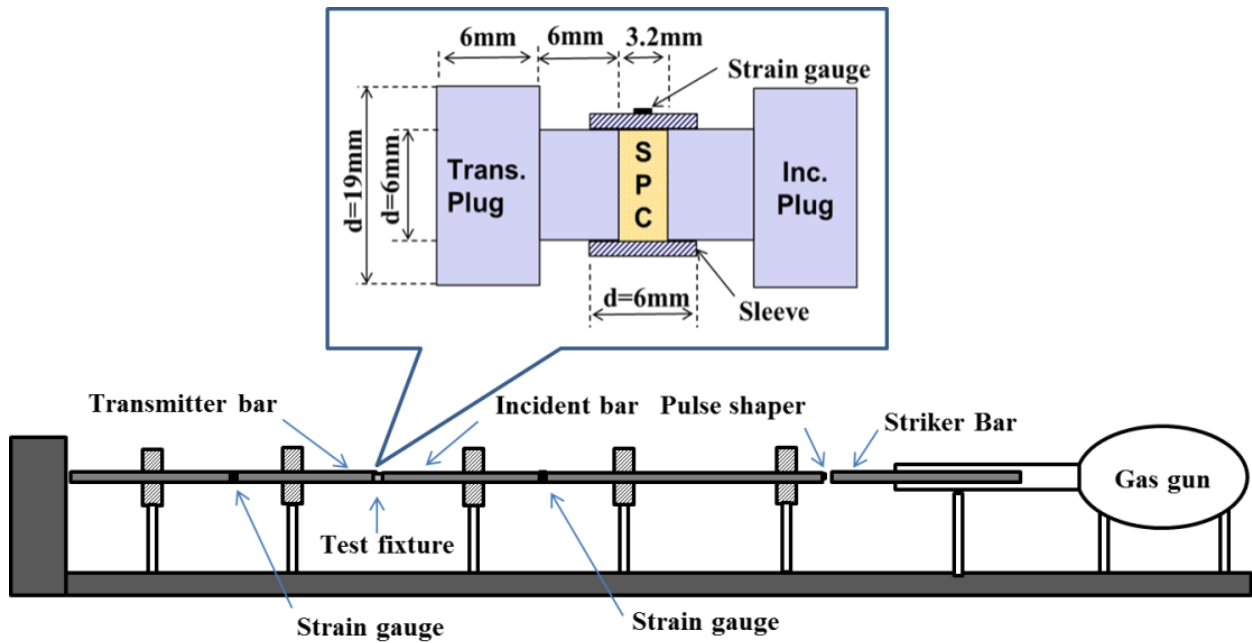


Figure 5.8. Schematic of SHPB apparatus, test fixture and specimen.

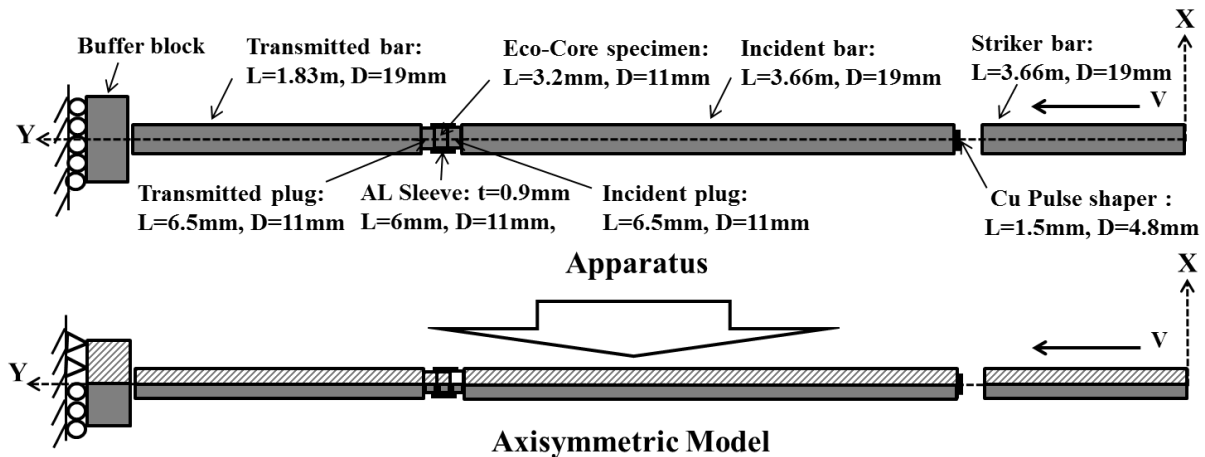


Figure 5.9. A 2-dimensional axisymmetric model of SHPB with specimen (hatched section).

The last figure shows the dimensions of all parts of the system. Specimen dimensions  $d=11$  mm and  $l= 3.2$  mm were used in the dynamic test and are used in the simulation. Once again element type PLANE 162 with axisymmetric option was used with all components of the model. The modified Low Density Foam model was used for Eco-Core with considering all the strain rate terms this time. A bilinear Isotropic model was used to simulate the annealed copper pulse shaper whereas; a Linear Elastic Isotropic model was used to simulate the rest of the components in the model. Area mesh was performed.

Boundary conditions were imposed on the model represented by constraining the displacement in the X-direction for all nodes of X-dimension = 0. In addition the nodes of the buffer block were constrained in all directions. 2-dimensional Automatic Surface to Surface contact was used among all components. This time load was applied to the model in the form of initial velocity acting on the striker bar in the Y-direction. The value of the initial velocity was changed every time and the simulation was run to indicate different strain rates. The finite element model with magnification of important parts is shown in Figure 5.10.

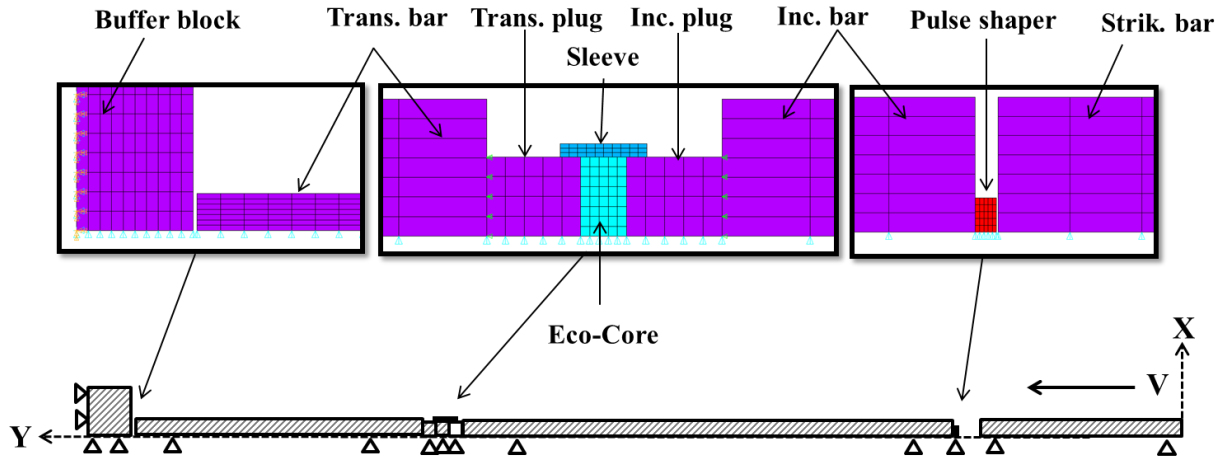


Figure 5.10. Finite element model of SHPB set up with zoomed sections.

**5.5.2 Results of dynamic test simulation.** Simulation results for different strain rates were obtained by assigning different initial velocities to the striker bar. Initial velocity for the desired outcome strain rate can be estimated by Eq. 5.4. Note that for the used specimen dimensions the obtained axial stress response was the same in all different locations in the specimen. Basically, with such a short specimen that is expected because of the dynamic equilibrium. Therefore, results were expressed to just one node located at the center of the specimen. Axial stress versus time was read directly from LS-DYNA result viewer whereas; axial strain was derived from the displacement response as before. Strain rate at each sub-step was determined by dividing the strain difference during a sub-step by the duration of the sub-step. Axial stress-strain response was derived from the stress and strain versus time responses.

Results were obtained at strain rates similar to the experimental ones; 500/s, 1600/s, 2220/s and 3120/s. Axial strain, axial stress and strain rate versus time responses and corresponding axial stress-strain response at 3120/s strain rate are shown in Figures 5.11a, b, c, and d, respectively. The results of axial stress-strain responses of Eco-Core at different strain rates were derived in the same manner and are plotted all together in Figure 5.12.

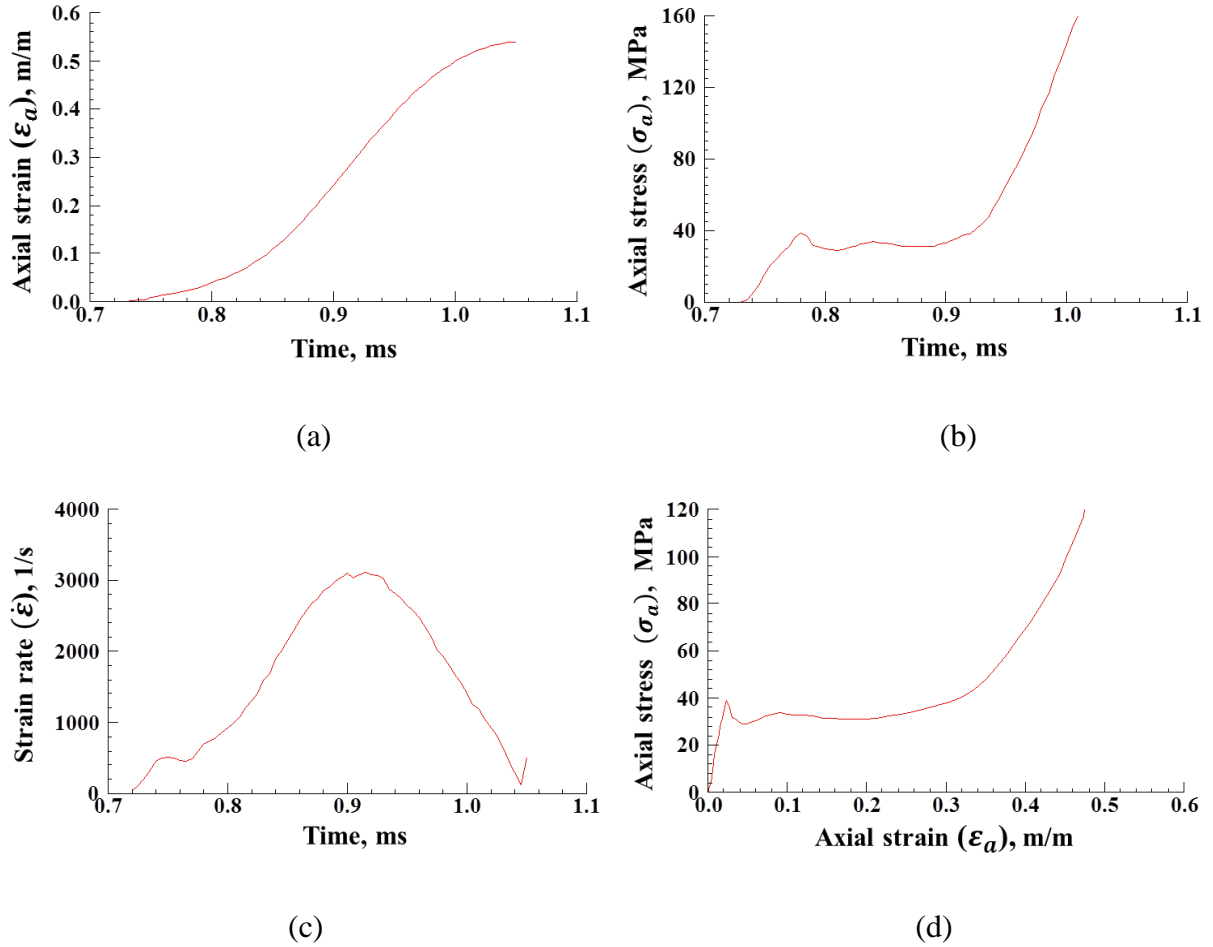


Figure 5.11. (a) Strain response at 3120/s, (b) Stress response at 3120/s, (c) Strain rate response at 3120/s, (d) Stress-strain response at 3120/s strain rate.

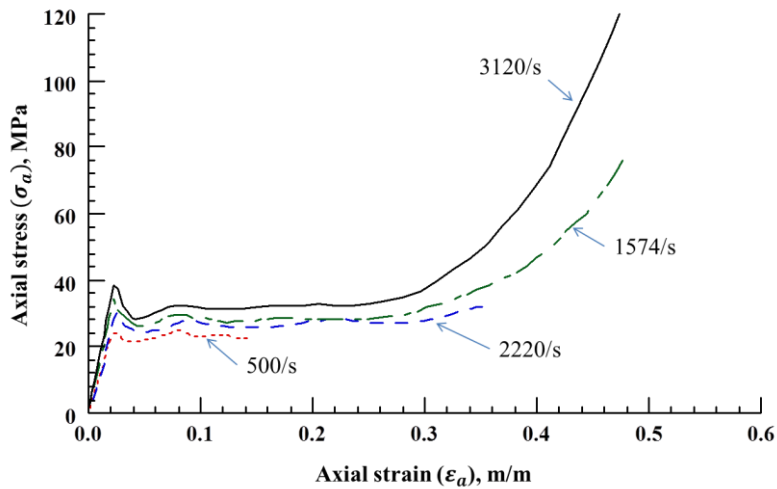


Figure 5.12. LS-DYNA results for different strain rates.

LS-DYNA plots for the stress propagation through Eco-Core specimen at 3120/s strain rate is shown in Figure 5.13. The figure shows the stress response at four different time-steps. The whole dynamic test simulation steps are listed in the APDL-Code presented in details in Appendix E.

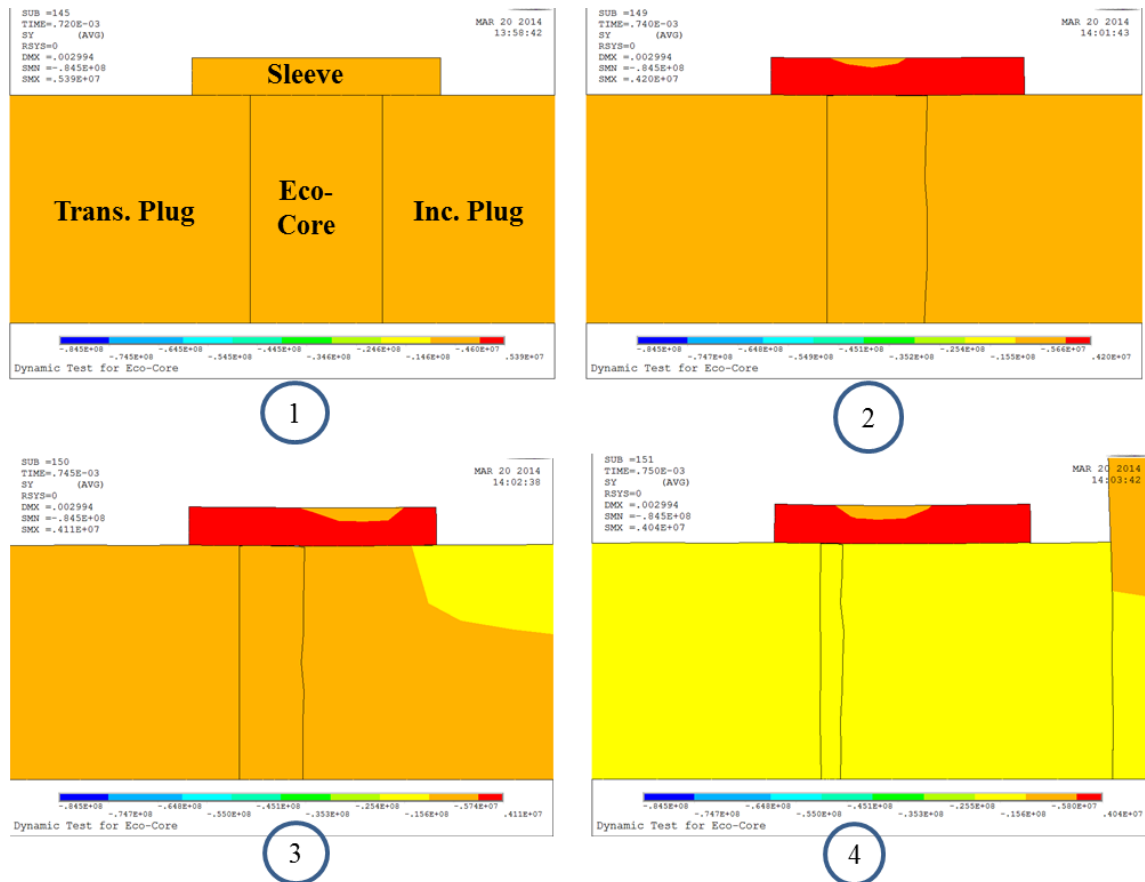


Figure 5.13. LS-DYNA predicted deformed shapes of specimen at four different time steps.

**5.5.3 Validation of dynamic test simulation results.** The stress-strain responses of LS-DYNA simulation results at different strain rates 512/s, 1602/s, 2220/s and 3111/s were compared to the experimental and constitutive equation responses. The comparison showed a very reasonable agreement among all responses. Figures 5.14, 5.15, 5.16 and 5.17 show the comparison of result at 512/s, 1602/s, 2220/s and 3111/s strain rate, respectively. The comparison indicated that LS-DYNA simulated the dynamic test of Eco-Core successfully.

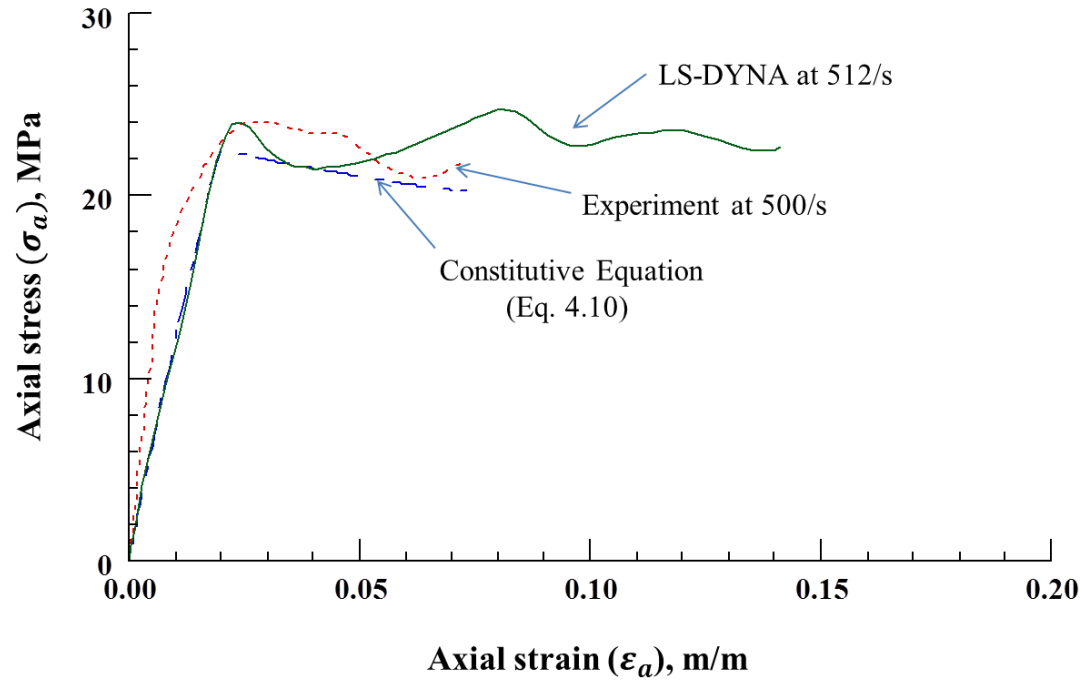


Figure 5.14. Comparison of LS-DYNA with experiment for 500/s strain rate.

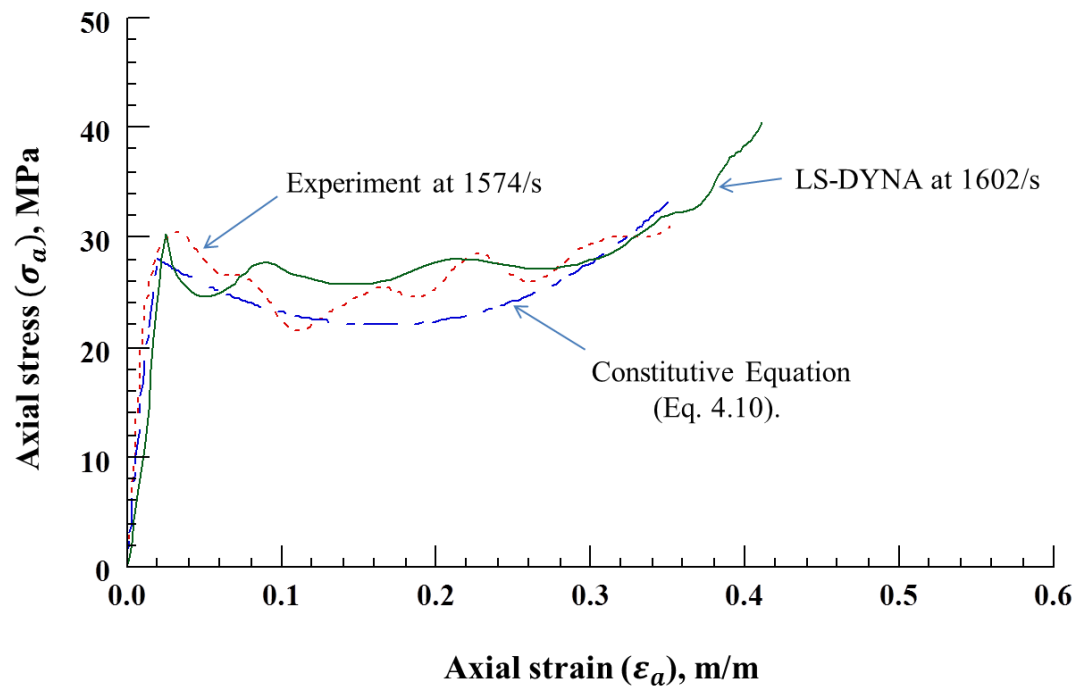


Figure 5.15. Comparison of LS-DYNA with experiment for 1574/s strain rate.

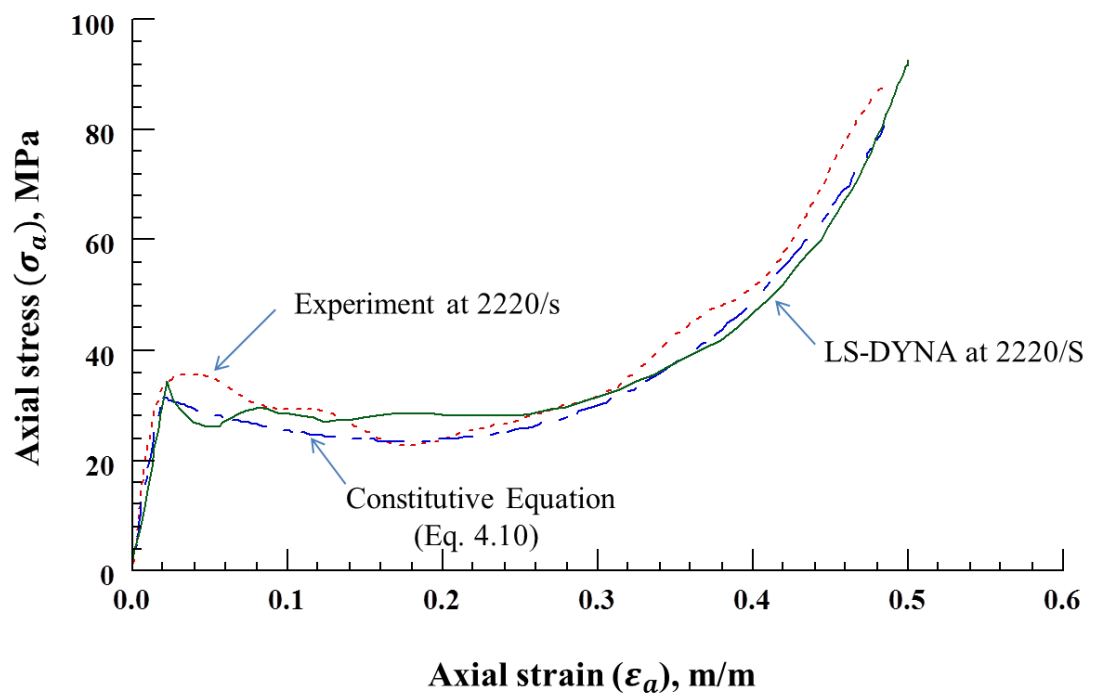


Figure 5.16. Comparison of LS-DYNA with experiment for 2220/s strain rate.

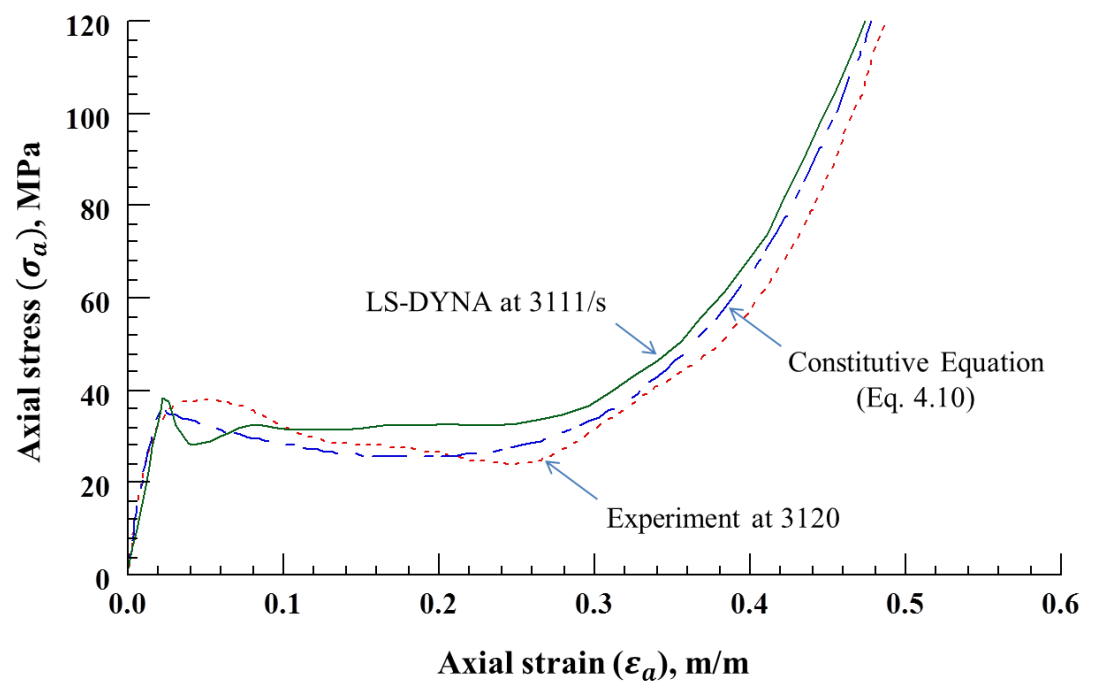


Figure 5.17. Comparison of LS-DYNA with experiment for 3120/s strain rate.

## 5.6 Applications of the LS-DYNA Simulation

After a finite element model has been developed by LS-DYNA code and was validated by the experimental results, it was employed in very useful applications. One of the major assumptions in the concept of SHPB testing is the dynamic equilibrium. The reliability of the test is pending on equilibrium of stresses all along the specimen. That is to be achieved; it imposes limitations in selection of specimen dimensions and geometry. Also it requires multiple trails and testes to decide if the selected dimensions are complying with the assumption. As it was mentioned before, high strain rate tests require considerable amount of time, cost and efforts. Therefore running a simulation program to check the dynamic equilibrium of specimens of different dimensions is a very practical approach.

In this case of study, an assumed Eco-Core specimen of 13.2 mm length and 11 mm diameter was used to run the LS-DYNA dynamic test simulation. Strain rate was managed to be 4000/s. Nodes at different locations in the specimen: N1, N2, N3, N4 and N5 were selected to obtain axial stress versus time response as shown in Figure 5.18. They were 3.25 mm apart from each other's. Last figure shows that the axial stresses all along the specimen occurred at the same time. That indicates the specimen was under dynamic equilibrium, thereby, specimen dimensions are acceptable to perform SHPB dynamic test.

Also, during the high strain rate tests, stress propagation in the specimen is impossible to measure. Besides, the short specimen requirement to achieve dynamic equilibrium makes it even harder to acquire any stress variation history of specimen during the test. Once again, an assumed Eco-Core specimen with exaggeration in specimen length of 100 mm and diameter of 11 mm was used to run LS-DYNA dynamic test simulation. Strain rate was managed to be 140/s. Five nodes were selected in different locations of specimen, Nodes: N1, N2, N3, N4 and N5.

They were 25 mm apart from each other's. Figure 5.19 shows schematic of the specimen and the axial stress versus time response of the five nodes. Last figure shows 15  $\mu$ s time interval for the stress wave to propagate from one node to another. That indicates the stress wave propagates in the Eco-Core specimen in a rate of 1666 m/s. Thanks to LS-DYNA simulation, these conclusions would not have been possible without it.

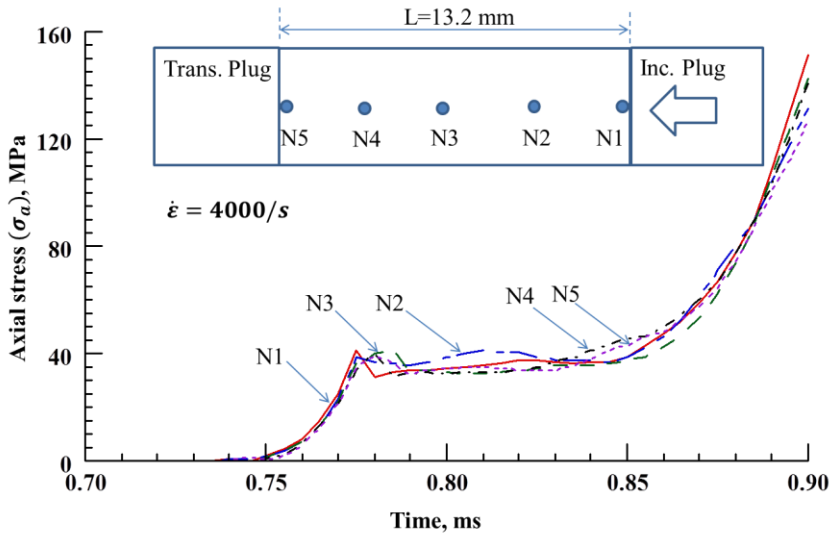


Figure 5.18. Axial stress response at different locations of 13.2 mm long specimen at 4000/s.

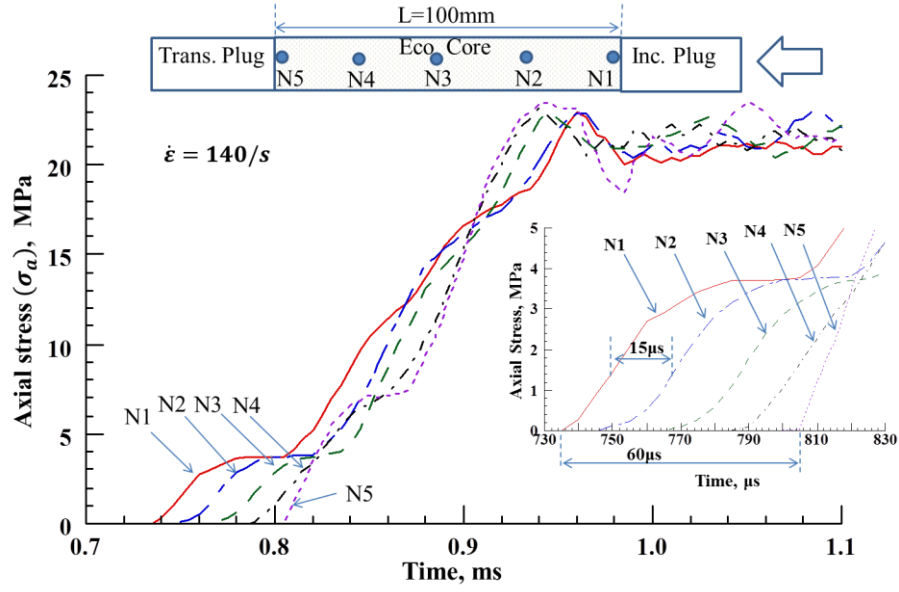


Figure 5.19. Axial stress propagation in a 100 mm long specimen at 140/s strain rate.

## 5.7 Summary

LS-DYNA simulation of static and dynamic confined compression tests of Eco-Core was conducted. The available “Low Density Foam” material model in LS-DYNA code was used to simulate the material properties of Eco-Core. A separate code was written to mimic Eco-Core material by the mentioned material model. Both static and dynamic tests at different strain rates were simulated. The LS-DYNA predicted stress-strain response was compared with experiment and the constitutive equation. All three results agreed very well with each other’s.

## CHAPTER 6

### Concluding Remarks and Future Work

#### 6.1 Concluding Remarks

Eco-Core is a unique fire resistant and non-toxic in fire foam that was conceived and developed at North Carolina A&T State University in 2003. The material was well characterized for composite sandwich structural applications. Performance of Eco-Core in multi-axial stress state, blast and shock conditions was not well understood. The present research fulfills this gap. The overall objective of this research was to develop a dynamic constitutive equation of Eco-Core that is valid for both static (low strain rate) and dynamic (high strain rate) conditions. Then validate the model by experiment. The dissertation was divided into four sections: material fabrication and specimen preparation; static and dynamic tests; development of constitutive model and validation by experiment; and finally implementation and validation by LS-DYNA. A summary and conclusions derived in each of those sections are given below.

Eco-Core panels were molded in two thicknesses, 25.4 mm and 12.7 mm, which are suitable for static and dynamic tests respectively. Static test specimen had 25.4 mm length and 28.5 mm diameter whereas the dynamic test specimen had 3.2 mm length and 11 mm diameter. A total 25 static test and 12 dynamic test specimens were prepared. The density of the static test specimens ranged from 0.50 to 0.52 g/cm<sup>3</sup> with an average of 0.507 g/cm<sup>3</sup>. The density of the dynamic test specimens ranged from 0.50 to 0.52 g/cm<sup>3</sup> with average of 0.51 g/cm<sup>3</sup>.

Static confined compression test of Eco-Core was conducted using five different sleeve materials (acrylic, aluminum, copper, steel and rubber) to simulate different confinement stress (pressure). The rubber sleeve represents the zero confinement. The confinement stress was calculated from the measured Hoop strain in the sleeve. The axial stress, radial confinement

stress and the friction between the specimen and the sleeve were reduced to a net-deviatoric stress (net-deviatoric stress = axial stress – friction equivalent stress – confinement stress). The net-deviatoric stress versus axial strain was found to be unique and independent of confinement stress. From these results, a static axial stress-strain constitutive equation was developed for Eco-Core under a multi-axial stress state. The equation was validated by experiment.

High strain rate confined compression testing of Eco-Core material was conducted for a strain rate ranged from 500/s to 3120/s using an aluminum sleeve confined compression test fixture in a SHPB apparatus. A special test fixture was developed to apply and measure both radial and axial stresses simultaneously. The designed specimen had 11 mm diameter and 3.2 mm length. The test instrumentation and data analysis were validated by comparing the measured stress-strain response of polycarbonate, nylon 6/6 and Eco-Core materials with data in literature. Test results showed that, like unconfined test results, the stress-strain response consists of three domains: linear (semi-linear), nonlinear or plateau (crushing) and densification. Unlike unconfined test, the stress-strain response and confined compression strength of Eco-Core are dependent on strain rate. Furthermore, the confined compression strength of Eco-Core increased with the increased strain rate.

An empirical dynamic axial stress-strain constitutive equation for Eco-Core was developed and is given by:

$$\frac{\sigma_a}{\sigma_c} = \begin{cases} 50 + ((25 \times 10^{-3})\dot{\varepsilon})\varepsilon_a - ((15 + 0.1\dot{\varepsilon})\varepsilon_a)^2 + \frac{q}{\sigma_c} \left[ 1 + 4\mu\left(\frac{l}{d}\right)(1 - \varepsilon_a) \right] & \text{for } \varepsilon_a \leq \varepsilon_c \\ 0.05(5.5\varepsilon_a)^{(2.5+7 \times 10^{-4}\dot{\varepsilon})} + (1.05 + 28 \times 10^{-5}\dot{\varepsilon})e^{-5\varepsilon_a} + \frac{q}{\sigma_c} \left[ 1 + 4\mu\left(\frac{l}{d}\right)(1 - \varepsilon_a) \right] & \text{for } \varepsilon_a > \varepsilon_c \end{cases}$$

Where  $\sigma_a$  is axial stress,  $\varepsilon_a$  is axial strain,  $\sigma_c$  is compression strength (20MPa),  $\varepsilon_c$  is compression yield strain (0.02),  $\dot{\varepsilon}$  is strain rate,  $\mu$  is coefficient of friction,  $l$  is specimen length and  $d$  is specimen diameter. This equation is valid for both static and dynamic conditions. The equation has two parts: One for initial semi-linear part ( $\varepsilon_a \leq \varepsilon_c$ , strain at compression strength) and non-linear part for  $\varepsilon_a > \varepsilon_c$ . The developed stress-strain equation was verified by experiment.

The dynamic energy absorption per unit volume of Eco-Core was found to be far superior to Balsa wood (more than 2 times) and other commercial polymer foams like PVC foam and Rohacell foam. The energy absorption per unit mass of Eco-Core is marginally better than other commercial materials.

LS-DYNA finite-element simulation of static and dynamic confined compression tests of Eco-Core was performed. The available “Low Density Foam” material model in LS-DYNA code was used to simulate the material properties of Eco-Core. A separate code was written to mimic Eco-Core properties by the above-mentioned material model. Both static and dynamic tests at different strain rates were simulated. The LS-DYNA predicted stress-strain response was compared with experiment and the developed constitutive equation. All three results agreed very well with each other’s. In conclusion, the present research developed a dynamic multi-axial constitutive equation for Eco-Core that can be used in a commercial code like LS-DYNA to analyze real life problems.

## 6.2 Future Work

Working on the static and the dynamic characterization of Eco-Core draw the attention to a few areas of possible development in the test methodology. These areas are:

- Conduct static test of Eco-Core or other syntactic foams under hydrostatic confinement. This method allows for applying constant level of confinement pressure on the specimen all

through the test and study the response of the material at that particular confinement pressure. Unlike, the sleeve confinement method where the confinement stress develops as the material is compressed. By using the hydrostatic confinement at different pressure levels, an alternate static constitutive equation can be developed.

- Direct measurement of the dynamic deformation of the specimen is proposed for the SHPB testing. Load cells (piezoelectric force sensors) can be installed on the incident and the transmitter bars for direct measurement of the forces acting on both sides of the specimen. Also, displacement laser sensors can be used with fixed marks on the bars to measure the displacement on both sides of the specimen for the entire period of impact, thereby the strain and the strain rate can be directly measured. This method will improve and develop the high strain testing since it overcomes the limitation of the narrow specimen configurations allowed by traditional SHPB testing.
- Material models in LS-DYNA need to be expanded to include materials like syntactic foams.

## References

1. Shivakumar, K. and H. Chen. *Eco-core and its performance in sandwich structural applications*. in *17th ICCM Technical Conference*. 2009. Edinburgh, UK.
2. Bardella, L. and F. Genna, *On the elastic behavior of syntactic foams*. International Journal of Solids and Structures, 2001. **38**(40): p. 7235-7260.
3. Wright, M.T., et al., *Composite material in aircraft mishaps involving fire 2003*, Naval Air Warfare Center Weapons USA, California.
4. NFPA. *An over view of the U.S. fire problem*. 2012 [cited 2012 January, 02]; Available from: <http://www.nfpa.org/assets/files/pdf/fireoverview.pdf>.
5. Sorathia, U., *Improving the fire performance characterizatic of composite materials for naval applications*. 2003, Naval Surface Warfare Center: West Bethada, MD.
6. Shivakumar, K., et al., *Processing and properties of a lightweight fire resistant core material for sandwich structures*. Journal of advanced materials, 2006. **38**(1): p. 32-38.
7. Shivakumar, K., M. Sharpe, and U. Sorathia. *Modification of eco-core material for improved fire resistance and toughness*. in *SAMPE05 International Conference*. 2005. Long Beach, California.
8. Sadler, R.L., et al., *Water immersion effect on swelling and compression properties of cco-core, PVC foam and balsa wood*. Composite Structures, 2009. **90**(3): p. 330-336.
9. Hossain, M.M. and K. Shivakumar, *Compression fatigue performance of a fire resistant syntactic foam*. Composite Structures, 2011. **94**(1): p. 290-298.
10. Hossain, M.M. and K. Shivakumar, *Flexural fatigue failures and lives of Eco-Core sandwich beams*. Materials & Design, 2014. **55**: p. 830-836.
11. Hossain, M.M., *Fatigue characterization of fire resistant syntactic foam core material*. 2013, NORTH CAROLINA AGRICULTURAL AND TECHNICAL STATE UNIVERSITY.
12. Shivakumar, K. and H. Chen, *Structural performance of eco-core sandwich panels*, in *Major Accomplishments in Composite Materials and Sandwich Structures*. 2010, Springer. p. 381-406.
13. Panduranga, R., L. Russell Jr, and K.N. Shivakumar. *Fracture toughness enhancement of fly ash based cco-core by glass fiber reinforcement*. in *22nd ASC Technical Conference*. 2007. Seattle, Washington.

14. Panduranga, R., K. Shivakumar, and L. Russell Jr. *Energy absorption of eco-core a syntactic foam*. in *48th AIAA/ASME/ASCE/AHS/ASC Structural, Structural Dynamic and Material Conference*. 2007. Waikiki, Hawaii.
15. Panduranga, R. and K. Shivakumar. *The high strain rate compression response of a fire resistant syntactic foam*. in *27th ASC Technical Conference*. 2012. Arlington, Texas.
16. Panduranga, R., *High strain rate response of eco-core and its modification*, in *Mechanical Engineering*. 2010, NC A&T State University: Greensborro, North Carolina.
17. Ramberg, W. and W.R. Osgood, *Description of stress-strain curves by three parameters*. 1943: National advisory committee for aeronautics.
18. Cowper, G. and P.S. Symonds, *Strain-hardening and strain-rate effects in the impact loading of cantilever beams*. 1957, DTIC Document.
19. Johnson, G.R. and W.H. Cook. *A constitutive model and data for metals subjected to large strains, high strain rates and high temperatures*. in *Proceedings of the 7th International Symposium on Ballistics*. 1983. The Netherlands.
20. Zerilli, F.J. and R.W. Armstrong, *Dislocation-mechanics-based constitutive relations for material dynamics calculations*. *Journal of Applied Physics*, 1987. **61**(5): p. 1816-1825.
21. Gibson, L. and M.F. Ashby, *Cellular solids structure and properties*. 2nd ed. 1997, Cambridge, UK.
22. Song, B., et al., *Confinement effects on the dynamic compressive properties of an epoxy syntactic foam*. *Composite Structures*, 2005. **67**(3): p. 279-287.
23. Subhash, G. and Q. Liu, *Quasistatic and dynamic crushability of polymeric foams in rigid confinement*. *International Journal of Impact Engineering*, 2009. **36**(10-11): p. 1303-1311.
24. Rittel, D., E. Hanina, and G. Ravichandran, *A Note on the Direct Determination of the Confining Pressure of Cylindrical Specimens*. *Experimental Mechanics*, 2007. **48**(3): p. 375-377.
25. Rittel, D. and A. Brill, *Dynamic flow and failure of confined polymethylmethacrylate*. *Journal of the Mechanics and Physics of Solids*, 2008. **56**(4): p. 1401-1416.
26. Forquin, P., et al., *Experimental study of the confined behaviour of PMMA under quasi-static and dynamic loadings*. *International Journal of Impact Engineering*, 2012. **40-41**: p. 46-57.

27. Huang, C. and G. Subhash, *Influence of lateral confinement on dynamic damage evolution during uniaxial compressive response of brittle solids*. Journal of the Mechanics and Physics of Solids, 2003. **51**(6): p. 1089-1105.
28. Bentayeb, F., K. Ait Tahar, and A. Chateaneuf, *New technique for reinforcement of concrete columns confined by embedded composite grid*. Construction and Building Materials, 2008. **22**(8): p. 1624-1633.
29. Chun, B.S., et al., *Development of a hyperbolic constitutive model for expanded polystyrene (EPS) geofom under triaxial compression tests*. Geotextiles and Geomembranes, 2004. **22**(4): p. 223-237.
30. *Fits and clearances pocket guide*, M.a.C. NSK, Editor. 2006: England.
31. Chen, W. and G. Ravichandran, *Dynamic compressive behaviour of ceramics under lateral confinement*. Le Journal de Physique IV, 1994. **4**(C8): p. C8-177-C8-182.
32. Hanina, E., D. Rittel, and Z. Rosenberg, *Pressure sensitivity of adiabatic shear banding in metals*. Applied Physics Letters, 2007. **90**(2): p. 021915.
33. Hoek, E. and J.A. Franklin, *A simple triaxial cell for field or laboratory testing of rock*. 1967: Imperial College of Science and Technology, University of London.
34. *Hoek Triaxial Cell Model HTC*, R. Limited, Editor. 2012: USA.
35. Chen, W., *Dynamic failure behavior of ceramics under multiaxial compression*. 1995, California Institute of Technology.
36. DIAB, A., *Sandwich Handbook*. 2003, Sandwich Concept.
37. Muthyala, V.D., *Composite sandwich structure with grid stiffened core*. 2007, Faculty of the Louisiana State University and Agricultural and Mechanical College In partial fulfillment of the requirements for the degree of Master of Science in Mechanical Engineering in The Department of Mechanical Engineering By Venkata Dinesh Muthyala BE, Osmania University.
38. Anon., *Testing at High Strain Rate*, A.P. Inc., Editor.: Miami/USA.
39. Timoshenko, S. and S. Woinowsky-Krieger, *Theory of Plates and Shells*. 2nd ed. 1959, New York, Toronto, London: McGraw-Hill Book Company.
40. Kully, R. and K. shivakumar. *Constitutive Equation of Syntactic Foam under Lateral Constraint*. in *29th ASC Techical Confernce*. 2014. San Diego, California, USA.
41. Chen, W., B. Zhang, and M. Forrestal, *A split Hopkinson bar technique for low-impedance materials*. Experimental Mechanics, 1999. **39**(2): p. 81-85.

42. Meyers, M., *Dynamic behavior of materials*. 1994, New York, NY: John Wiley & Sons Inc.
43. Salisbury, C., *Spectral analysis of wave propagation through a polymeric Hopkinson bar*, in *Mechanical Engineering*. 2001, University of Waterloo: Waterloo, Ontario, Canada.
44. Chou, S., K. Robertson, and J. Rainey, *The effect of strain rate and heat developed during deformation on the stress-strain curve of plastics*. *Experimental Mechanics*, 1973. **13**(10): p. 422-432.
45. LSTC. *LS-DYNA*. 2011 [cited 2014 May 05]; Available from: <http://www.lstc.com/products/ls-dyna>.
46. Sirijaroonchai, K., S. El-Tawil, and A.E. Naaman, *Numerical simulation of the Split Hopkinson Pressure Bar test technique for concrete under compression*. *International Journal of Impact Engineering*, 2010. **37**(2): p. 141-149.
47. Lu, Y., Z. Song, and Z. Tu. *Numerical simulation study of the strain rate effect on concrete in compression considering material heterogeneity*. in *DYMAT-International Conference on the Mechanical and Physical Behaviour of Materials under Dynamic Loading*. 2009. EDP Sciences.
48. Rong, Z., W. Sun, and Y. Zhang, *Dynamic compression behavior of ultra-high performance cement based composites*. *International Journal of Impact Engineering*, 2010. **37**(5): p. 515-520.
49. Dong, S., Y. Wang, and Y. Xia, *A finite element analysis for using Brazilian disk in split Hopkinson pressure bar to investigate dynamic fracture behavior of brittle polymer materials*. *Polymer testing*, 2006. **25**(7): p. 943-952.
50. Challita, G. and R. Othman, *Finite-element analysis of SHPB tests on double-lap adhesive joints*. *International Journal of Adhesion and Adhesives*, 2010. **30**(4): p. 236-244.
51. Majzoobi, G., et al., *Determination of materials parameters under dynamic loading. Part I: Experiments and simulations*. *Computational Materials Science*, 2010. **49**(2): p. 192-200.
52. Wang, Z., L. Wu, and J. Wang, *A study of constitutive relation and dynamic failure for SFRC in compression*. *Construction and Building Materials*, 2010. **24**(8): p. 1358-1363.
53. Adrian, R., B. Mihai, and C. Tudor. *Finite elements method in split Hopkinson pressure bar developing process*. in *Proceedings of the 6th WSEAS international conference on System science and simulation in engineering*. 2007. World Scientific and Engineering Academy and Society (WSEAS).

54. Lacy, J., et al. *A Method for Selecting Software for Dynamic Event Analysis I: Problem Selection*. in *Transactions 19th International Conference on Structural Mechanics in Reactor Technology*. 2007.
55. Gupta, S. and S. Moulick, *Study the Effect of Different SHPB Test Parameters Using Numerical Simulation Technique*.

## Appendix A

### ***Measurement of Coefficient of Friction Between Eco-Core and Sleeves***

This appendix describes the measurement of coefficient of friction between Eco-Core and four different types of sleeve materials (acrylic, aluminum, copper and steel) used in this study.

#### ***Test set up:***

Test setup appears in Figure A1. Sleeve tubes of 20 cm long and 28.5 mm diameter were cut and held at an angle as an inclined plane using a stand. A protractor was used to measure the angle of inclination ( $\theta$ ). Inner sides of the metal tubes were polished with sand paper grade 600-grit. Same type of polishing was done in the confined compression test. Cylindrical Eco-Core specimen with 12.7 mm diameter and 12.7 mm length was prepared by turning a larger specimen on the lathe machine in the same manner of preparing static confined test specimens. The specimen was inserted inside the tube and inclination of the tube was varied until the specimen was about to slide down. This initiation of sliding angle was noted. The experiment was repeated five times for all sleeve tubes. The critical sliding angle ( $\theta_c$ ) of sliding was recorded and are listed in Table A1.

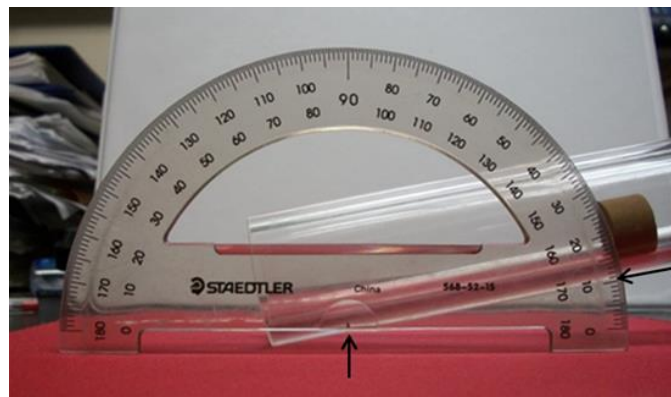
#### ***Test results:***

The critical sliding angles varied from  $9^0$  to  $11^0$  for acrylic and aluminum tubes where as it varied from  $10^0$  to  $11^0$  for copper and steel tubes. The average critical angle is found to be  $10^0$ . The corresponding coefficient of friction ( $\mu$ ) is calculated from the equation  $\mu = \text{Tan}(\theta_c^0)$ . The result is  $\mu = 0.18$  with an error of less than 2%.

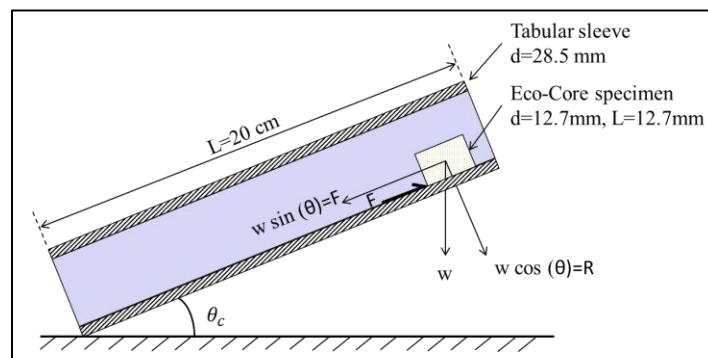
Table A 1

*Critical friction angle*

| Test no. | Angle of sliding ( $\theta_c$ ), deg. |          |        |       |
|----------|---------------------------------------|----------|--------|-------|
|          | Acrylic                               | Aluminum | Copper | Steel |
| 1        | 10                                    | 11       | 11     | 10    |
| 2        | 11                                    | 10       | 11     | 10    |
| 3        | 9                                     | 11       | 10     | 10    |
| 4        | 10                                    | 10       | 10     | 10    |
| 5        | 10                                    | 9        | 10     | 11    |
| Ave.     | 10                                    | 10       | 10     | 10    |
| STD      | 0.6                                   | 0.7      | 0.5    | 0.4   |



(a)



(b)

Figure A 1. (a) Photograph of friction test setup, (b) Schematic of friction test setup.

*Appendix B*

***Calibration of Confinement and Friction Stresses versus Axial Strain***

The effect of confinement stress ( $q$ ) and the effect of the equivalent friction stress between the specimen and the sleeve in the axial direction ( $\sigma_\mu$ ) from the experimental data were added together as  $(q + \sigma_\mu)$ . The value of  $(q + \sigma_\mu)$  is not effected by the strain rate. But, it differs for different sleeve types. The  $(q + \sigma_\mu)$  versus  $\varepsilon_a$  response of the used aluminum sleeve of  $d=11$  mm and  $h=0.9$  mm and specimen of  $d=11$  mm and  $l=3.2$  mm is plotted in Figure B1. A fourth order polynomial equation was found to be the best fit to the experimental curve of  $(q + \sigma_\mu)$  for  $\varepsilon_a > 0.02$ . The curve fitting equation is denoted by Eq. B1.

$$(q + \sigma_\mu) = 4.2 - 21.5\varepsilon_a + 709.3\varepsilon_a^2 - 2621.2\varepsilon_a^3 + 2973.7\varepsilon_a^4 \quad (B1)$$

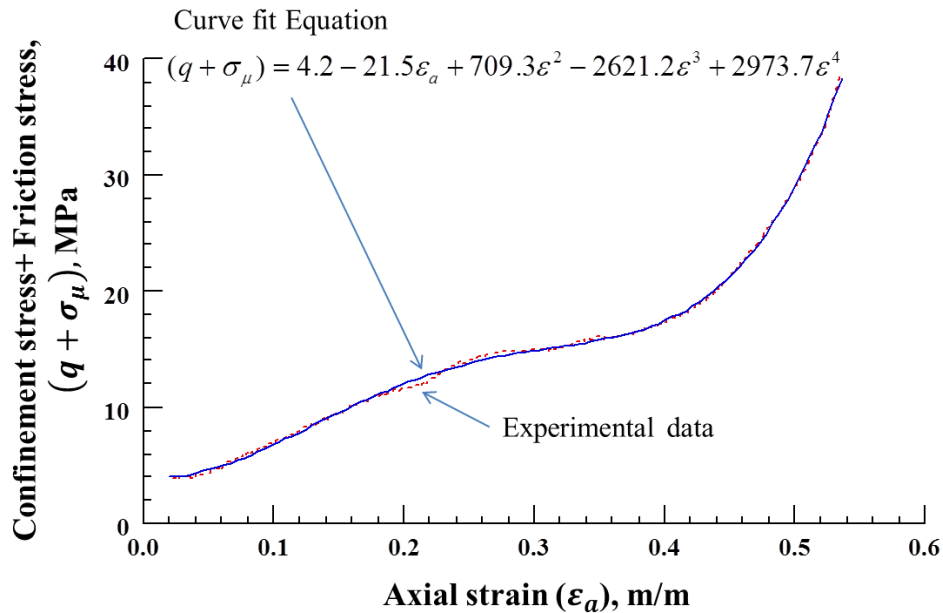


*Figure B 1.* Experimental and curve fitting for  $(q + \sigma_\mu)$  versus  $\varepsilon_a$  response.

### *Appendix C*

#### ***Calibration of Strain Rate versus Impact Velocity and Specimen Length***

The modified material model (Low Density Foam Material Model) has become a strain rate dependent after it was defined by the strain rate sensitive constitutive equation. Therefore the strain rate of the test has to be determined for the material model. The strain rate can be related to impact velocity of the striker bar and determined accordingly by the following procedure:

- LS-DYNA simulation code for the SHPB dynamic test was prepared using specimen length of 3.2 mm. Initially the material model (developed by constitutive equation) is a function of a strain rate.
- A 500/s strain rate value was substituted in the strain rates of the material model in the code.
- The impact velocity imposed on the striker bar was assigned low value and then the code was run and outcome strain rate of the specimen was determined and compared to the 500/s strain rate.
- The velocity of impact was increased gradually until the outcome strain rate matched 500/s. That impact velocity was found to be 3.3 m/s as shown in Figure C1a.
- Same steps were repeated to 1574/s, 2220/s and 3120/s strain rates and every time the impact velocity was determined as shown in Figures C1b, c and d, respectively.
- The values of the impact velocities and the outcome strain rates were listed in Table C1.
- Strain rate was plotted versus impact velocities as shown in Figure C2. The correlation equation between strain rate and impact velocity ( $V$ ) for the specimen length ( $l$ ) of 3.2 mm was found to be:

$$\dot{\epsilon} = 299V - 480 \quad (C1)$$

- Since the strain rate varies inversely proportional with the length of the specimen, general strain rate equation as a function of velocity and specimen length was approximated as:

$$\dot{\epsilon} = (299V - 480) \times \frac{0.0032}{l} \quad (C2)$$

- This equation was checked for very high speed and very long specimen and the results agreed very well with the equation (see Table C2).

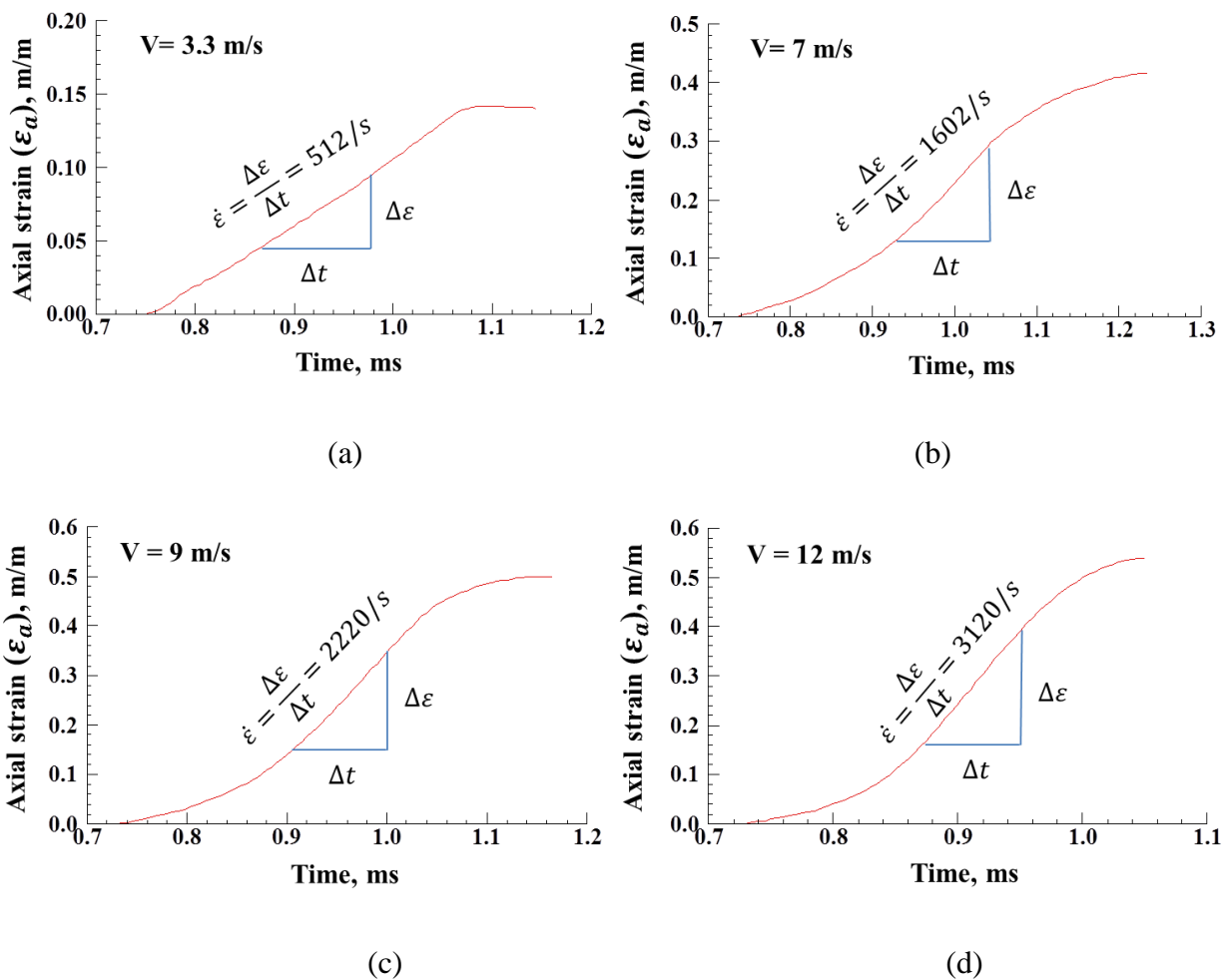


Figure C 1. (a) Strain response of 3.2 mm long specimen at 3.3 m/s impact velocity, (b) Strain response at 7 m/s impact velocity, (c) Strain response at 9 m/s impact velocity, (d) Strain response at 12 m/s impact velocity.

Table C 1

Strain rate versus impact velocity ( $L=3.2$  mm)

| Velocity of Impact ( $V$ ), m/s | Output strain rate ( $\dot{\epsilon}$ ), 1/s |
|---------------------------------|--|
| 3.3                             | 512  |
| 7                               | 1602   |
| 9                               | 2220   |
| 12                              | 3111   |

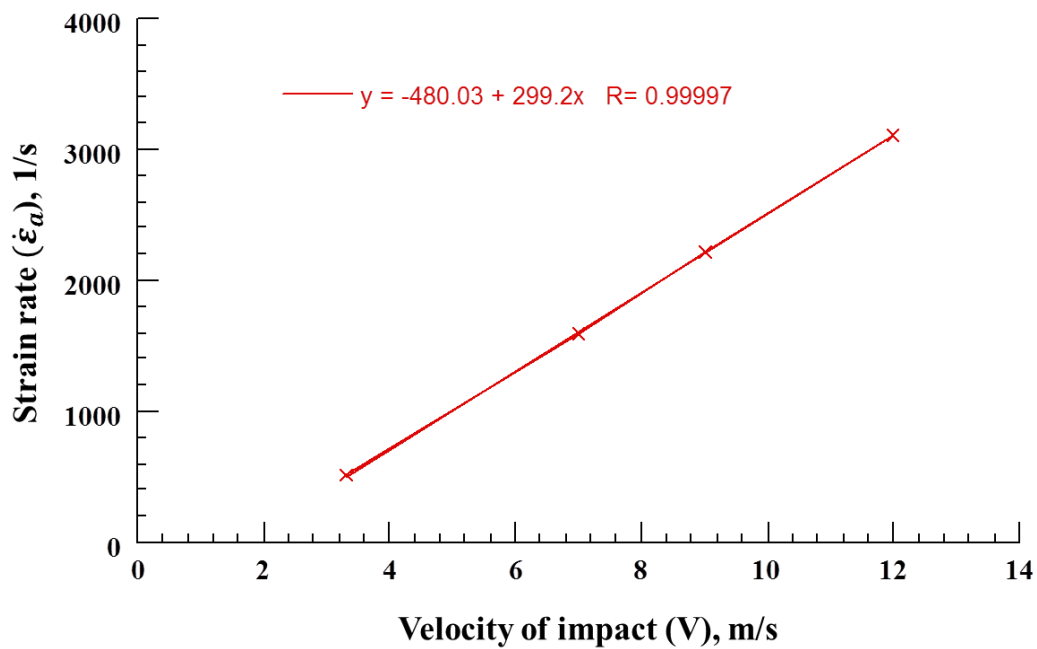


Figure C 2. Calibration of strain rate versus impact velocity for 3.2 mm long specimen.

Table C 2

Strain rate responses of Eq. C2 and LS-DYNA for different  $l$  and  $V$

| Specimen length ( $l$ ),<br>mm | Impact velocity ( $V$ ),<br>m/s | Strain rate, Eq. C2<br>( $\dot{\epsilon}$ ),1/s | Strain rate, LS-DYNA<br>( $\dot{\epsilon}$ ),1/s |
|--------------------------------|---------------------------------|---|--|
| 3.2                            | 3.3                             | 512   | 512  |
| 13.2                           | 50                              | 3600  | 4000   |
| 100                            | 15                              | 130   | 140  |

## Appendix D

**APDL Code for Static Test Simulation**

```

FINISH
/CLEAR
/TITLE, Static Test for Eco-Core
/FILNAM, EC-Dy
!!!!!!Define units!!!!!!
!N,m,pascal
/NOPR                ! Entering dynamic solver
KEYW,PR_SET,1
KEYW,PR_STRUC,1
KEYW,LSDYNA,1
KEYW,PR_DYNA,1
/PREP7              ! Entering preprocessing
!!!!!!!!!!!!!!!!!!!!!! Define element type!!!!!!!!!!!!!!!!!!!!!!
ET,1,PLANE162
KEYOPT,1,3,1        ! For element 1 Key option K3 is option #1 "Axisymmetric"
KEYOPT,1,2,1        ! For element 1 Key option K2 is option #1 "volume weight"
!!!!!!!!!!!!!!!!!!!!!! Define materials properties!!!!!!!!!!!!!!!!!!!!!!
!!!!!!!!!!!!!!!!!!!!!! LOW DENSITY FOAM MODEL!!!!
*DIM,SN,,51         ! Strain
*DIM,SS,,51         ! Stress
*DIM,CF,,51         ! Confinement stress + friction stress
*DIM,A,,51          ! Part A of the polynomial equation for (Conf+fric)
*DIM,B,,51          ! Part B of the polynomial equation for (Conf+fric)
*DIM,C,,51          ! Part C of the polynomial equation for (Conf+fric)
*DIM,D,,51          ! Part D of the polynomial equation for (Conf+fric)
*DIM,E,,51          ! Part E of the polynomial equation for (Conf+fric)
*SET,SN(1),0
*SET,SS(1),0
*SET,CF(1),0
*Do,I,2,51,1
*SET,SN(I),(I-1)*0.02
*SET,A(I),2973.7*(SN(I))**4
*SET,B(I),2621.2*(SN(I))**3
*SET,C(I),709.33*(SN(I))**2
*SET,D(I),21.519*(SN(I))
*SET,E(I),4.1922
*SET,CF(I),A(I)-B(I)+C(I)-D(I)+E(I)
*SET,SS(I),((5.5*SN(I))**2.5+21*EXP(-5*SN(I))+CF(I))*1000000 !Constitutive. Eq.
*ENDDO
EDCURVE,ADD,1,SN,SS ! Define curve 1 of Eco-Core by strain stress
MP,DENS,1,500        ! Density of Eco-Core
MP,EX,1,1E9         ! Modulus of Eco-Core

```

```

MP,NUXY,1,0.16          ! Poisson's ratio of Eco-Core
TB,FOAM,1,,2           ! Foam model type 2 "Low Density Foam"
TBDATA,1,1             ! Use curve 1
TBDATA,2,6.5E6         ! Tension strength of Eco-Core
TBDATA,5,0.15          ! Viscous coeff.
MP,DENS,2,8050         ! Steel density
MP,EX,2,200E9          ! Steel modulus of elasticity for material 1 in Pascale
MP,NUXY,2,0.33         ! Poisson's ratio for material 1
MP,DENS,3,2810         ! Aluminum density
MP,EX,3,69E9           ! Aluminum modulus of elasticity for material 1 in Pascale
MP,NUXY,3,0.3         ! Poisson's ratio for material 1
!!!!!!!!!!!!!!!!!!!!!! Define key points!!!!!!!!!!!!!!!!!!!!!!
!EC
k,1,0,0
k,2,0.0127,0
k,3,0.0127,0.0127
k,4,0,0.0127
!PLUNGER
K,5,0,0.0127
K,6,0.0127,0.0127
K,7,0.0127,0.0327
K,8,0,0.0327
!SLEEVE
k,9,0.0127,0
K,10,0.0144,0
K,11,0.0144,0.0254
K,12,0.0127,0.0254
!!!!!!!!!!!!!!!!!!!!!! Define lines by joining key points!!!!!!!!!!!!!!!!!!!!!!
L,1,2
L,2,3
L,3,4
L,4,1
L,5,6
L,6,7
L,7,8
L,8,5
L,9,10
L,10,11
L,11,12
L,12,9
!!!!!!!!!!!!!!!!!!!!!! Define areas!!!!!!!!!!!!!!!!!!!!!!
A,1,2,3,4
A,5,6,7,8
A,9,10,11,12
!!!!!!!!!!!!!!!!!!!!!! Define line divisions!!!!!!!!!!!!!!!!!!!!!!
LESIZE,1,,10

```





## Appendix E

*APDL Code for Dynamic Test Simulation*

```

FINISH
/CLEAR
/TITLE, Dynamic Test for Eco-Core
/FILNAM, EC-Dy
!!!!!!!!!!!!!!!!!!!!!!!!!!!!!!!!!!!! Define units!!!!!!!!!!!!!!!!!!!!!!!!!!!!!!!!!!!!
!N,m,pascal
/NOPR                      ! Entering dynamic solver
KEYW,PR_SET,1
KEYW,PR_STRUC,1
KEYW, LSDYNA,1
KEYW,PR_DYNA,1
V=12                       ! Velocity of impact
l=0.0032                   ! SPC thickness in m
SR=299*V-480*(0.0032/l)   ! Strain rate
/PREP7                     ! Entering preprocessing
!!!!!!!!!!!!!!!!!!!!!!!!!!!!!!!!!!!! Define element type!!!!!!!!!!!!!!!!!!!!!!!!!!!!!!!!!!!!
ET,1,PLANE162
KEYOPT,1,3,1              ! For element 1 Key option K3 is option #1 "Axisymmetric"
KEYOPT,1,2,1              ! For element 1 Key option K2 is option #1 "volume weight"
!!!!!!!!!!!!!!!!!!!!!!!!!!!!!!!!!!!! Define materials properties!!!!!!!!!!!!!!!!!!!!!!!!!!!!!!!!!!!!
!!!!!!!!!!!!!!!!!!!!!!!!!!!!!!!!!!!! LOW DENSITY FOAM MODEL!!!!
*DIM,SN,,51               ! Strain
*DIM,SS,,51               ! Stress
*DIM,CF,,51               ! Confinement stress + friction stress
*DIM,A,,51                ! Part A of the polynomial equation for (Conf+fric)
*DIM,B,,51                ! Part B of the polynomial equation for (Conf+fric)
*DIM,C,,51                ! Part C of the polynomial equation for (Conf+fric)
*DIM,D,,51                ! Part D of the polynomial equation for (Conf+fric)
*DIM,E,,51                ! Part E of the polynomial equation for (Conf+fric)
*SET,SN(1),0
*SET,SS(1),0
*SET,CF(1),0
*Do,I,2,51,1
*SET,SN(I),(I-1)*0.02
*SET,A(I),2973.7*(SN(I))**4
*SET,B(I),2621.2*(SN(I))**3
*SET,C(I),709.33*(SN(I))**2
*SET,D(I),21.519*(SN(I))
*SET,E(I),4.1922
*SET,CF(I),A(I)-B(I)+C(I)-D(I)+E(I)
*SET,SS(I),((5.5*SN(I))**2+(2.5+0.0007*SR)+(21+0.0056*SR)*EXP(-5*SN(I))+CF(I))*1000000
*ENDDO

```





L,26,27  
L,27,28  
L,28,25  
L,29,30  
L,30,31  
L,31,32  
L,32,29  
L,33,34  
L,34,35  
L,35,36  
L,36,33  
!!!!!!!!!!!!!!!!!!!!!!!!!!!!!!!!!!!! Define areas!!!!!!!!!!!!!!!!!!!!!!!!!!!!!!!!!!!!  
A,1,2,3,4  
A,5,6,7,8  
A,9,10,11,12  
A,13,14,15,16  
A,17,18,19,20  
A,21,22,23,24  
A,25,26,27,28  
A,29,30,31,32  
A,33,34,35,36  
!!!!!!!!!!!!!!!!!!!!!!!!!!!!!!!!!!!! Define line divisions!!!!!!!!!!!!!!!!!!!!!!!!!!!!!!!!!!!!  
LESIZE,1,,7  
LESIZE,2,,150  
LESIZE,3,,7  
LESIZE,4,,150  
LESIZE,5,,5  
LESIZE,6,,5  
LESIZE,7,,5  
LESIZE,8,,5  
LESIZE,9,,7  
LESIZE,10,,600  
LESIZE,11,,7  
LESIZE,12,,600  
LESIZE,13,,4  
LESIZE,14,,5  
LESIZE,15,,4  
LESIZE,16,,5  
LESIZE,17,,8  
LESIZE,18,,5  
LESIZE,19,,8  
LESIZE,20,,5  
LESIZE,21,,4  
LESIZE,22,,5  
LESIZE,23,,4  
LESIZE,24,,5





